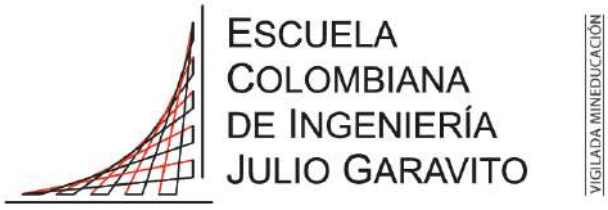

Master Thesis

DEVELOPMENT OF PHYSICAL INTERFACES TO PROMOTE KINEMATIC COMPATIBILITY FOR AGORA LOWER-LIMB EXOSKELETON

Felipe Ballén Moreno

Supervisor:

Prof. Dr. Marcela Múnera

Co-supervisor:

Prof. Dr. Carlos A. Cifuentes

A thesis submitted in fulfillment of the requirements for the degree of

Master in Electronic Engineering

November 2020

"Intelligence is the ability

to adapt to change."

Stephen Hawking

Acknowledgements

This thesis contributes to the scope and objectives of the AGoRA research project "Development of an Adaptable Robotic Platform for Gait Rehabilitation and Assistance". I would like to acknowledge the sponsors involved in this project, such as the Ministry of Science, Technology and Innovation Minciencias (Grant 801-2017) and the Colombian School of Engineering Julio Garavito. Besides, I also would like to acknowledge the collaboration with the EPF Eć ole d'ingénieur through Prof. Dr. Thomas Provot and Prof. Dr. Maxime Bourgain, and *Universidad Autónoma de Coahuila* through Prof. H. A. Moreno, which guides me to establish the grounds of this work.

Undoubtedly, the support of a large group of people allowed me to fulfill this work. First of all, I would like to thank my mother, Angela, and my grandmother Cecilia, who gives me strength, wisdom, and love to be the person I am. To my father, Fernando, who gave me the resilience to overcome any barrier, even though he is gone. Additionally, I would like to thank my thesis advisors, who always guided me along this challenging path but satisfying. To Marcela, who taught me that I could beat my limits every day and be multi-tasking and efficient without losing my mind. To Carlos, whose vision taught me that the only limit is our imagination and the ability to manage as many projects as you can. Finally, I want to express my full appreciation and gratitude to my colleagues and friends, that day after day works to achieve some goal within the endless research path. The past two years were unique in my life and each one brought the best to make it unforgettable. Thanks to Daniel, Sergio, Luis, Alejandro, Daniel Jr., Andrés, Nathalia, Jonathan, Maria José, Margarita, Orión, Juan, Ricardo, Tim, and Diego.

Esta tesis contribuye al alcance y los objetivos del proyecto de investigación AGoRA "Desarrollo de una plataforma robótica adaptable para la rehabilitación y asistencia de la marcha". Quisiera agradecer a los patrocinadores que participan en este proyecto, como el Ministerio de Ciencia, Tecnología e Innovación Minciencias (Grant 801-2017), y la Escuela Colombiana de Ingeniería Julio Garavito. Además, también me gustaría reconocer la colaboración a la EPF Eć ole d'ing'enieur a través del Prof. Dr. Thomas Provot y el Prof. Dr. Maxime Bourgain,

y a la Universidad Autónoma de Coahuila a través del Prof. H. A. Moreno, que me guiaron para establecer las bases de este trabajo.

Sin lugar a duda, el apoyo de un gran grupo de personas me permitió realizar este trabajo. En primer lugar, me gustaría agradecer a mi madre Angela, y a mi abuela Cecilia, que me dan la fuerza, sabiduría y amor para ser la persona que soy. A mi padre Fernando, que me dio la resislencia para superar cualquier barrera, aunque ya no esté. Además, quiero agradecer a mis asesores de tesis, que siempre me guiaron por este duro camino pero satisfactorio. A Marcela, que me enseñó que soy capaz de superar mis límites cada día y que puedo ser multi-tasking y eficiente sin perder la cabeza. A Carlos, cuya visión me enseñó que el único límite es la imaginación y la capacidad de gestionar tantos proyectos como se pueda. Por último, quiero expresar todo mi aprecio y gratitud a mis colegas y amigos, que día tras día trabajan para lograr algún objetivo dentro del interminable camino de la investigación. Los últimos dos años fueron únicos en mi vida y cada uno aportó lo mejor para que sea inolvidable. Gracias a Daniel, Sergio, Luis, Alejandro, Daniel Jr/, Andrés, Nathalia, Jonathan, María José, Margarita, Orión, Juan, Ricardo, Tim y Diego.

Abstract

Over the years, exoskeletons are included in clinical, industrial, and military applications to enhance and assist the human body. Regarding lower-limb exoskeletons in clinical applications are intended to provide aid during daily living activities. Lower-limb exoskeletons are equipped with a mechanical structure, actuators, sensors, attachments, and interfaces that interact physically with the user. These features are focused on being adequately designed for suitable human-robot interaction. However, the features' design has multiple complexities and limitations to solve and assess. On one hand, the human hip joint has intricacy behavior due to the three degrees of freedom that are not resolved by commercial exoskeletons. On the other hand, there is a lack of robotic devices' performance indicators that properly assess the physical interfaces.

In this sense, this master's thesis presents the design and modeling of a passive hip joint intended to assist the hip ab/adduction motion. Besides, it also presents a novel three-dimensional relative motion methodology to assess the human-robot interaction of the AGoRA lower-limb exoskeleton. The passive hip joint presents the design principles used to estimate the interaction torque allowing the understanding of energy provided to the user. Moreover, it also raises the three-dimensional relative motion methodology's theoretical concepts and the implementation in a pilot study. The principal outcomes are aimed to improve the AGoRA lower-limb exoskeleton's understanding of the Physical Human-Robot Interaction. On the one hand, the passive hip joint is characterized along different preloads, giving the user a maximum torque of 15.8 Nm at a preload of 472.43 N. Likewise, the joint's stiffness provided a maximum of 4.24 Nm/deg. On the other hand, the proposed three-dimensional relative motion methodology demonstrated the exoskeleton's interaction among the three principal planes of motion, identifying undesirable motions in the secondary planes. The proposed joint's results revealed multiple improvements for the user's assistance. Similarly, the three-dimensional relative motion's results suggested a physical interfaces' enhancement to reduce the undesirable motions and improve AGoRA lower-limb exoskeleton's human-robot interaction and its kinematic compatibility.

Keywords: Human-Robot Interaction, Biomechanics, Lower-limb Exoskeleton, Hip Exoskeletons, Exoskeleton Performance Evaluation.

List of Tables

List of Figures

Contents

Chapter 1

Introduction

This work presents the development and assessment of physical interfaces for the AGoRA lower-limb exoskeleton. Design features are considered to understand how those interfaces are involved in gait assistance. A preliminary study is also presented using a novel metric developed to understand the user-device interaction. This chapter shows the motivation of this study and its objectives.

1.1 Motivation

Locomotion can be affected by a work-related accident or a neurological injury. After-effects vary according to the location and type of injury suffered (e.g., spinal cord injury, stroke, cerebral palsy)[1]. Mainly, stroke is defined as a sudden interruption of blood flow in the brain involving different impairments. These effects depend on the location and nature (i.e., ischemic or hemorrhagic) of the lesion [2]. Stroke's consequences may cause impairments in the lower and upper limbs, which reduce the ability to perform daily tasks and deteriorate the life quality. The most common impairments are pain, impaired motor control, spasticity, and muscle weakness [3]. Focusing on lower-limbs, spasticity consequences affect the ankle and knee adduction and extension, as well as equinovarus foot [4]. In this sense, the neuromusculoskeletal structure needs support and assistance to mitigate pathological mechanisms. The

rehabilitation process is critical to start the recovery of post-stroke patients. Consequently, the first choice is physical therapy.

Physical Therapy (PT) usually consists of repetitive movements performed by a therapist to overcome pathological mechanisms. In consequence, PT engages sensorimotor mechanisms triggering neuroplasticity [5]. PT has been demonstrated to be effective in recovering for different activities of daily living (ADL), using standardized metrics such as functional independence measure (FIM) [6]. Despite this evidence, PT has certain limitations. For instance, the distal joints have been proven to be more difficult to rehabilitate and obtain a full range of motion [7]. Besides, therapists' burden is exhaustive due to the demanding assistance for increasing patients [8], [9].

Emerging robotic technologies can be used as a tool to include in PT, allowing better results in earlier stages of the patient's recovery [10]. These devices' development considers different kinds and degrees of impairments caused by neurological injuries. For example, cerebral palsy patients have gait issues produced by an injury in the immature brain [11]. These specific devices for children need complete support, and the forces' magnitude is lower because of their lighter body. On the contrary, stroke patients have a more comprehensive population spectrum. Therefore, the population's physical characteristics and the impairment's aspects become in design parameters for the robotic device [7].

Robotic devices' design parameters should promote the kinematic compatibility between the user and the device, allowing a proper physical Human-Robot Interaction (pHRI) [12]. The design parameters are used to develop robotic devices that are adaptable, suitable, ergonomic, and comfortable that multiple users can benefit from their usage without reducing the device's performance. Following these robotic devices' features, the device's structure allowed a smooth interaction with the user. The kinematic compatibility involves the main components that must be adequately designed and developed such as the mechanical structure, several actuators, control strategies, and physical interfaces [13].

Over the years, robotic devices' progress has been unbalanced because the design and assessment of physical interfaces have been overlooked [14]. Even though a few studies have been taken into account physical interfaces, there is a lack of performance indicators to assess them [5], [13], [14]. Hence, this scope can have meaningful breakthroughs in the understanding and improvement of the pHRI.

Following this scope, this interdisciplinary project seeks to improve current approaches in wearable robots. This project comprises a robotic platform to conduct clinical and laboratory studies regarding robotic aid for gait. This work intends to enhance the kinematic compatibility of the AGoRA lower-limb exoskeleton (AGoRA-LLE) by better understanding the physical interfaces' development and assessment. In this work, kinematic compatibility is assessed in terms of interaction torques in a passive joint and relative rotations during gait.

1.2 Background

This thesis is developed in the context of the research project "*Development of an Adaptable Robotic Platform for Gait Rehabilitation and Assistance*" AGoRA supported by the Ministry of Science and Technology *Minciencias* (grant 801-2017), as well as internal funding from the Colombian School of Engineering Julio Garavito (ECIJG).

The AGoRA project is led by Prof. Dr. Carlos A. Cifuentes and Prof. Dr. Marcela Munera (professors at the Department of Biomedical Engineering and head of the *Center for Biomechatronics* at ECIJG). This project's research team is a cooperative network, including national and international research groups and institutions. A clinical insight given by the trauma and rehabilitation group at *Universidad Clínica La Sabana* (led by Dr. Catalina Gómez) constitutes the project's medical partner. Besides, the engineering partners of the project team are composed of three international research groups: (1) the Neural and Cognitive Engineering group of the Center for Automation and Robotics at the Spanish National Research Council, Spain (led by Dr. Eduardo Rocon), (2) the Institute of Automation of

the University of San Juan, Argentina (led by Dr. Ricardo Carelli) and, (3) the Robotics and Industrial Automation Group of the Federal University of Espíritu Santo in Vitória, Brazil (led by Dr. Anselmo Frizera-Neto). Additionally, Prof. Dr. Thomas Provot and Prof. Dr. Maxime Bourgain (professors at the EPF École d'ingénier) were collaborators for the biomechanical analysis involved in the project.

This project aims to develop and validate a robotic platform for gait rehabilitation and assistance through a smart walker and an active lower-limb exoskeleton. This project seeks an appropriate interaction between the user, the robotic platform, and the environment employing different communication channels. Multiple sensors and actuators of both robotic devices are used for estimating physical interaction given by the user, environment variables, and feedback to the system and user. This overall arrangement is known as Human-Robot Interaction (HRI), which is detailed in Fig. 1.1.

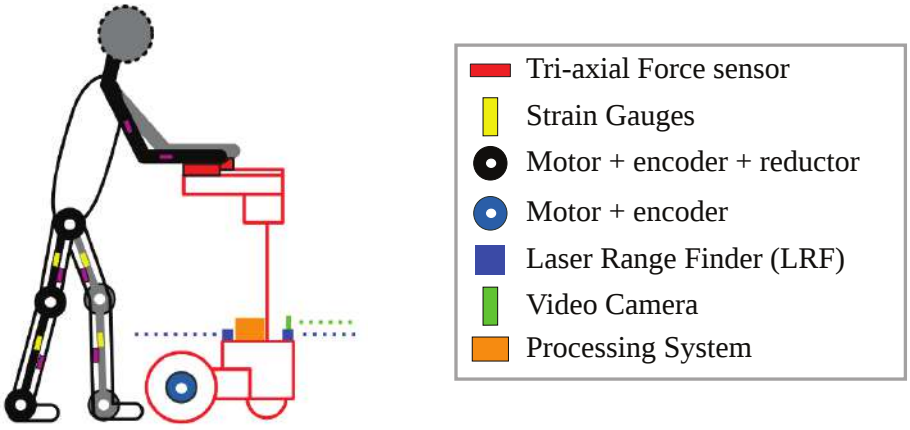

Figure 1.1: AGoRA Project. Smart walker and lower-limb exoskeleton components for rehabilitation and assistance.

According to the above and within this project's scope, this master thesis contributes to the development and assessment of the active lower-limb exoskeleton. It seeks to build and evaluate its physical interfaces to understand the kinematic compatibility during a specific task. In this sense, this work looks forward to answering the following research question: Is the AGoRA-LLE kinematic compatible during gait?

1.3 Objectives

Under the project's aim, it is proposed the development of the physical interfaces for a lower-limb exoskeleton (LLE), along with its assessment to understand the interaction between the user and the device. It is also presented as a methodology to assess the pHRI given by the physical interfaces. The following objectives are described to reach this proposal.

1.3.1 General Objective

To develop physical interfaces to promote kinematic compatibility for AGoRA lower-limb exoskeleton.

1.3.2 Specific Objectives

- To conduct a literature review to understand the kinematic compatibility in rehabilitation devices.
- To develop the AGoRA lower-limb exoskeleton hip joint's mathematical model, which represents the force transmission to the anatomical joints.
- To design and integrate ergonomic interfaces for AGoRA lower-limb exoskeleton.
- To evaluate the kinematic compatibility through a biomechanical assessment of the developed platform.

1.4 Contributions

The significant contributions of this work are meant to accomplish the main goals of the AGoRA lower-limb exoskeleton to ensures gait rehabilitation and assistance. This master thesis carried out technical and scientific contributions as follows:

1. The design and development of physical interfaces for an active lower-limb exoskeleton to ensure the user's assistance. They were designed to be comfortable and followed ergonomic principles according to the targeted population.

2. The mathematical model of the passive hip joint of the AGoRA lower-limb exoskeleton: this model is based on a variable stiffness system providing complaint assistance, and its interaction can be adjusted at different levels. This model was estimated to understand the user's interaction along with gait.

3. The development and implementation of a three-dimensional methodology to analyze the performance of the AGoRA lower-limb exoskeleton's physical interfaces. The method follows biomechanical principles, along with an analysis that fully describes the pHRI.

1.5 Publications

The progress of this thesis has been reported to the scientific community as follows:

1. (Conference Proceedings) **F. Ballen-Moreno**, C. A. Cifuentes, T. Provot, M. Bourgain, and M. Marcela, "3D Relative Motion Assessment in Lower-limb Exoskeletons: A Case of Study with AGoRA exoskeleton," in The International Symposium on Wearable Robotics (WeRob2020), no. 1, pp. 2–3.

2. (Journal article) **F. Ballen-Moreno**, H. A. Moreno, D. F. Casas, C. A. Cifuentes, M. Múnera, "Design of a Hip Passive Joint for Lower-limb Exoskeleton Aimed to Rehabilitation" *to be submitted*

3. (Journal article) **F. Ballen-Moreno**, M. Bautista, T. Provot, M. Bourgain, C. A. Cifuentes, M. Múnera, "Physical Interfaces Assessment of the AGoRA Exoskeleton through 3D Relative Motion Analysis" *to be submitted*

4. (Conference Proceedings) M. Manchola, D. Serrano, D. Gomez, **F. Ballen**, et al., "T-FLEX: Variable Stiffness Ankle-Foot Orthosis for Gait Assistance," in Wearable

Robotics: Challenges and Trends, vol. 16, J. González-Vargas, J. Ibáñez, J. L. Contreras-Vidal, H. van der Kooij, and J. L. Pons, Eds. Springer International Publishing, 2019, pp. 160–164. https://doi.org/10.1007/978-3-030-01887-0_31

5. (Book chapter) Sierra S., Arciniegas L., **Ballen-Moreno F.**, Gomez-Vargas D., Munera M., Cifuentes C.A. (2020) Adaptable Robotic Platform for Gait Rehabilitation and Assistance: Design Concepts and Applications. In Exoskeleton Robots for Rehabilitation and Healthcare Devices. SpringerBriefs in Applied Sciences and Technology. Springer, Singapore. https://doi.org/10.1007/978-981-15-4732-4_5

6. (Conference Proceedings) D. Gomez-Vargas, M. J. Pinto-Bernal, **F. Ballen-Moreno**, et al., "Therapy with t-flex ankle-exoskeleton for motor recovery: A case study with a stroke survivor," 8th IEEE RAS & EMBS International Conference on Biomedical Robotics and Biomechatronics (BioRob), 2020.

1.6 Document Organization

The structure of this document details the development and assessment of the AGoRA lower-limb exoskeleton. It presents the passive frontal hip joint's design and modeling given the interaction torque provided for the user. Moreover, it introduces a novel three-dimensional relative motion methodology to assess the physical interfaces of the AGoRA-LLE. In this context, the document is organized as:

- **Chapter 1** presents the motivation and background involved in this work. Within this chapter explains the research question and the contributions related to this thesis are also described.

- **Chapter 2** establishes the design features in the lower-limb exoskeletons focused on the physical interfaces' targeted goal. Each feature gives a guideline to developing the

lower-limb exoskeleton, which is expanded along with this chapter.

- **Chapter 3** describes the current development of the AGoRA lower-limb exoskeleton according to the design features. It also presents the passive frontal hip joint through its mathematical model and simulation.

- **Chapter 4** presents the novel three-dimensional relative motion methodology to analyze the user's interaction with the lower-limb exoskeleton. It also reports the implementation of the proposed method through a pilot study.

- **Chapter 5** resumes the conclusions and highlights of this work. This chapter also proposes primary future outcomes to improve AGoRA-LLE performance.

Chapter 2

Lower limb exoskeletons

The applications for lower-limb exoskeletons (LLEs) are mainly oriented to rehabilitation and assistance, and they have been focused on populations that suffered from work-related accidents or neurological injuries (i.e., stroke, cerebral palsy, spinal cord injury) [15]. Robotic aid has been divided into execution scenarios, such as treadmill-based or overground tasks [16]. Accordingly, the lower-limb exoskeleton could include different functionalities and approaches to interact with the clinician and the user. However, these approaches have some limitations. In this sense, populations' needs and activities lead to guidelines defined as design features for the robotic devices [17].

Design features are related to the anatomic concepts, targeted goal, mechanical structure, actuation, control strategies, and physical interfaces, as is showed in Fig. 2.1. These features are linked between each one, and they will define LLE capabilities. In this sense, this chapter describes each feature involved in an LLE. First, human-centered features relate the anatomic concepts (e.g., anthropometric measurements and joint kinematics) that are focused on hip and knee joints, and the targeted goal (e.g., therapeutical or ADL aid). Then, device-based features are explained through developments presented in the literature.

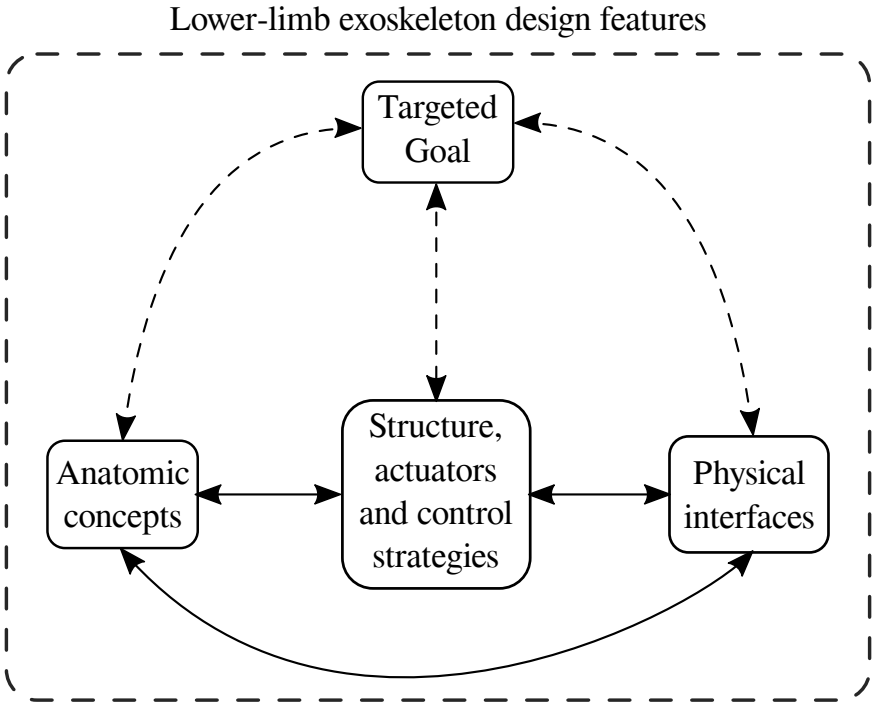

Figure 2.1: A diagram that illustrates the design features relationship.

2.1 Anatomic concepts

The targeted population delimits user features, usually remarked through gender (e.g., male or female) and age group (e.g., infant, child, adolescent, young adult, adults, and older adults) [18]. Anthropometric measurements and human joint kinematics are defined within a range or approximation that follows the gender and age group.

2.1.1 Anthropometric measurements

Anthropometric measurements are paramount for different design features for LLE, where its process is user-centered. They can be estimated using three approaches: (1) user's height, (2) cadaver studies, and (3) ergonomic information of the targeted population. The ergonomic approach has been used to determine user lower-limb measurements. These values are highly related to the targeted population' region, and they have been estimated under specific

postures (i.e., standing and sit-down) [19]. In this context, the Colombian population is considered, and Table 2.1 summarizes the main anthropometric measurements [20].

Dimensions	**Women**			
	Young adults (20-29 y.o.)	*Adults (30-39 y.o.)*	*Middle aged (40-49 y.o.)*	*Elderly (50-59 y.o.)*
Umbilical perimeter	80.8 (8.13)	85.9 (8.16)	90.3 (9.66)	91.0 (9.31)
Thigh's superior perimeter	55.0 (4.80)	56.2 (4.57)	57.8 (5.18)	55.5 (4.79)
Middle shank perimeter	33.7 (2.57)	34.1 (2.39	35.0 (2.82)	34.2 (2.62)
Knee height	48.5 (2.32)	48.4 (2.29)	48.4 (2.40)	47.8 (2.51)
Medial iliac crest height	93.4 (4.25)	92.6 (4.24)	92.1 (4.93)	91.0 (4.74)
	Men			
Umbilical perimeter	83.1 (8.04)	89.3 (8.18)	92.4 (8.59)	94.1 (8.66)
Thigh's superior perimeter	54.7 (4.90)	55.6 (4.14)	55.0 (4.54)	53.9 (4.47)
Middle shank perimeter	35.3 (2.59)	36.3 (2.38)	36.3 (2.71)	36.0 (2.58)
Knee height	52.9 (2.56)	52.4 (2.49)	52.2 (2.43)	51.7 (2.84)
Medial iliac crest height	101.6 (4.78)	100.4 (4.69)	99.7 (4.64)	98.7 (5.47)

Table 2.1: Colombian anthropometric measurements relevant for LLE, in centimeters, mean (standard deviation) [20].

2.1.2 Human joints

The anatomical composition of human joints allows different patterns of movements. It provides intricate functionalities while they collaborate independently. Most human joints' biological behavior is not straight forward due to their intrinsic geometry [21]. Besides, the constituent elements have non-linearities (i.e., mechanical properties and configuration) increasing the modeling difficulty. These anatomical elements are bones, ligaments, tendons, and muscles. Human joints often exhibit several degrees of freedom (DOF) and increased complexity [22].

To correctly interpret the motion generated by human joints, they have to be described as an approximation where a model resembles their kinematic outcome. Accurate joint modeling remarks have been addressed by 2D and 3D registration techniques such as X-ray fluoroscopy [23], [24]. On the other hand, joint dissection has been aimed at the same problem through a 3D digital electrogoniometer [25]. Although previous approaches could deliver a precise outcome, they require expensive equipment and their results are exclusive to a particular user.

Despite these limitations, joint models are useful input models as an arrangement of theoretical joints. In this sense, it could be represented as part of each joint into 1-DOF joints (e.g., revolute or prismatic) and, depending on their configuration (e.g., series or parallel), it might resemble the joint model [26]. The joint representation is widely analyzed in several devices through theoretical joints, and the arrangement of joints types and configurations are often referred to as the device's kinematic chain. Moreover, the joints' design is involved in ergonomics within the human-robot interaction [21]. Besides, this design is also used inside the control scheme build for the device [27].

The human joint and theoretical joint are also delimited by targeted activities addressed in the next section. These activities will establish principal planes of operation, together with the range of each DOF. Within this context and in this thesis's scope, the hip and knee joints will be described and highlighting their behavior during gait.

2.1.3 Human hip joint

The hip joint's general anatomy is defined between the femoral head and the acetabulum of the pelvis. Through ligaments and muscles, the human joint can perform different movements in three principal planes known as coronal, transverse, and sagittal, shown in Fig. 2.2. Moreover, the femoral head and the acetabulum are attached by capsular ligaments divided by iliofemoral, pubofmeoral, and ischiofemoral ligaments [28]. Besides, several muscle groups

are intertwined along with the hip movements, as seen in Table 2.2.

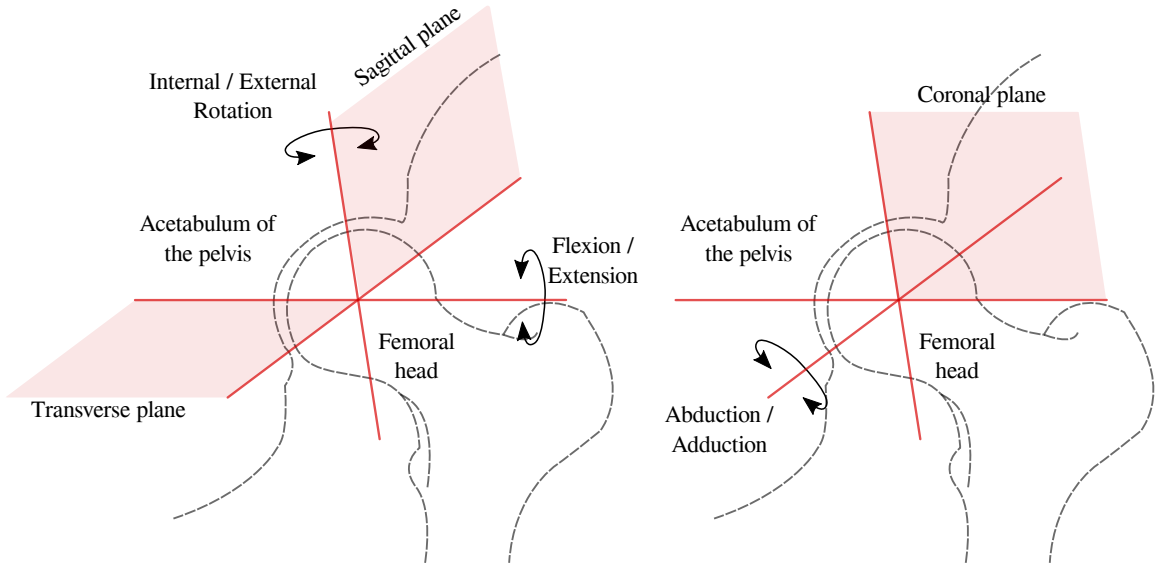

Figure 2.2: A descriptive scheme of the hip joint degrees of freedom. The scheme describes the hip joint's three principal planes of motion.

Plane	**Hip motion**	**Muscles**	**Gait ROM [deg]**
Sagittal	*Flexion*	Psoas major, iliacus pectineus, rectus femoris, and sartorius.	40
	Extension	Gluteus maximus and hamstring muscles.	
Frontal	*Abduction*	Gluteus medius, gluteus minimus, tensor fascia latae, and sartorius.	10
	Adduction	Adductor longus, brevis, magnus, gracilis, and pectineus.	
Transverse	*Internal rotation*	Tensor fascia, fibers of the gluteus medius, and minimus.	8
	External Rotation	Obturator muscles, quadrutus femoris, gemelli, gluteus maximus, sartorius, and piriformis.	

Table 2.2: Anatomical features and range of motion of the human hip joint[28], [29]. The gait ROM is presented in degrees.

The ligaments and muscles' arrangements define the maximum range of motion (ROM) for

each hip movement [29]. Under these biological limitations, targeted goals' ROM should be inside these ranges. In gait, the hip motion has been defined as a specific ROM shown in Table 2.2 [3]. Likewise, the hip motion also varies along with the gait periods known as stance and swing, which describes a full gait cycle [3]. Each DOF of the hip followed a characteristic waveform, as is presented in Fig. 2.3. Along the sagittal plane, hip extension and flexion present the higher ROM after the loading response (i.e., at 10% of gait percentage) and the end of middle swing (i.e., 87% of the gait percentage), respectively, as is shown in Fig. 2.3A. Within the coronal plane, the hip adduction occurs during the loading response and the hip abduction at the initial swing (i.e., 60% of the gait percentage) as shown in Fig. 2.3B. Finally, hip internal and external rotation have a maximum variation during the mid-swing phase (i.e., 73% of the gait percentage) as it is presented in Fig. 2.3C [30].

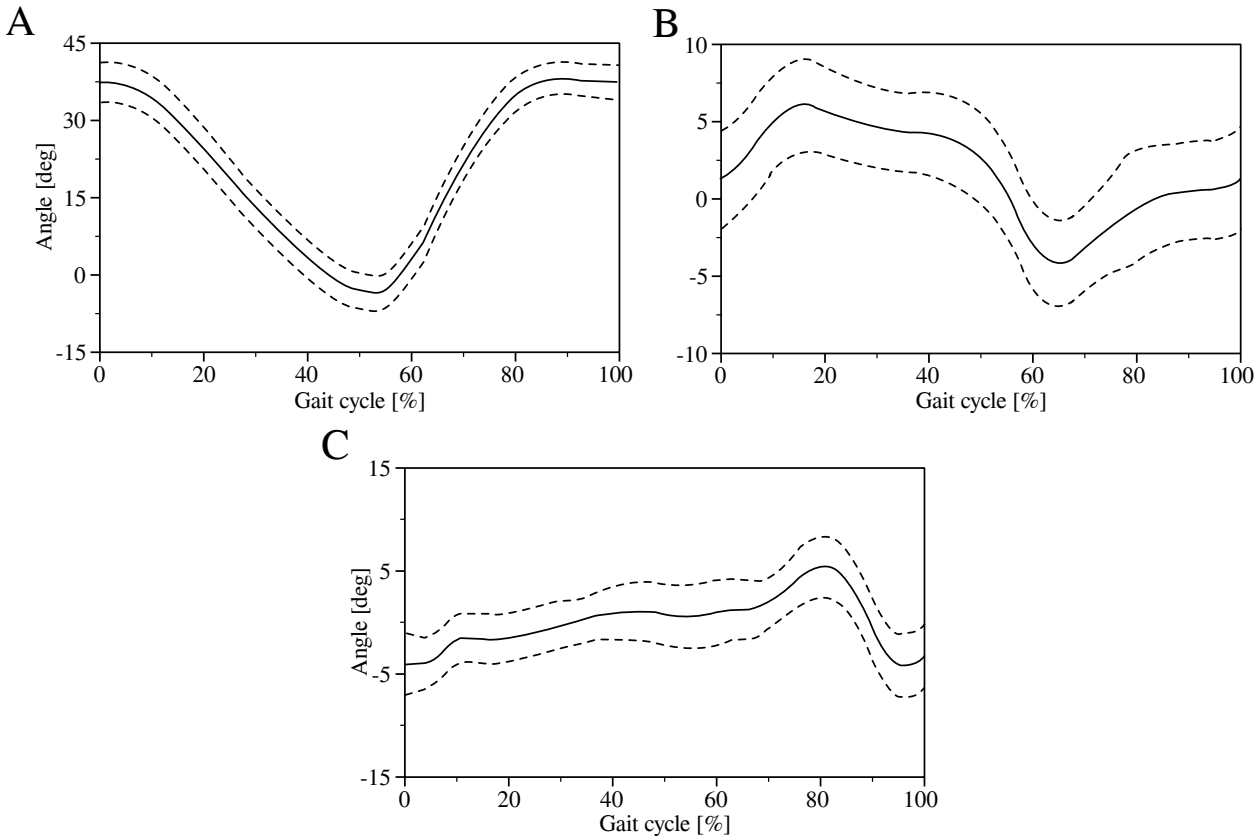

Figure 2.3: Hip angles behavior along the three principal planes of motion during gait. A. Flexion and extension motion. B. Abd/adduction motion. C. Internal and external rotation motion. Kinematic outcomes extracted from [30].

2.1.4 Human knee joint

Several approaches are introduced to understand the knee's kinematic behavior through the methodologies mentioned above. In this case, the knee is composed of the femoral condyles, the tibial plateau, and the patella. It has a joint capsule to provide strength and lubrication. It also has an intricate group of ligaments and fluids that empower the weight-bearing, such as intracapsular and extracapsular ligaments [31]. Besides, a predominant group of muscles is involved in each knee motion, as seen in Table 2.3. Each group of muscles assists during the user's tasks given biological limitations. Moreover, these motions delimited the biological knee to 4 DOF, as is shown in Fig. 2.4.

Plane	**Knee motion**	**Muscles**	**Gait ROM [deg]**
Sagittal	*Flexion*	Articularis genus, rectus femoris, vastus lateralis, vastus intermedius, and vastus medialis.	55-60
	Extension	Biceps femoris, semitendinosus, semimembranosus, gastrocnemius, plantaris, gracilis, and popliteus	
Frontal	*Abduction*	Gluteus medius and minimus, obturator externus, gemelli, and sartorius.	8
	Adduction	Adductor group of muscles.	
Transverse	*Internal rotation*	Biceps femoris.	8
	External Rotation	Semimembranosus, semitendinosus, gracilis, sartorius, and popliteus.	

Table 2.3: Anatomical features and range of motion of the human knee joint [31].

Knee kinematics might change according to the task performed by the user. For instance, knee motion during gait has a specific waveform for each plane, as is shown in Fig. 2.5 [30]. Within the sagittal plane presented in Fig. 2.5A, the knee flexion at the initial contact (i.e., 0% of the gait percentage) to the loading response. Then, the knee extends during the mid-stand (i.e., 10% to 30% of the gait percentage) and starts to flexing at the terminal

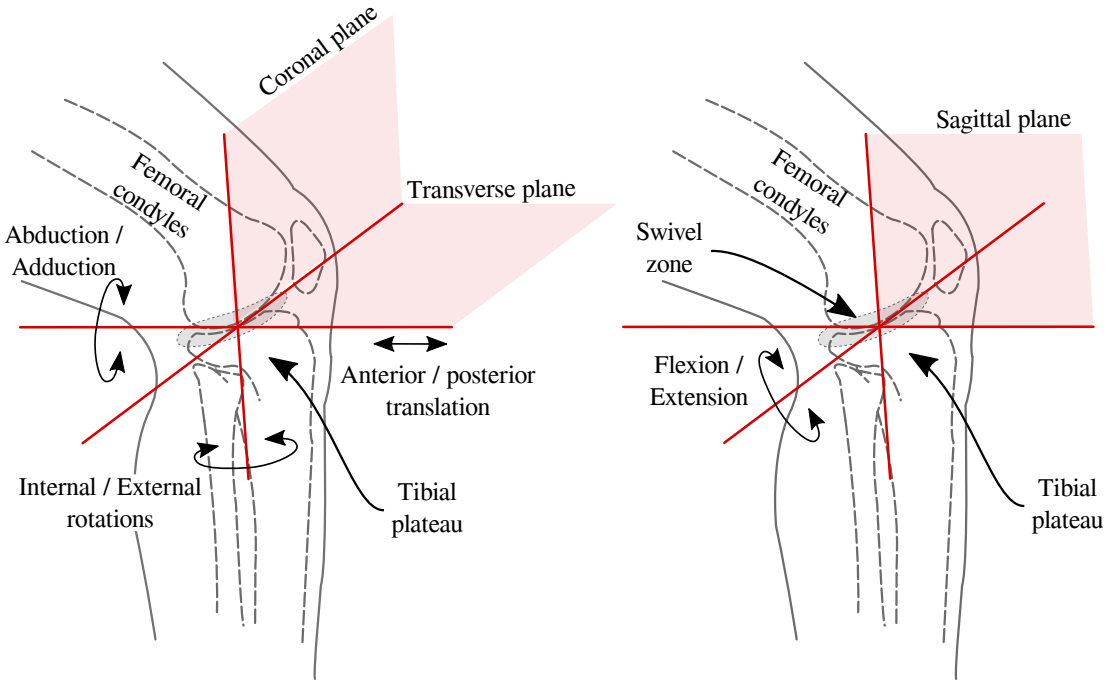

Figure 2.4: A descriptive scheme of the knee joint's degrees of freedom illustrates its principal planes of motion.

stance (i.e., 50% of the gait percentage) to the initial swing. At last, the knee extends to the end of the gait cycle [3]. Most of the knee motion within the coronal plane relies on the terminal stance and the swing period, as shown in Fig. 2.5B. Finally, the knee motion along the transverse plane varies at the initial contact and the initial swing, as is shown Fig. 2.5C [30].

2.2 Targeted goal

The primary guideline for developing an LLE, or any robotic device, is their purpose and essential objectives given by the clinicians' or the daily living activities' (ADL) requirements [32]. Each one leads to robot-assisted therapy and robotic aid for ADLs, respectively. Hence, device functionalities obey those objectives, and they could be deployed within a clinic or at the user's home.

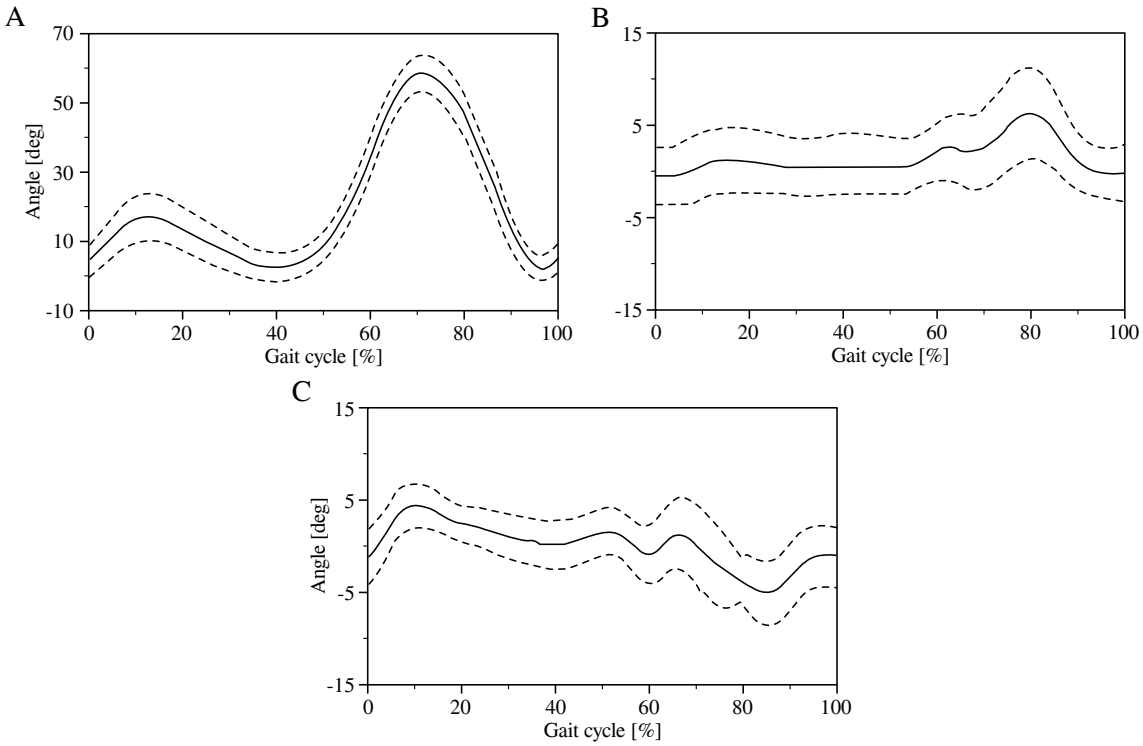

Figure 2.5: Knee angles behavior along the three principal planes of motion during gait. A. Flexion and extension motion. B. Abd/adduction motion. C. Internal and external rotation motion. Kinematic outcomes extracted from [30].

2.2.1 Robot-assisted therapy

Clinicians' needs are aimed to support the rehabilitation process of the patients. Physical therapy (PT) requires demanding training to provoke neural plasticity [8]. They are also focused on training and building muscle strength, regain healthy patterns and balance. In this scenario, the overall goal is aimed to reduce the burden of the clinicians. Simultaneously, robotic aid eases repetitive motor tasks ensuring patient recovery and reduced locomotor dysfunctions [33].

This overall goal supports multiple steps along with PT, where it defines main functionalities to improve a specific task, for instance, gait. In this sense, many gait rehabilitation systems have been deployed and designed for a clinical environment known as treadmill-based LLEs [7]. The treadmill-based LLE has a standard functionality known as body weight support

(BWS), widely used in early locomotion training. BWS has been designed to reduce the patient's weight while walking through an LLE [34]. Moreover, BWS eases the pelvis aid to mend asymmetric changes among the gait, either by passive or active setups [16], [35].

Within a clinical environment, the Lokomat has been extended along with one thousand devices within 646 facilities (Fig. 2.6A). Other treadmill-based LLEs have been developed to research proposes such as ALEX [36] or LOPES [37], as is shown Fig. 2.6B. Although another kind of LLE is deployed within this environment, treadmill-based LLEs are only applicable in clinical scenarios due to their robustness. However, they provide helpful functionalities in people who suffered a neurological injury [38].

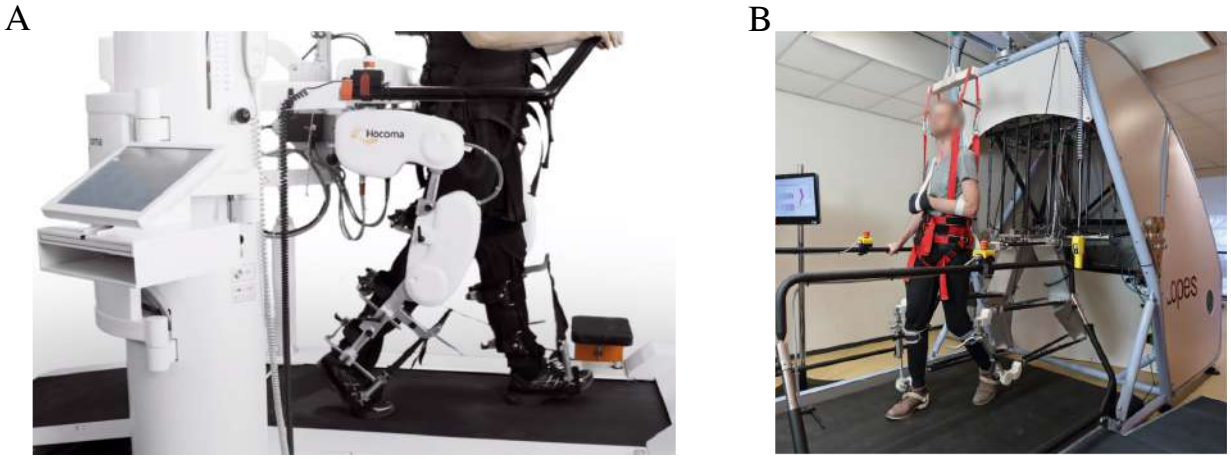

Figure 2.6: Representative examples of treadmill-based exoskeletons. A. Lokomat, Hocoma. Extracted from [39]. B. LOPES II, Roessingh rehabilitation center in Enschede, the Netherlands. Extracted from [37].

2.2.2 Robotic aid for Activities of Daily Living

Other devices have been designed to assist ADLs, which are also required by the patient, such as stand-to-sit, sit-to-stand, walking up/downstairs, among others [15]. The execution of ADLs could pursue a therapeutic objective, as mentioned before, through gait rehabilitation. Nevertheless, they also have been targeted to increase the ability to perform ADL as well as the user's quality of life (QoL) [40], [41].

Therefore, LLE's requirements are related to assistive tasks for the user's ADLs. Over-

ground LLEs have been arranged as portable devices such as Indego [42], HAL [43], and MINDWALKER [44]. These devices can be exemplified through ReWalk shown in Fig. 2.7A for home-setting [45]. Similarly, overground LLE applied for clinical proposes as H2 [46]. In particular, robotic functionalities have been mainly focused on the user's daily independence within these scenarios. These functionalities required a suitable arrangement of sensors and actuators to perform a proper aid, which will be addressed in the following section.

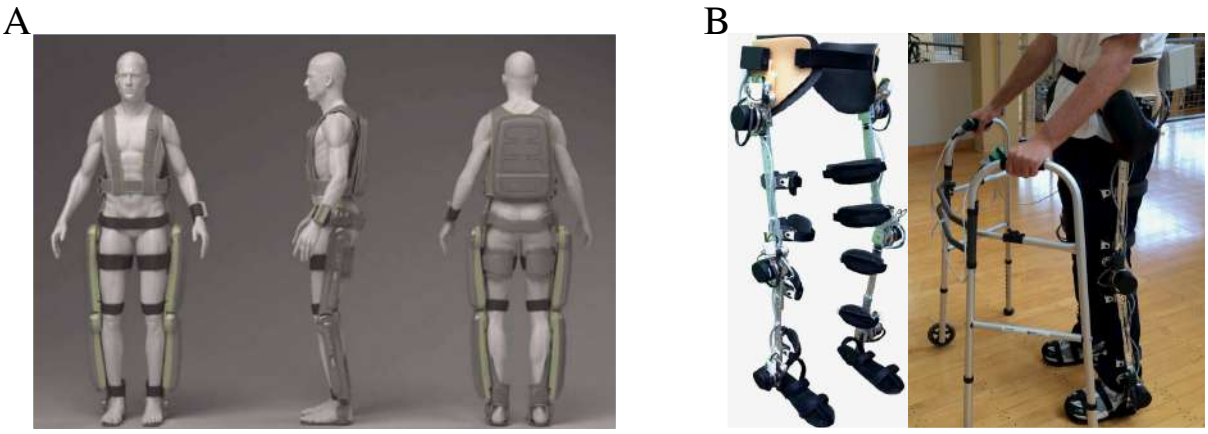

Figure 2.7: Representative examples of overground exoskeletons. A. ReWalk exoskeleton suit, extracted from [45]. B. H2 robotic exoskeleton, extracted from [46]

2.3 LLE Structure, Actuation, and Control Strategies

The LLE features are determined by the user's joints' kinematic and kinetic behavior during a targeted goal. Several approaches have been proposed to resemble human joints regarding the mechanical structure, which enhance ergonomics and comfort [13]. They have been classified as anthropomorphic and non-anthropomorphic [47]. Moreover, they have coupled actuators that provide the energy from the user's joints. These actuators obeyed different types of control strategies, which ensure proper pHRI.

2.3.1 Mechanical structure

Once the human features are analyzed, the LLE's kinematic chain's definition provides the mechanical structure's initial requirements. Regarding this information, two design approaches allow the device to follow the user's movement pattern presented in Fig. 2.8. The

most common method is the Anthropomorphic Structure (AS), in which the structure's shape follows the assisted limb by placing the actuators near the user's joints. This approach is the most commonly used in active lower-limb exoskeletons, such as HAL-3, BLEEX, and ALEX [36], [48], [49]. In contrast, Nonanthropomophic Structures (NS) differ from the human shape extending the design possibilities. Although these structures provide several mechanical advantages (i.e., back drivability, proper distribution of masses), the design process's complexity may increase [47].

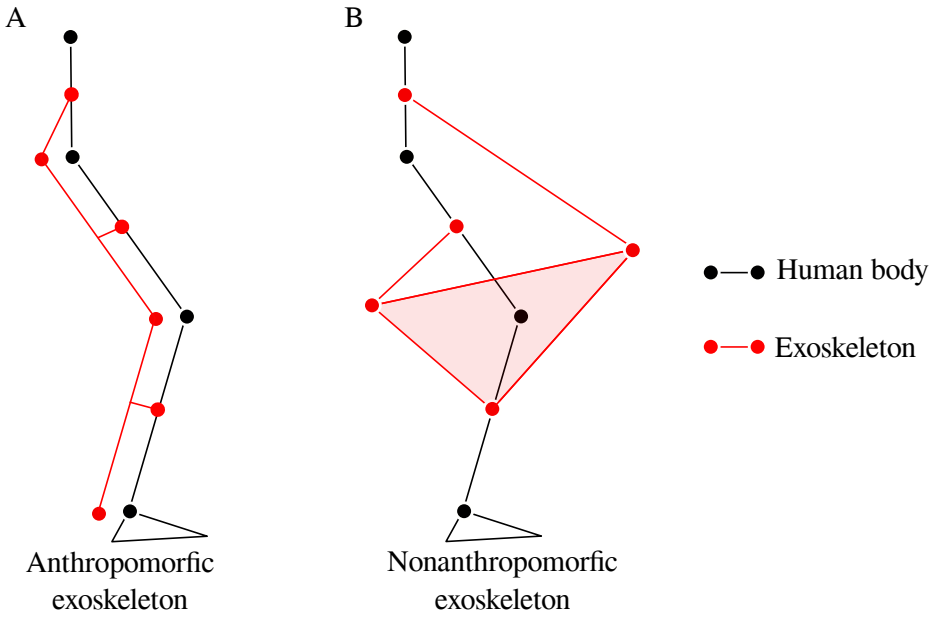

Figure 2.8: Types of the mechanical structure for lower limb exoskeletons. A. A descriptive diagram of an anthropomorphic exoskeleton. B. A descriptive diagram that presents one example of a nonanthropomorphic exoskeleton.

The exoskeleton joints have been widely addressed within the mechanical structure because of their influence on the device's kinematic compatibility. This can be achieved by mimicking or simplifying the joint structure of interest. Besides, they also follow the type of structure, either AS or NS. Furthermore, joint proposals to AS are targeted to align with the user's joints employing: (1) manual adjustment, (2) compliant mechanisms, or (3) kinematic redundancy [50]. The first scenario has been deployed in many commercial LLE such as Lokomat [38], HAL [43], ReWalk [45], and Indergo [42]. Nevertheless, their manual adjustment maybe exhaustive and requires considerable practice to reduce the time to install the device. Other

joints proposals are intended to overcome the limitations of previous devices.

Two principles are used in compliant joints considering the material's mechanical behavior and the represented linkage through the joint's geometry [51]. Regardless of their intricate design, it allows the motion in the central plane and multiple differed motions. In other words, it also has a degree of flexibility among other planes. Another joint proposal approach is the kinematic redundancy by adding DOF for the same joint through revolute or prismatic theoretical joints [52]. This can be achieved at different levels, Naf et al. proposed multiple joints in series such as three revolute joints as presented in Fig. 2.9A, two revolute joints, and one prismatic as seen in Fig. 2.9B, one revolute joint and two prismatic joints as shown in Fig. 2.9C and three prismatic joints represented in Fig. 2.9D. These solutions are aimed to enhance kinematic compatibility [21], [50].

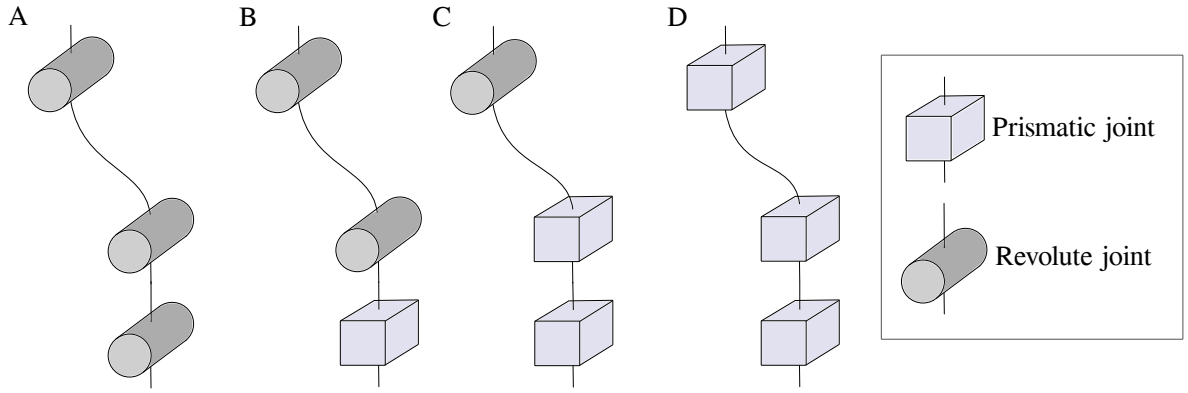

Figure 2.9: Kinematic redundancy. Proposal kinematic chains using three joints in series to enhance the kinematic compatibility. These kinematic chains could be deployed along with the structure and within the physical interfaces [50]. A. Series of three revolute joints. B. Series of two revolute joints and one prismatic joint. C. Series of one revolute joint and two prismatic joints. D. Series of three prismatic joints.

2.3.2 Actuation

The energy applied to the LLE's joints can be derived from multiple sources to generate motion and assist with the targeted goal. These energy sources delimit LLE's response features (i.e., device bandwidth, weight, power) affected by the actuator type and the relation between the supplied torque to the user device's weight [13]. Therefore, more robust or more

straightforward actuators may be suitable for different scenarios.

Three of many aspects are summarized in Table 2.4 according to six different kinds of actuators used in LLE. The first aspect presents a general configuration according to the type of actuator highlighting the main components. These components define the actuator's back drivability, which is related to the characteristic impedance; in other words, the capability of response against a contrary motion [53]. Even though this capability depends on their components' constraints, they present a common trend of whether it is back drivable. Another central aspect is the trade-off between the power and the weight. The actuators showed that electric-based actuators (e.g., series elastic actuator (SEA), variable stiffness actuator (VSA)) weigh double than hydraulic or pneumatic actuators (e.g., pneumatic artificial muscle (PAM)), defining the power/weight ratio as low for electric-based actuators, and high for hydraulic or pneumatic [54].

Type	**Configuration**	**Power/weight ratio**	**Back drivability**
Electric	Motor - Gearbox - Load	Low	No
SEA	Motor - Spring - Load	Low	Yes
VSA	Motor - Nonlinear spring - Load	Low	Yes
Pneumatic	Air source - Linear or rotatory transfer - Load	High	No
PAM	Air source - Artificial muscle - Load	High	Yes
Hydraulic	Fluid source - Linear or rotatory transfer - Load	High	No

Table 2.4: Type of actuators commonly used in LLE. The most common actuators are described according to their generalized configuration, power/weight ratio, and back drivability [54].

Several actuators have been frequently coupled in rehabilitation or assistance LLE, for instance, the motor drive (e.g., electric motor and gearbox) [55]. This actuator has been deployed in most commercial exoskeletons because of its ease of implementation, opposite

pneumatic actuators' side due to its heavyweight energy source. However, as a linear actuator, it has to be outweighed by a control strategy.

Throughout the years, novel actuators emerged in LLE applications, and they have been widely used in treadmill-based (e.g., LOPES [37], ALEX [36], [56], MINDWALKER [44]) and overground exoskeletons (e.g., Soft exosuit [57], Rex [58]). These actuators use passive elements coupled to motors (i.e., series or parallel elastic actuators, variable stiffness actuator), giving back drivability to the joint, in which they are capable of uncoupling the shaft [7]. Moreover, their kinematic and kinetic outcome can be specifically designed to joint requirements for mechanical leverage by springs or dampers configurations [59].

2.3.3 Control Strategies

Designers have comprised mechanical statements or properties (e.g., joints modeling, dynamic constraints, type of actuator) into several control strategies to achieve the targeted main goal based on the features mentioned above. These strategies are defined as high-level control strategies focusing on the user's intention [54]. In contrast to the low-level control strategies, which handle the response of the actuators directly.

The control strategies could be based on multiple signals from the user or the device to acquire the user's intention. On the one hand, electromyographic (EMG) signals have been used in single-joint LLE, selecting the principal muscle or muscle group during the task [53]. On the other side, the device has been used as an input to the control strategies through the actuators or other sensors attached to the structure [54].

Many control strategies have been intended for specific rehabilitation tasks or to improve the interaction regarding the source of the control signals. Moreover, they have been divided into two categories: (1) trajectory tracking control (TTC) and (2) assist-as-needed control (AAN) [60], [61]. The first approach was adapted from industrial robots [61]. TCC is a conventional method used in the initial stages of the rehabilitation process for gait training. This approach has developed several kinds of TTC (e.g., reference trajectory, model-based stability,

predefined motion, sensitivity magnification control strategies), which predominately guide the user to perform a specific movement [60]. However, these approaches provided a fixed amount of assistance during the tasks.

Current approaches vary the level of assistance according to the user leading to AAN control strategy, enhancing the patient's neuroplasticity within rehabilitation scenarios. To fully detect the human effort, it has been defined as compensation systems intrinsically to the device, such as friction and gravity compensation [60]. Considering these systems, one of many approaches is based on bioinspired control that addressed AAN through impedance controllers [62]. Besides, path control algorithms have been included in compliant virtual walls to amend gait patterns, which could be based on position or force fields [60].

2.4 Physical interfaces

To ensure the transmission of energy from the actuator to the user, the physical interface is the most important feature that affects the exoskeleton's performance [50]. The real progress in generating motion begins at the actuators' energy and then transferred to the mechanical structure. The physical interfaces are attached and carry the energy to human joints [63], [64]. Thus, the design and development of physical interfaces must consider the overall features to provide a suitable solution. Moreover, they have to ensure comfort and ergonomics to the user. Within this framework, diverse materials and arrangements have been deployed to secure the LLE to the user.

2.4.1 Manufacture and materials

Physical interfaces have to be comfortable along with the targeted goal. From an ergonomic perspective, critically, avoid safety hazards such as skin injuries or pressure points [65]. In this context, the interaction between the user's skin and the physical interfaces must be compliant and secure its safety against pain and lesions. Moreover, it also has to be strong enough to transfer energy as efficiently as possible. Hence, the physical interfaces' materials

are one of the main aspects to enhance the device's performance.

Many approaches include orthopedic components integrating commercial solutions for LLE's applications, as is shown in Fig. 2.10. These solutions can combine compliant materials (i.e., foams, fabrics, thermoplastics) to leverage ergonomics and comfort [66], [67]. These components embrace a broader population through an adjustable design, and they could reduce the costs of the physical interfaces. However, physical interfaces have also been tailored based on LLE's design features [13].

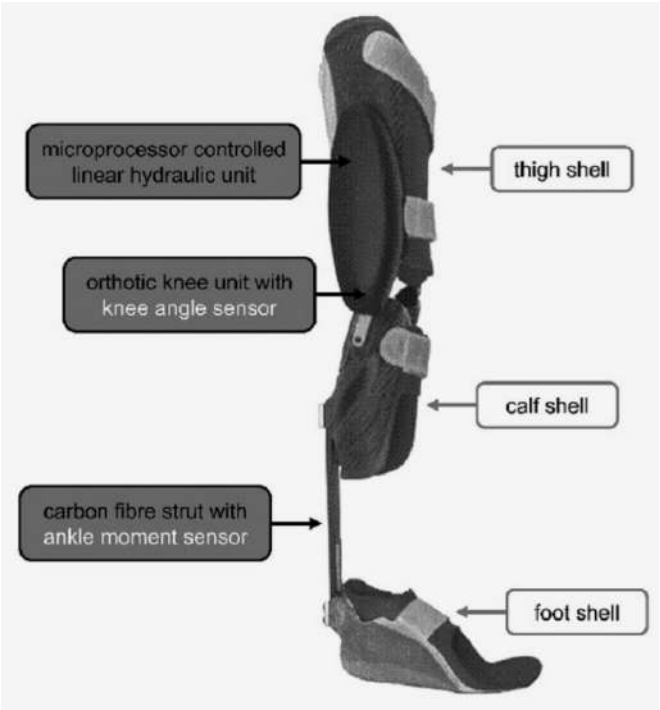

Figure 2.10: Commercial solutions for LLE. C-Brace by Ottobock from a knee-ankle-foot orthosis [68].

Most physical interfaces are designed in two sections: (1) rigid interface to transfer the actuators' energy and (2) flexible or soft interface to adapt to user limb' geometry and provide comfort. The ratio of each section depending on the material selection. For instance, the proposed exoskeleton by Asbeck et al. uses fabrics for the physical interfaces under their bowden cable actuation [57]. Hence, most of the material used in this case was mainly flexible due to the design's physical interfaces aimed to fit different users.

Another case presented a rigid physical interface predominantly for the active ankle-foot exoskeleton of Langlois et al. made of PLA and carbon fiber reinforcement, shown in Fig. 2.11B [69]. The design and development of physical interfaces were customized through 3D scanners and 3D printers technologies [13], [69], as is shown in Fig. 2.11A. These techniques are highly adaptable to different geometries, either rigid or flexible materials, though, for rigid interfaces, they have to be reinforced via carbon fiber or resins.

A

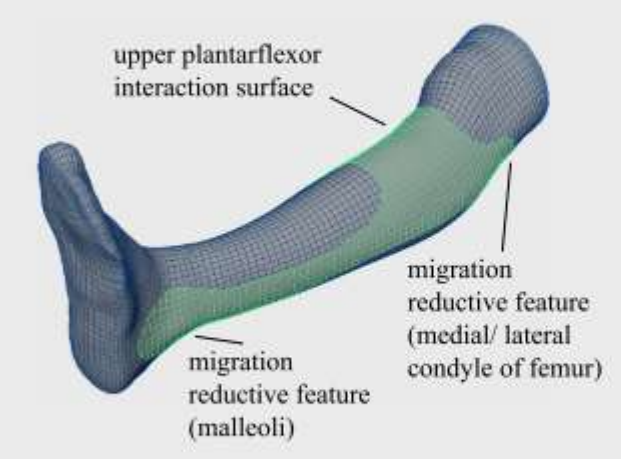

B

Figure 2.11: A customized physical interface for an ankle-foot orthosis. Extracted from [69]. A. The 3D scanner of the user's limb and CAD model for the physical interface. B. The customized physical interface to a powered ankle-foot exoskeleton.

2.4.2 Physical Interfaces' Layout and Assessment

Despite the extensive development of LLE, physical interfaces have been overlooked compared to other design features. Consequently, several layouts have been defined to the same application (e.g., number of physical interface per body segment, best material aimed at a rehabilitation or assistance task) [70]. These layouts involved an ergonomic, kinematic, and kinetic cost, affecting the device's performance.

Within the physical interface layout, the user's limb location plays an essential role in ensuring comfort. Nevertheless, a few studies have been focused on this topic [14]. The physical interfaces' assessment is divided between quantitative (i.e., kinematics or kinetics) and qualitative (i.e., QUEST or user-centered evaluation) studies. In this sense, quantitative studies have been emerged to understand the interaction between the device and the user through optoelectronic systems. These studies are presented in Table 2.5. Kinematic approaches are performed through reflective markers placed in the user and the device during a specific task (e.g., walking or sit-to-stand). Moreover, the studies are aimed to analyze the displacement or rotation along the sagittal plane of the study. However, frontal and transverse planes are omitted in the analysis and the planes' displacements or rotations. These studies could include multiple performance indicators such as, joint kinematics, interface displacements, and adaptability to different height ranges.

Author	**Device**	**Task**	**Variable**		**Plane of study**			**Outcome**	
			D	*R*	*S*	*F*	*T*	*D [mm]*	*R [deg]*
D'Elia et al. [71]	Pelvis orthosis	W	x	-	x	-	-	5.4	-
Langlois et al. [69]	Ankle-foot orthosis	W	x	-	x	-	-	3.4	-
Akiyama et al. [72]	Lower-limb exoskeleton	StS	x	x	x	-	-	58	21

Table 2.5: Kinematic studies of lower limb devices. The variables involved are one-dimensional displacement (D) and one-dimensional rotation (R). The tasks are defined as walking (W) and sit-to-stand (StS). Within the planes of study are divided into sagittal (S), frontal (F), and transverse (T). The outcomes involved the full displacement in millimeters (D) and the maximum rotation in degrees (R).

Another quantitative approach uses kinetics performance indicators to comprehend the transmission of energy along with the tasks. Within these studies, kinetic assessment is presented and summarized in Table 2.6. Each study used a sensory interface (e.g., force-sensitive resistors or six-axis force/torque sensors) to capture the forces and torques, and they are implemented in two locations: (1) inside of the physical interfaces [73], [74] and (2) between the

mechanical structure and physical interfaces [75]. Furthermore, a preliminary study analyzed the interaction forces during a knee flexion/extension movement, contrary to other studies focused on gait. In particular, the kinetic approach addressed more planes of study than kinematic studies, analyzing several performance indicators such as, global torques, global power, and ground reaction forces.

Author	**Device**	**Task**	**Variable**			**Plane of study**			**Outcome**		
			F	T	*P*	*S*	*F*	*T*	*F [N]*	*T [Nm]*	P [W]
Leal-Junior et al. [73]	Knee exoskeleton	MT	x	-	-	x	-	-	26	-	-
Rathore et al. [74]	REX	G	x	-	-	x	-	-	24	-	-
Li et al. [75]	Lower-limb exoskeleton	G	x	x	-	x	x	x	20	1.8	-
Yandell et al. [76]	Ankle-foot orthosis	G	-	-	x	x	-	-	-	-	5.4

Table 2.6: Kinetic studies of lower limb devices. The tasks are defined as movement tasks (MT) and gait (G). The variable of analysis is the force (F), torque (T) and power (P). Within the planes of study are divided into sagittal (S), frontal (F) and transverse (T).

The further kinetic analysis allows quantifying transmission losses involved during the task. The factors entailed energy losses depend on the physical interfaces' location and the number of physical interfaces per body segment [14]. For instance, the Soft Exosuit analyzed by Yandell et al. presented a power dynamics study to understand the losses within the physical interface. The analysis considered the power of the actuator compared to the ankle's power during gait. The primary outcome was the absorption of 55% by its physical interfaces [76]. However, this study has been performed using only one physical interface and overlooked the interface migration over time.

Kinematic and kinetic studies also include other sensors to enhance the understanding of kinematic compatibility during a specific task. These sensors could be added inside the device, as a wearable sensor (e.g., EMG electrodes, cuff's force sensors), or equipped externally (e.g., instrumented treadmill, force ground sensors) [72], [76]. The kinematic compatibility

assessment using one or more of these sensors afford a wide range of information from different performance indicators. The data could be also related to assessing the device's performance, understanding the HRI, and how affect the user's outcomes (i.e., spatial-temporal parameters, metabolic cost, joint kinematics).

On the other hand, qualitative studies are widely used to assess the exoskeleton focusing on the user's insight [14]. These studies provided an overall assessment of the exoskeleton in terms of comfort and ergonomic aspects, although with clinical proposes [77]. However, a recent ergonomic study has been related to the physical interface location of an LLE and the users' discomfort through multiple questionnaires and a usability test [78]. This study's outcomes of this study provided a meaningful guideline to ensure a painless and comfortable interaction that improved the design of the physical interfaces.

Reviewing the literature, the physical interfaces' kinematic assessment presented a common trend analyzing one-dimensional outcomes of the sagittal plane, as it is summarized in Table 2.5. This evidence reveals a knowledge gap among the kinematic assessment that can be extended to more planes. Contrary to the kinetic evaluation, a few studies presented a further analysis for other planes. However, this analysis was focus on forces and torques outcomes.

This work's primary goal is to assess the interaction between the user and the AGoRA-LLE. Throughout this assessment, a methodology is proposed to analyze the physical interfaces to increase the understanding of the kinematic compatibility of the lower-limb exoskeleton.

Chapter 3

AGoRA lower-limb exoskeleton

The mechatronic development of the AGoRA lower-limb exoskeleton (AGoRA-LLE) has been focused on the enhancement of the control strategies to achieve a suitable pHRI along with the gait [79], [80]. Even though control strategies have been improved, other features involved in the LLE such as joint design or physical interfaces have to be considered. Furthermore, this chapter's structure follows the guidelines previously established in chapter 2, involving the current development of the AGoRA lower-limb exoskeleton, as described in the next section and showed in Fig. 3.1.

Additionally, it also presents the design of the passive hip joint of the exoskeleton for the ab/adduction motion in the frontal plane, using variable stiffness' principle. The hip ab/adduction motion can be restricted according to the stiffness adjusted within the mechanism given a torque interaction produced by the exoskeleton joint. This interaction is simulated, enclosing several scenarios to delimit the amount of energy delivered to the user.

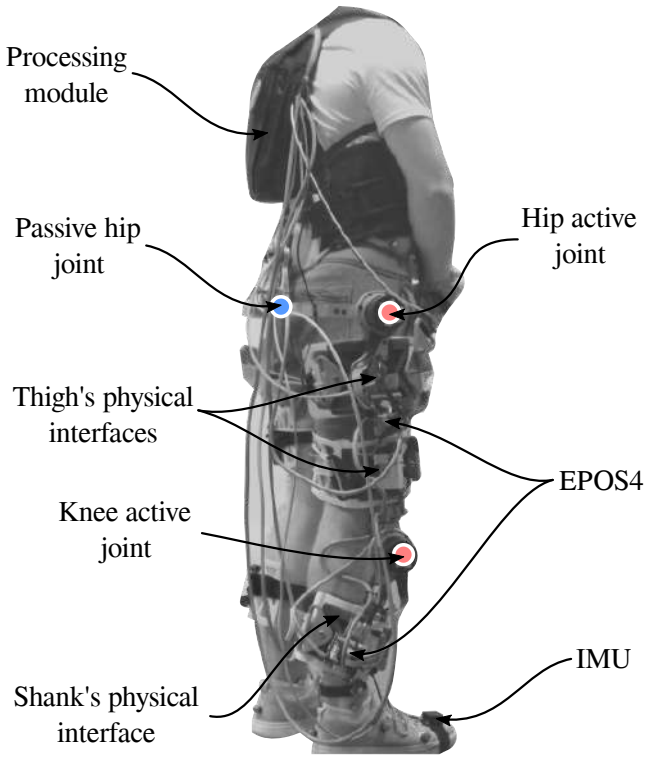

Figure 3.1: Current version of the AgoRA lower-limb exoskeleton. A illustration that describes the AGoRA lower-limb's principal features.

3.1 Design features

The development of the AGoRA-LLE can be divided into design features, as presented in chapter 2. Each feature has been aimed at multiple goals delimiting the functionalities and design's outcomes of the device. Besides, the physical interfaces' feature will be addressed in detail, presenting the improvement between versions.

3.1.1 Targeted activity and anatomic concepts

Among the development of the AGoRA-LLE, it has been established different boundaries within robotic aid. For instance, the ADLs have been limited to walking and sit-to-stand activities. Moreover, the anthropometric measurements followed Table 2.1, and exoskeleton's thigh and shank links were estimated for young adults to older people. In this sense, the

targeted population is also limited by a maximum weight of 90 Kg, and the user's height range is defined from 1.70 to 1.83 m [81].

On the other hand, the hip joint model has been considered two out of three DOF according to the boundaries shown in Fig. 2.2, specifically, the flexion/extension and the ab/adduction rotations. Furthermore, the knee joint model has been also simplified as one out of four DOF, and it was select as its main rotation, i.e., flexion/extension. In this way, human joints have been defined due to their importance during gait [22].

3.1.2 Mechanical structure and actuators

The structure of AGoRA-LLE is classified as AS, defined in chapter 2, where the mechanical structure follows the human anatomy to hold the different components of the device. This structure is made of duralumin, a lightweight and high-resistant material. Within the structure, multiple links have been designed as a variable to adjust to the user's anthropometric measurements. These links are placed between (A) the sagittal hip actuator and the frontal hip joint, (B) the backrest and the frontal hip joint, (C) the knee actuator and the shank's physical interfaces, and (D) the hip and knee actuators are shown in Fig. 3.2.

The mechatronic development of the AGoRA lower-limb exoskeleton (AGoRA-LLE) has been focused on the enhancement of the control strategies to achieve a suitable pHRI along with the gait [79], [80]. Even though control strategies have been improved, other features involved in the LLE such as joint design or physical interfaces have to be considered. Furthermore, this chapter's structure follows the guidelines previously established in chapter 2, involving the current development of the AGoRA lower-limb exoskeleton, as described in the next section.

Additionally, it also presents the design of the passive hip joint of the exoskeleton ab/adduction in the frontal plane, using variable stiffness actuation (VSA). The hip ab/adduction motion can be restricted according to the stiffness adjusted within the mechanism given a torque interaction produced by the exoskeleton joint. This interaction is simulated, enclosing several

scenarios to delimit the amount of energy delivered to the user.

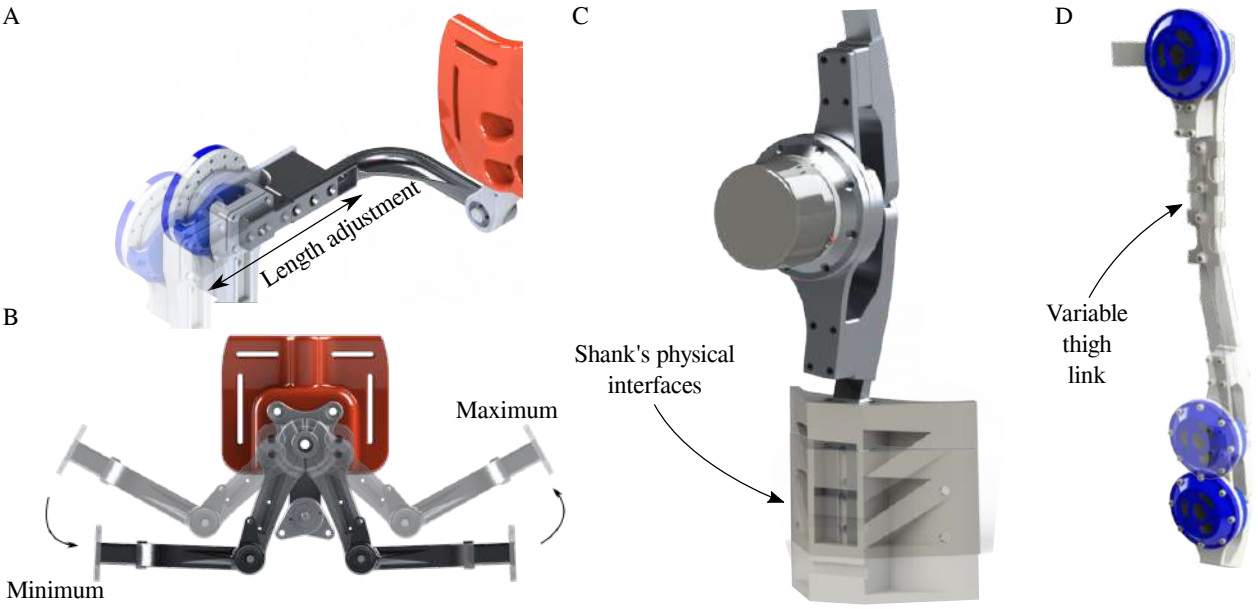

Figure 3.2: Adjustable links of the AGoRA exoskeleton. Each adjustable link is located between A. Sagittal hip actuator and the frontal hip joint. B. Backrest and the frontal hip joint. C. Knee actuator and the shank's physical interfaces. D. Hip and knee actuators.

The actuators used in the AGoRA-LLE are mainly active joints defined as motor drive actuators. They are composed of a brushless DC motor (EC-60 flat 408057, Maxon Motor AG, Switzerland) coupled with a gearbox (CSD-20-160-2AGR, Harmonic drive LLC, USA). The actuators can provide a peak torque up to 180 Nm through these components, either for the knee or hip joint in the sagittal plane. Likewise, a passive joint designed in this thesis for the frontal hip joint will be deeply addressed in the next section. The overall scheme of the active and passive joints of the AGoRA-LLE is summarized in Fig. 3.3.

3.1.3 Control scheme

The software architecture of the AGoRA-LLE is built in a Robotic Operative System (ROS) framework through a package known as *ros_ control*. This package eases the implementation and management of real-time controllers and, the monitoring of the controllers. The overall software scheme is divided into three primary levels, which are presented in Fig. 3.4. Within the high-level of the AGoRA-LLE' software architecture, the gait phase detection drives the

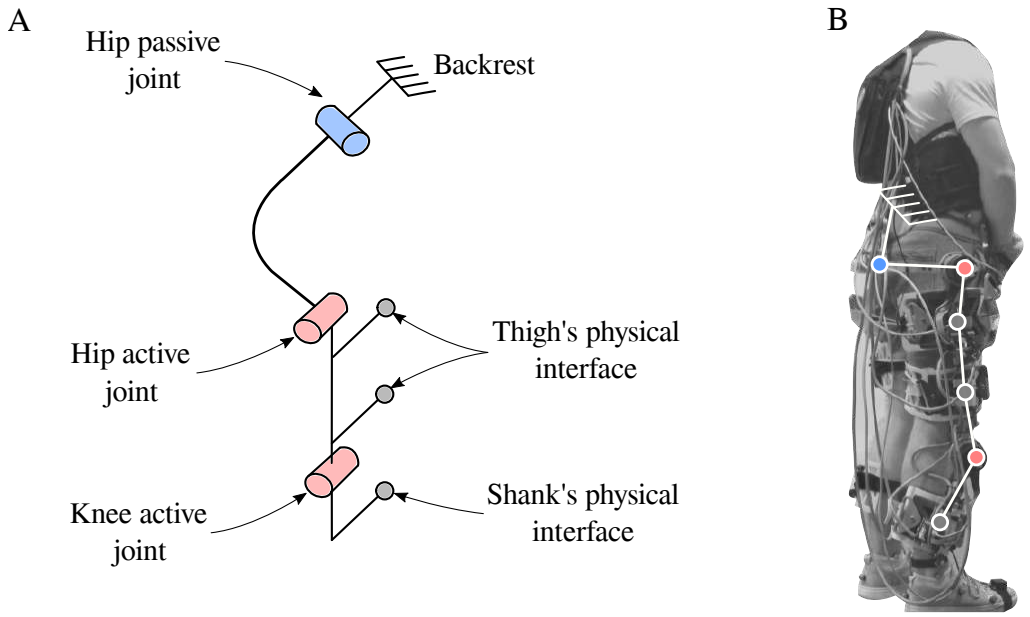

Figure 3.3: Scheme of the mechanical structure. A. A diagram of the kinematic chain illustrating the active and passive joints, the physical interfaces, and the backrest as the exoskeleton's ground. B. Representative kinematic chain on the user.

exoskeleton guided by different controllers [79]. Moreover, the exoskeleton has transparent and assistance mode based on admittance and impedance controllers, respectively.

The middle-level control compresses key models and considerations regarding the device and the actuators to achieve the these controllers' proper performance. Kinematic and kinetic models are deployed to understand and compensate inherent to the exoskeleton. Initially, the AGoRA-LLE is defined by the Denavit-Hartenber parameters according to the kinematic chain, is shown in Fig. 3.3. The friction within the motor and gearbox and the device's weight must be adjusted through kinetic compensation systems [80].

Subsequently, the low-level control gathers specific controllers that directly handle the actuator, such as velocity and torque controllers. These controllers communicate with the EPOS4 driver and manage motor directly. As shown in Fig. 3.4, within the low-level control there are sensory interfaces that allow bidirectional communication between the actuator and the controllers. Additionally, the sensory interfaces are also implemented between each control level to monitor and manage the overall device's response.

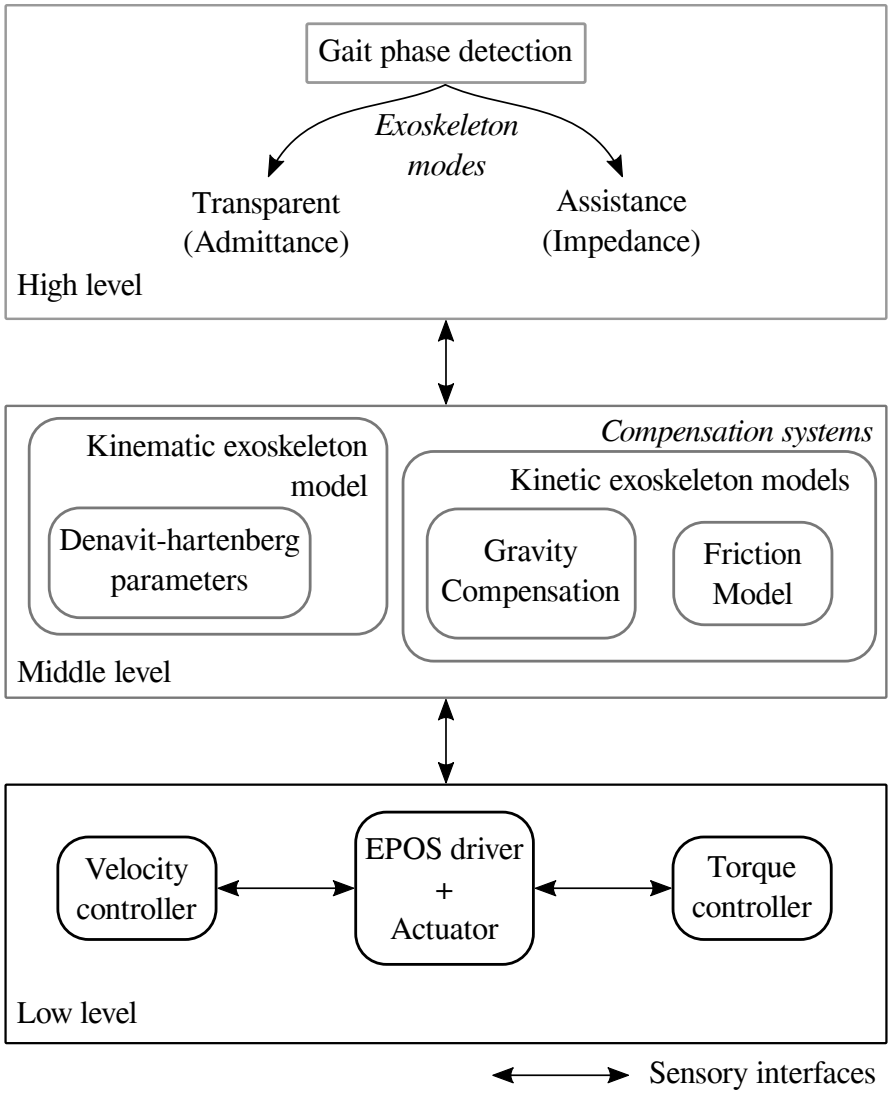

Figure 3.4: The overall control scheme of the AGoRA lower-limb exoskeleton.

3.1.4 Physical interfaces

The development of the AGoRA-LLE's physical interfaces is divided into two design approaches: (1) overlapped design and (2) embedded design. The first approach leads to a prototype shown in Fig. 3.5. The overlapped version is designed to match the structure geometry and resemble a part of the limb's using a rigid 3D printed part. A fabric and fastener are connected to the rigid 3D printed part which fully adapts to the remaining limb's geometry. However, the preliminary experimental test showed that the physical interfaces

were shifted due to the vibration produced by the task's motion. As a consequence, the fasteners were loosened during the gait. The rigid parts were uncomfortable to the user creating pressure points either in the shank or thigh links.

Figure 3.5: AGoRA-LLE's physical interfaces first version. An overlapped version of physical interfaces made of 3D printed Nylon, fabric, and fastener.

To overcome these issues, the physical interfaces' design is aimed to embed into the structure is presented to assembly the physical interfaces inside the exoskeleton's mechanical structure, as shown Fig. 3.6. Moreover, they are split into two sides: a rigid side to ensure the mechanical structure's location and a flexible side to adapt ergonomically to the user's limb. The rigid side is made of 3D printed polylactid acid with Particulate Carbon fiber (PLA-PC) and the flexible side is made of 3D printed thermoplastic polyurethane (TPU). This flexible side is also attached to a flexible fabric that adjust the TPU part to the user's limb.

The version's improvements ensure the physical interfaces' location and avoid the vibrations seen in the previous version, as shown in Fig. 3.7. Moreover, the embedded version's surface area increased to ease the energy transmission without pressure points that affect the comfort. This version's assessment will be presented regarding a relative motion approach in the next chapter.

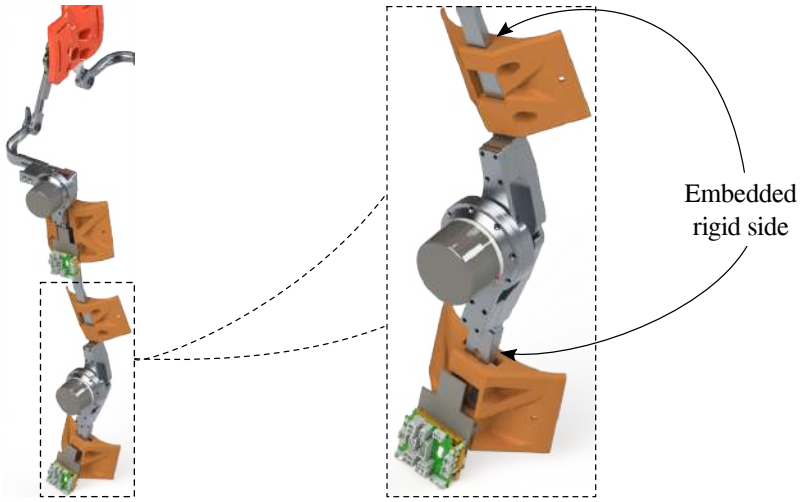

Figure 3.6: AGoRA physical interfaces' CAD design. The mechanical structure's assembly shows the physical interfaces embedded on the exoskeleton's links.

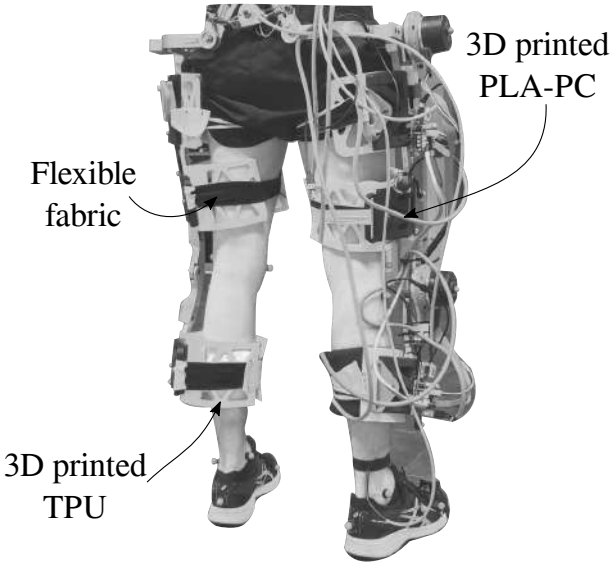

Figure 3.7: AGoRA-LLE's physical interfaces second version. The embedded version of physical interfaces are made of PLA-PC, TPU and flexible velcro.

3.2 Passive frontal hip joint

Most of the LLE's joints include several planes of motion (i.e., sagittal or coronal plane) to perform a ADLs [7], [16]. These joints can be designed as active joints including actuators, or passive joints, using spring and dampers elements. Both of these joints should allow complaint interaction [53]. Nevertheless, active joints need heavier actuators and robust algorithms to

perform a proper interaction, as presented in previous chapters. Hence, passive joints can be a suitable solution for secondary planes of motion, and enhance the HRI.

The passive joints are used to decoupling an undesired DOF by adding adjacent to exoskeleton's joints to improve the user's interaction [71]. They are also implemented as self-aligning mechanisms to ease the joint's alignment during the task [82]. Moreover, passive joints could be designed through complaint elements or include passive elements (e.g., springs or dampers) to transmit forces to the user [50]. Therefore, the passive joints constitute a key role within an exoskeleton, providing several benefits to the user.

The proposed passive hip joint is aimed to provide support along the frontal plane. The joint's design followed the human joint feature, which considered the ROM of the user's hip joint along the frontal plane. This joint combines three main design principles: variable stiffness's principle (VSP), four-bar mechanism, and bio-inspired tendons. Each one plays a role during the passive interaction between the user and the exoskeleton, providing an adjustable system to satisfy users' needs. Following these principles, the interaction torque is estimated through mathematical modeling to understand and quantify the energy and support deployed to the user.

3.2.1 Four-bar mechanism

Links arrangement has been addressed since the 13th century, which allowed technological development in multiple scopes [83]. Moreover, they have been used to transform wind or water energy as source power. Their arrangement belonged to the simplest mechanisms, such as the four-bar mechanism. In particular, during the 19th century, Pointsot, Willis, Reuleaux, and Chasles accomplished several breakthroughs, which gave the foundations to understand four-bar mechanisms [83]. In parallel, the overall progress also considered the kinetic analysis through the law of conservation of energy or Newton's laws [84].

Over the years, four-bar mechanisms have been specified by the boundaries conditions of the implementation. These boundaries conditions involved the type of links (i.e., binary, tertiary, quaternary) and mobile or fixed joints (i.e., prismatic or revolute joint). The most common mechanism is known as double-rocker, presented in Fig. 3.8A, crank-rocker mechanism, shown in Fig. 3.8B, and crank-slider, shown in Fig. 3.8C. Within these scenarios, the double rocker mechanism is one part of the VSP is designed to transfer the energy to the user.

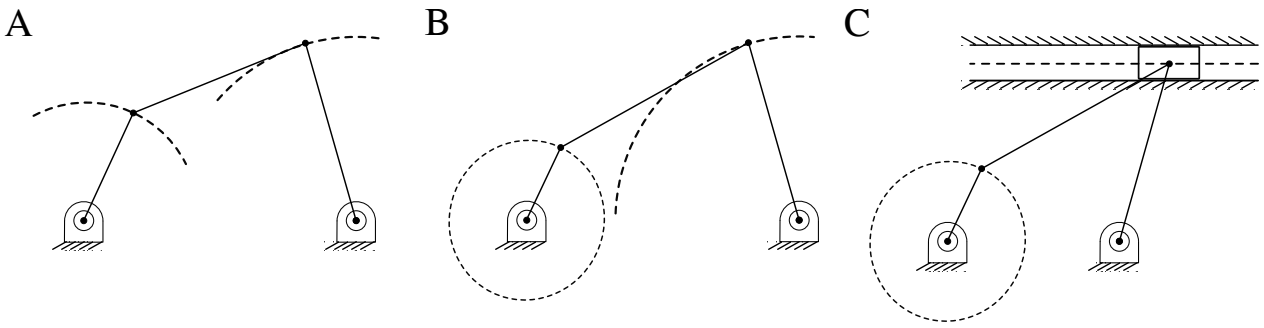

Figure 3.8: Basic configurations of the four-bar mechanism. A. Double rocker mechanism. B. Crank-rocker mechanism. C. Crank-slider mechanism.

Two double-rocker mechanisms are merged on the backside of the AGoRA-LLE. Each mechanism is configured per side, as it is shown in Fig. 3.9. Focused on the right side of the exoskeleton, one of the rocker links directly interacts with the user's leg and it pivots in O_2. Moreover, the opposite rocker pivoted in O_4 is loaded with the bio-inspired tendons' external forces.

3.2.2 Bio-inspired tendons

The passive elements involved in the VSP were designed to resemble the stiffness of a human tendon as a spring-like component. It was accomplished by a braided material formed by (1) elastic filament (Filaflex, 2.85mm, Recreus, Spain) and (2) fishing rod (eight filaments, Sufix 832, USA). These filaments were intertwined following a volumetric fraction of 14% to accomplish a variable stiffness performance regarding the elongation. To assess this configuration, a tensile test was carried out through a universal machine, fixing a specimen between two jaws, as shown Fig. 3.10. Besides, the tensile tests followed the ASTM C1557-14 [85].

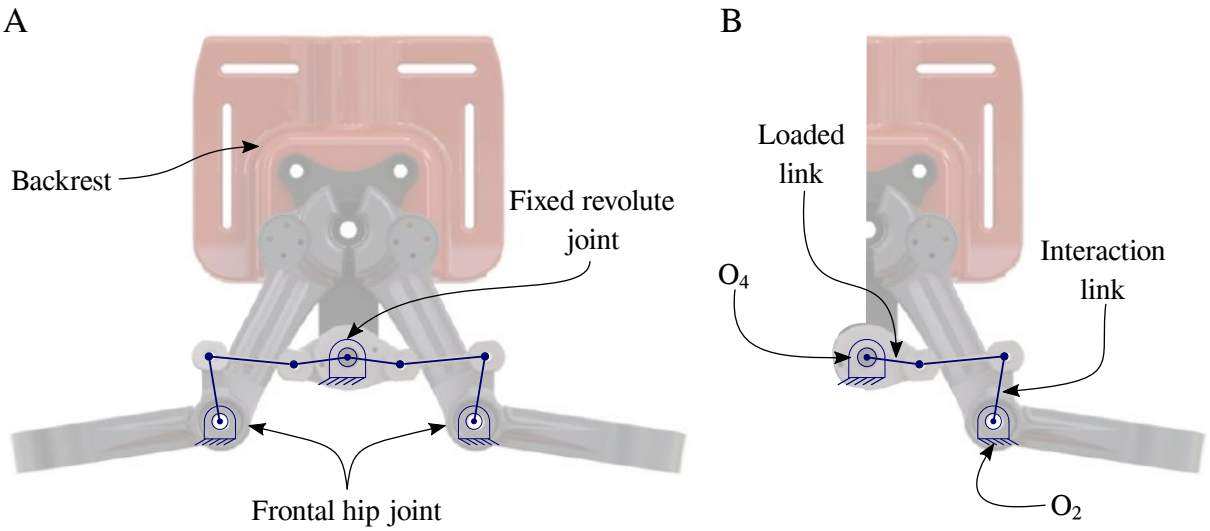

Figure 3.9: Description of the passive frontal hip joint. A. Global overview of the passive frontal hip joint for both sides. B. Right side description of the mechanism detailing the loaded and interaction links.

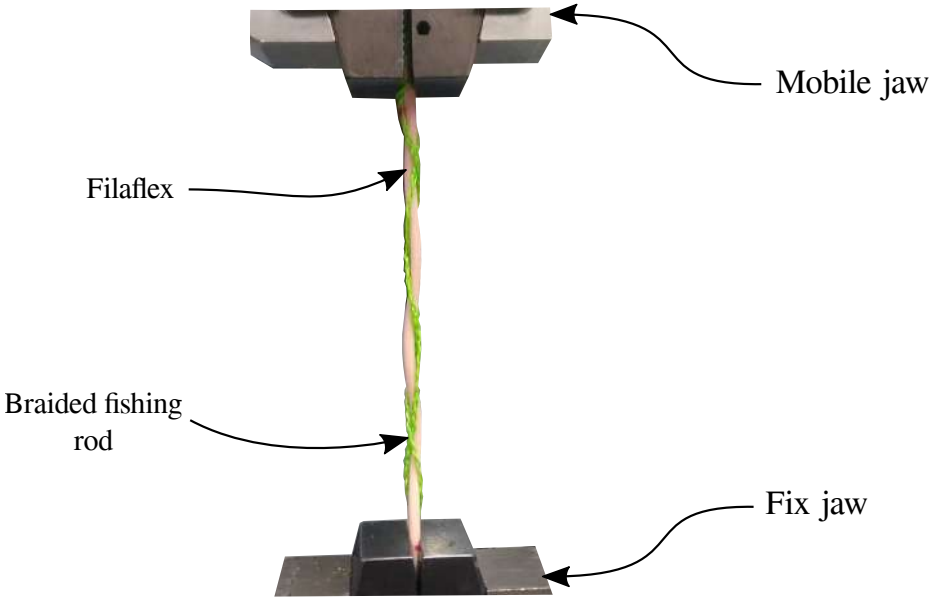

Figure 3.10: Tensile test experimental setup.

Stress-strain results are used to estimate two elastic zones and their Young's modulus as is shown in Fig. 3.11.A range of strain defines each zone: zone A between 0 to 0.10 mm/mm and zone B between 0.1 to 0.15 mm/mm. Nevertheless, zone C presented inconsistent stress values and rupture point. However, this last zone is not taken into account in the analysis because the bio-inspired tendons will be loaded with forces smaller than the required for the

rupture point.

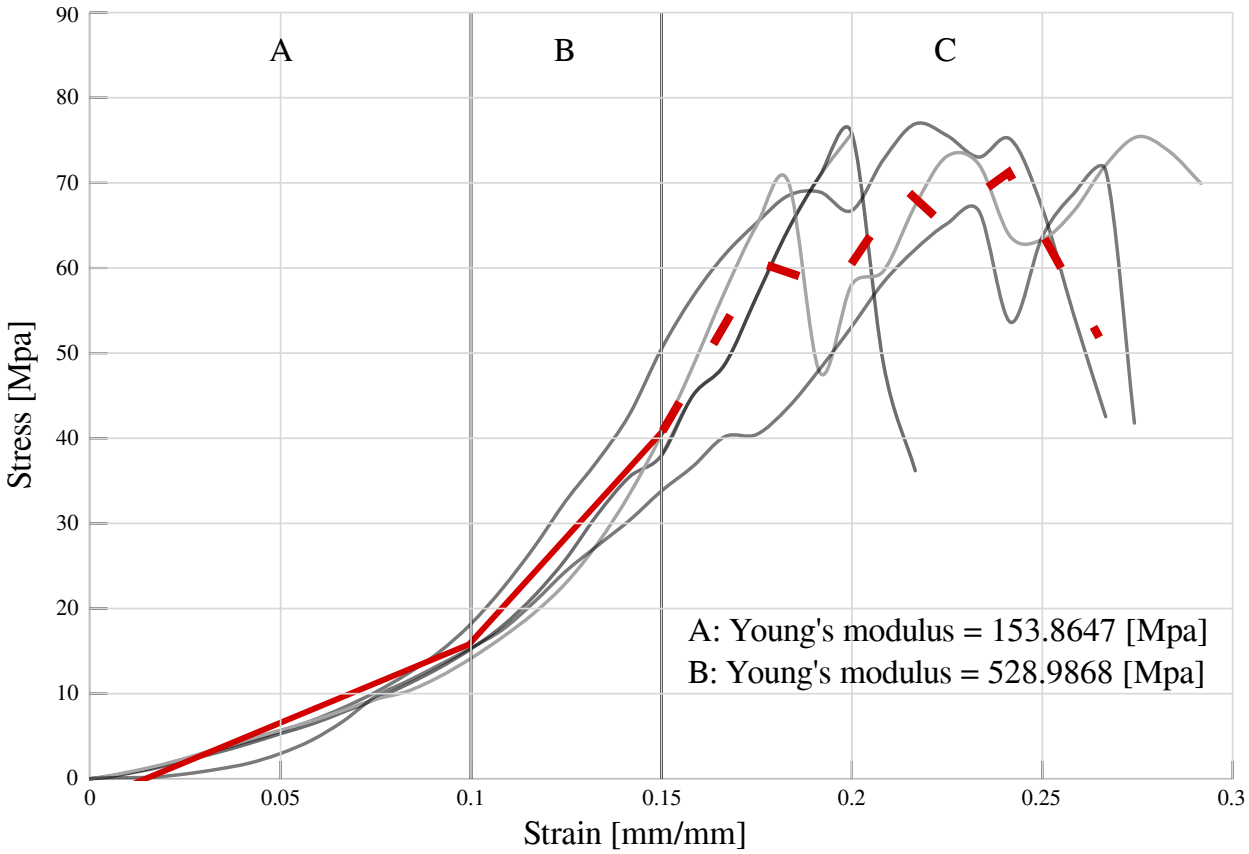

Figure 3.11: Tensile results of the bio-inspired tendons. The stress-strain curve presents the Young's modulus for the A and B zone.

3.2.3 Variable stiffness principle

The variable stiffness principle (VSP) has been defined within the passive compliant actuators, it allows an active impedance control, inherent compliance or inherent damping [59]. Regarding the passive actuators based on inherent compliance, they have intrinsic compliant elements that provide a fixed or variable stiffness due to their mechanical properties. According to these mechanical properties, they are divided into two categories: (1) Series Elastic Actuator (SEA) and (2) Variable Stiffness Actuator (VSA) [59]. However, the VSP could be delimited into many configurations regarding the mechanical interlink and the passive components (i.e., spring or damper). In this sense, the proposed passive joint is defined as a four-bar mechanism and a spring-like element previously described.

3.2.4 Mathematical modeling

The theoretical framework employed the design principles aforementioned, given the overall layout of the passive frontal hip joint divided into the details of the variables shown in Fig. 3.12A and the points' coordinates regarding the global frame O_2 as seen in Fig. 3.12B. As was presented in Fig. 3.2B, frontal adjustment can affect the passive hip joint's the initial parameters. For this reason, the frontal adjustment was configured at the minimum range. Therefore, the links' length, initial parameters, and links features are defined in Table 3.1.

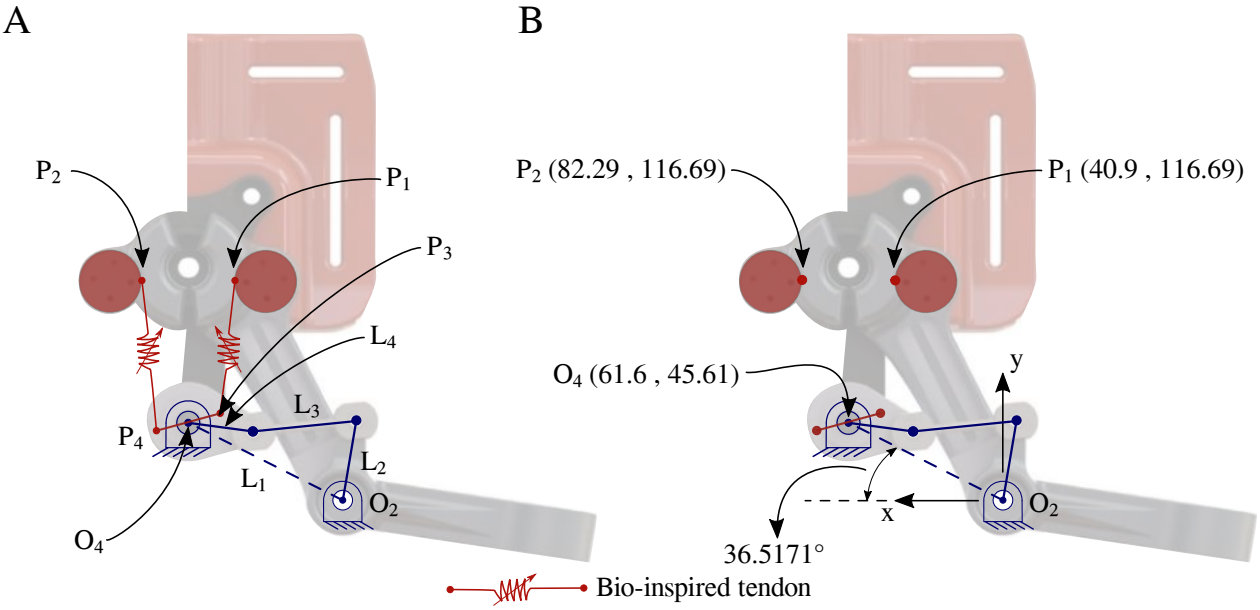

Figure 3.12: Scheme of the passive frontal hip joint. A. Details of variables and boundaries are taken into account to understand the torque of interaction generated by the passive joint. B. The main referenced points show their coordinates regarding the global frame in O_2. Units in millimeters.

	Length [m]	**Weight [kg]**	**Inertia [kgm^2]**	**Angular velocity [rad/s]**	**Angular accel. [rad/s^2]**
L_1	76.65e-3	-	-	-	-
L_2	40.00e-3	26.31e-3	1.00e-1	0	0
L_3	65.02e-3	140.0e-3	1.00e-1	-	-
L_4	31.00e-3	26.31e-3	1.00e-1	-	-

Table 3.1: Initial parameters and features for each link of the double rocker mechanism.

The bio-inspired tendons are attached between the P_1 to P_3 and P_2 to P_4. Besides, the points P_1 to P_2 are fixed in the structure, and the points P_3 to P_4 pivot in O_4. Moreover, the double

rocker mechanism has external forces applied in P_3 and P_4 affecting only L_4. The global frame system is located in O_2 which refers to the fixture points P_1 and $P2$, and the pivot O_4 coordinates, which are also referenced to O_2. According to the global frame system, the L_2 ROM is defined as 20° bisected by the global frame's Y-axis. This ROM is due to the human hip motion along the frontal plane of ab/adduction.

To ease the passive hip joint modeling, the global frame is rotated $\alpha = 36.5171°$, aligning the L_1 to the X-axis, as is shown in Fig. 3.13A. This rotation allows us to analyze the double rocker mechanism as a classic approach. Moreover, the interest points (e.g. O_4, P_1, P_2) are also rotated using a two-dimensional rotation matrix ($\mathbf{R}$), as is shown in Eq. 3.1. Following these adjustments, the double rocker mechanism involved in the passive hip joint is summarized, as is shown in Fig. 3.13B.

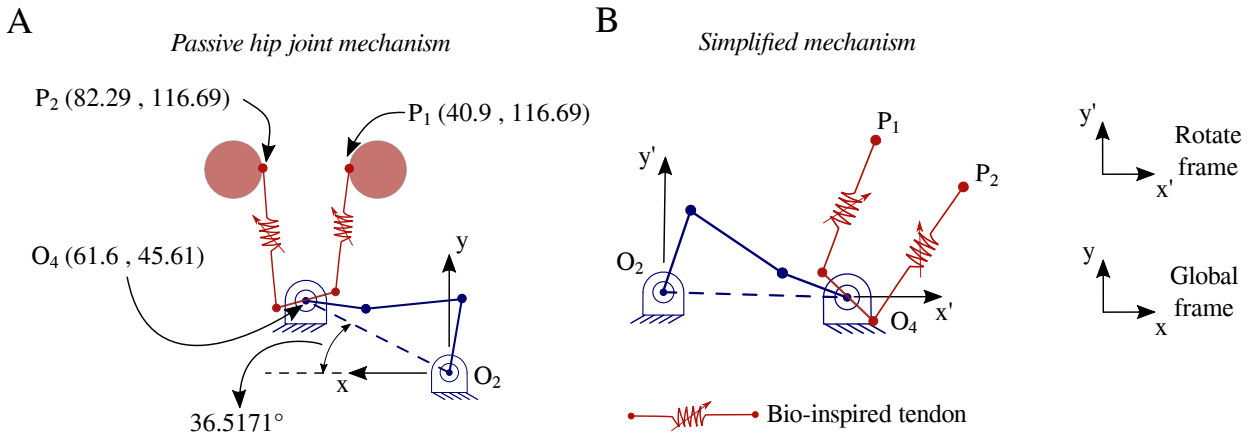

Figure 3.13: General scheme of the four-bar mechanism. A. The passive hip joint mechanism's summarize scheme is adjusted to ease the mathematical modeling. B. Simplified mechanism according to the frame's rotation.

$$\mathbf{R} = \begin{bmatrix} cos\alpha & -sin\alpha \\ sin\alpha & cos\alpha \end{bmatrix} \tag{3.1}$$

3.2.5 Kinematic modeling

Based on the boundary conditions of the double rocker mechanism, the position of each link has to be defined using the baseline angles which provide the orientation of the links (i.e., θ_3 related L_3, and θ_4 related L_4) regarding the input variables (i.e., links' length, θ_2, $\dot{\theta}_2$, and $\ddot{\theta}_2$).

To determine links position, a vector loop is employed using the links as vectors represented in Eq. 3.2 and shown in Fig. 3.14. These vectors are defined using complex numbers in a polar representation (e.g., $r\exp(j\theta)$) as is seen in Eq. 3.3. They are also extended by the Euler's identity (i.e., $\exp \pm j\theta = cos\theta \pm jsin\theta$), as is shown in Eq. 3.4.

$$\mathbf{R}_2 + \mathbf{R}_3 - \mathbf{R}_4 - \mathbf{R}_1 = 0 \tag{3.2}$$

$$a\exp(j\theta_2) + b\exp(j\theta_3) - c\exp(j\theta_4) - d\exp(j\theta_1) = 0 \tag{3.3}$$

$$a(cos\theta_2 + jsin\theta_2) + b(cos\theta_3 + jsin\theta_3) - c(cos\theta_4 + jsin\theta_4) - d(cos\theta_1 + jsin\theta_1) = 0 \tag{3.4}$$

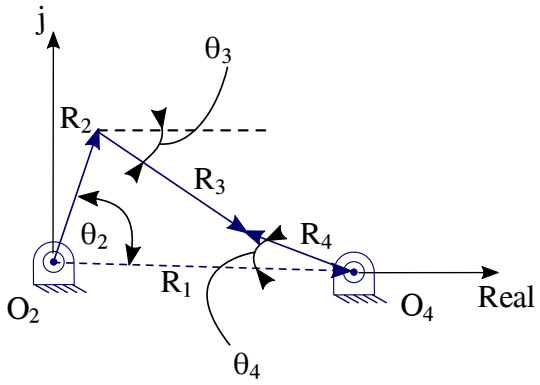

Figure 3.14: Kinematic scheme of the simplified mechanism. The four-bar mechanism is represented through the vector loop approach and defined each links' angle.

The equations' system is divided into real and imaginary equations to solve the unknown angles (i.e., θ_3 and θ_4) in terms of θ_2, a, b, c and d. The solution for each unknown angle is defined in Norton et al. by several constants for an overall formula presented in Appendix A.1.

3.2.6 Kinetic modeling

Following the initial boundary conditions and the kinematic outcome, the kinetic analysis is addressed by Newton's laws for each link defining the sum of all forces (F) and torques (τ) by Eq. 3.5 and Eq. 3.6, respectively. Both definitions could be expressed by a linear system of equations such as $A \cdot x = B$. Specifically, matrix A defines the geometrical features

of the mechanism. The column vector x gather the unknown variables related to internal forces and torques between the links and the vector column B store the dynamic equilibrium and external forces. Moreover, the centroid of the mass is placed in the middle of each link. The kinetic analysis presents the internal and external forces and the resulting acceleration of each link shown in Fig. 3.15. As a result of the links' small mass and inertia, the links' weight is not considered in the kinetic modeling.

$$\sum \overrightarrow{F} = m \cdot \overrightarrow{a} \tag{3.5}$$

$$\sum \tau = I\alpha \tag{3.6}$$

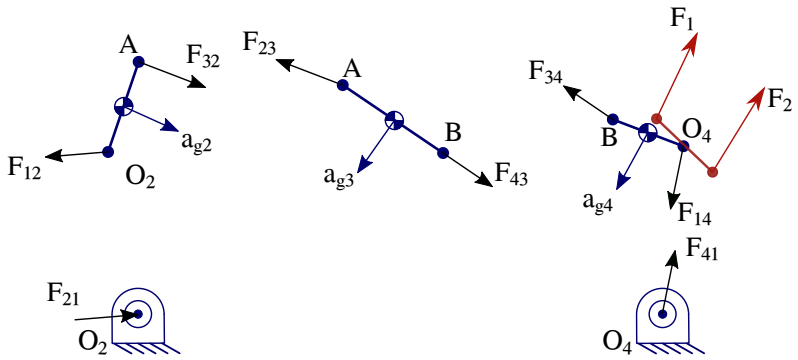

Figure 3.15: Kinetic scheme of the simplified mechanism. The links' free body diagram is presented summarizing the internal and external forces.

The external forces involve the position of the fixation points (i.e., P_3 and P_4) and the mechanical behavior of the bio-inspired tendons. The fixation points' location depends on the angle θ_4, as is shown in Fig. 3.16, the links red and blue belongs to the same body. Moreover, the tendon's force depends on the strain (i.e., ϵ_1 or ϵ_2) resulting from the motion of link 4. This strain of each tendon relies on two lengths: (1) the initial length (l_{ini}) calculated between the P_1 to P_3 or P_2 to P_4 and (2) the current length ($l_\bullet$) between the P_1 to P_3 or P_2 to P_4 according to the variation of θ_4. The strain is also used to estimate the tendon's force defining each Young's modulus, according to Fig. 3.11. Finally, the cross area ($a = 6.379mm^2$) of the tendons is constant along with the tendons. These considerations to calculate the external forces are summarized in Appendix A.2.

The kinetic analysis summary is presented as a system of equations of the passive frontal hip joint shown in Appendix A.3. The system of equations defines the sum of all forces and torques for each link. The $A \cdot x = B$ system is solved by multiplying the inverse of A (A^{-1}) in both sides of the equation given $x = A^{-1}B$. Within the vector, $\mathbf{x}$ relies on the main output of the model, the torque of interaction.

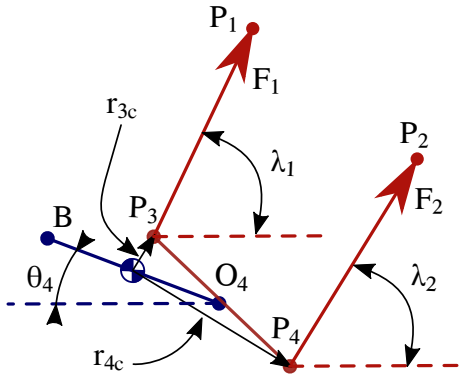

Figure 3.16: Kinetic scheme of the external forces applied to link 4.

3.2.7 Matlab simulation

Kinematic and kinetic modeling are solved within the hip ab/adduction ROM (i.e., 20°) to understand the passive frontal hip joint interaction. Algorithm 1 presents the pseudo-code implemented in *Matlab R2018b* to quantify the torque interaction (i.e., τ_2). Three main functions are employed to estimate τ_2 divided into (1) *kinematic*, (2) *external forces*, and (3) *kinetic*. According to the main parameters of the four-bar mechanism, τ_2 is estimated in different scenarios as a result of the variable stiffness configuration. These scenarios are delimited by the initial elongation, which can be adjusted in P_1 and P_2.

Within these scenarios, the *kinematic* function uses the equations showed in Appendix A.1 to estimate the unknown angles. The *external forces* function calculates the current tendons' force, considering the initial elongation and the θ_4 that involves the tendons' fixation points. Finally, the *kinetic* function gives the main output defined as the interaction torque using the kinematic and the external forces as an input.

Algorithm 1 Kinematic and kinetic solution's pseudo-algorithm.

$mech \leftarrow L_1, L_2, \theta_2, \dot{\theta}_2, \ddot{\theta}_2, L_3, L_4$ ▷ Parameters of the mechanism shown in Table 3.1.
$ROM \leftarrow 20°$ ▷ Hip ab/adduction range of motion.
$np \leftarrow 200$ ▷ Number of divisions within the ROM.
for $i \leftarrow 0$ **to** 0.15 **do** ▷ Initial elongation. Steps of 0.1.
    for $j \leftarrow 0$ **to** np **do** ▷ Steps of 1.
        $\theta_3, \dot{\theta}_3, \ddot{\theta}_3, \theta_4, \dot{\theta}_4, \ddot{\theta}_4 \leftarrow$ KINEMATIC$(mech, \theta_2, ROM, j)$ ▷ Appendix A.1
        $F_1, F_2 \leftarrow$ EXT. FORCES(θ_4, i) ▷ Appendix A.2
        $\tau_2 \leftarrow$ KINETIC$(F_1, F_2, \theta_3, \dot{\theta}_3, \ddot{\theta}_3, \theta_4, \dot{\theta}_4, \ddot{\theta}_4)$ ▷ Appendix A.3
        $\theta_2 \leftarrow \theta_2 + j \cdot (ROM/np)$
    return τ_2 ▷ Store each τ_2 per i

3.3 Results

The interaction torque is presented through fourteen scenarios as a result of the variable stiffness configuration Fig. 3.17. According to the tendon's stiffness, these scenarios are gathered into two groups (1) ten curves preloaded between 0 N to 88.3 N and (2) 4 curves preloaded between 371.1 N to 472.43 N. These configurations preloads are estimated using the mechanical properties of the bio-inspired tendon, as presented in Appendix A.2. The first group represents the lower stiffness of the bio-inspired tendon which the interaction torque slightly changes at lower preload. In contrast to the second group, the torque interaction increase given the preload magnitude, as well as the torque variation of 4 N.

Further analysis of these results provides the rotational stiffness for each preloaded scenario by integrating the interaction torque regarding θ_2. The joint stiffness is divided into low and high stiffness gathering the blue and red curves of Fig. 3.17, respectively, as is shown in Fig. 3.18. Within the low stiffness, the outcomes are estimated between 0.56 to 1.25 Nm/rad at a range of preload between 0 to 176.7 N. In contrast to the high stiffness' outcomes between 3.45 to 4.24 Nm/rad which need a preload of 742.4 to 944.9 N.

According to the interaction torque results, an approximation model is estimated to fully characterize the interaction torque and the user's hip ab/adduction. To achieve this, each

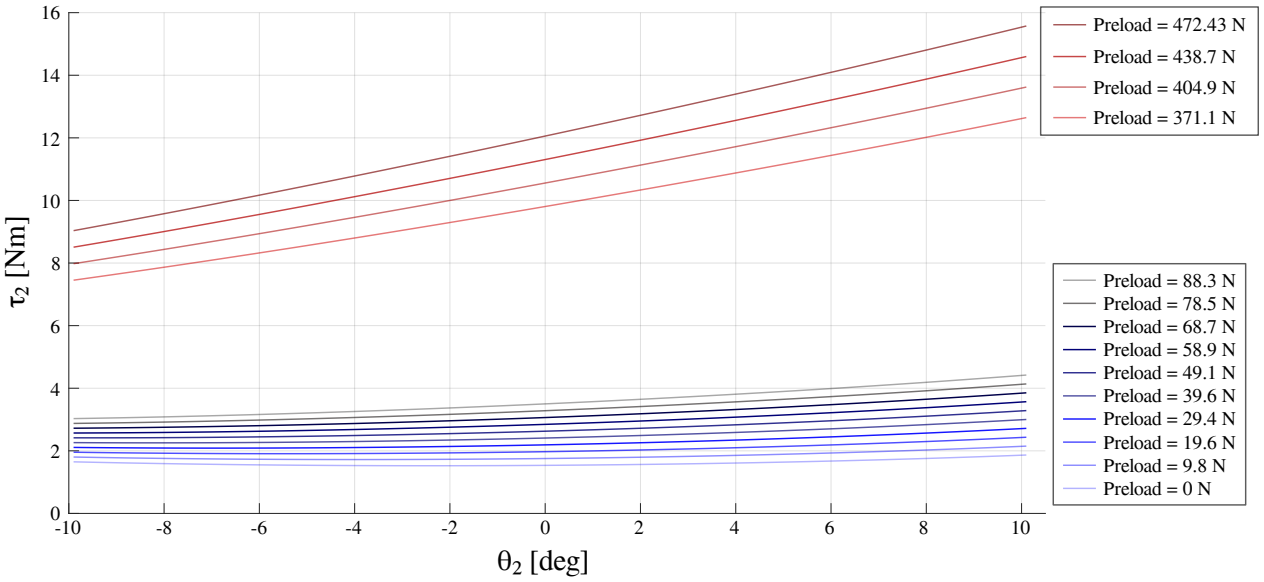

Figure 3.17: Interaction torque of the passive frontal hip joint along with several preload cases.

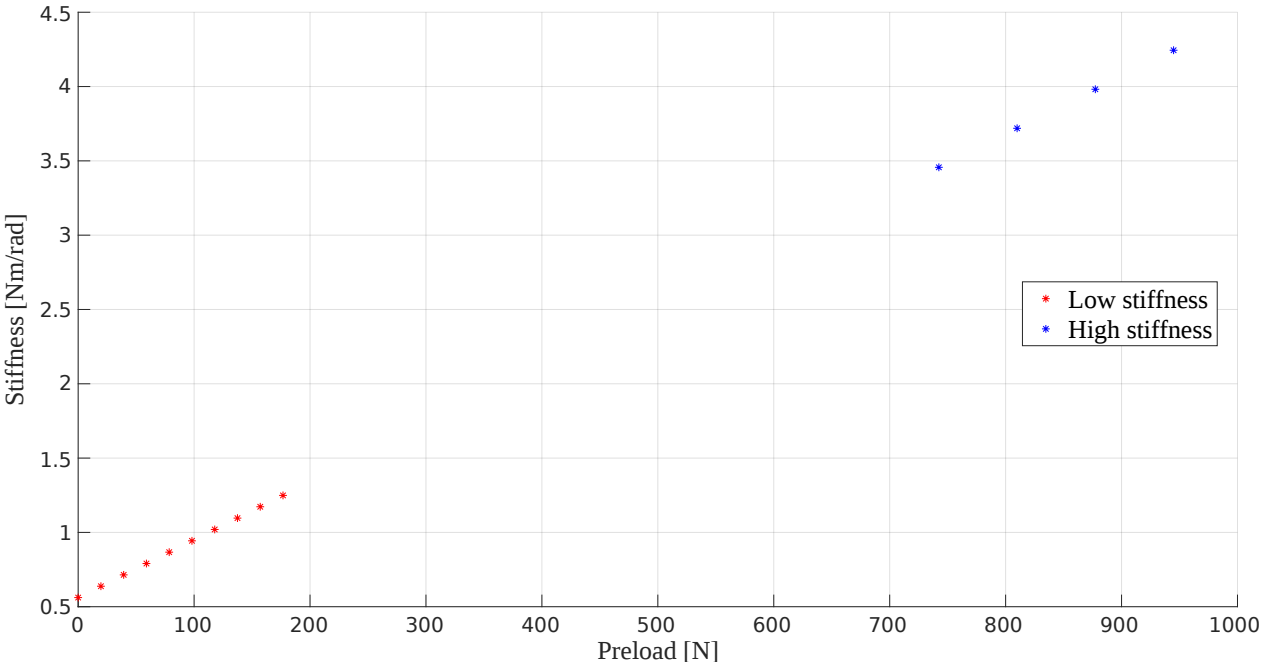

Figure 3.18: Joint stiffness regarding the preloaded scenarios.

scenario is fitted to a polynomial equation of second degree (i.e., a, b, and c are the fitting coefficients) dividing this analysis into the same two groups previously established. The Eq. 3.7 resumes the interaction torque within the lower tendon's stiffness, representing the blue curves in the Fig. 3.17. Moreover, the Eq. 3.8 summarizes the interaction torque (τ) of

the higher tendon's stiffness corresponding to the red curves. These equations define the relationship between the interaction torque (τ) and the hip ab/adduction motion (θ_2).

$$\tau(\theta_2) = a\theta_2^2 + b\theta_2 + c; a = 0.0022, 0.0103 \leq b \leq 0.0691, 1.5347 \leq c \leq 3.4988 \tag{3.7}$$

$$\tau(\theta_2) = a\theta_2^2 + b\theta_2 + c; a = 0.0021, 0.2595 \leq b \leq 0.3268, 9.8049 \leq c \leq 12.0558 \tag{3.8}$$

These approximation models and the analytical data are compared to understand the curve fitting for each scenario. The relative error estimates the fitting error, as is presented in Eq. 3.9 and the error between the data and the fit function is shown in Fig. 3.19. In this sense, the overall error was lower for the second group of curves (i.e., red curves) and higher for the first group of curves (i.e., blue curves). Moreover, the variation of the first group was greater than the second group. Nevertheless, the maximum relative error of all the scenarios was 2.48% at 0 N of preload.

$$\tau_{error} = \frac{data - fit}{data} \tag{3.9}$$

3.4 Discussion

The passive hip joint's mathematical model was developed to quantify the interaction torque and stiffness according to the system's preload. The passive frontal hip joint required higher preload forces to increase the interaction torque delivered to the user. In the first group of curves, the preload ratio needed to obtain the Maximum interaction Torque (RPMT) is delimited between 9.8 to 42.1. Likewise, the RPMT within the second group of curves is defined between 59.8 to 59.9. On the other hand, stiffness outcomes are also divided into two groups which can be adjusted according to the preload force. Even though the stiffness and

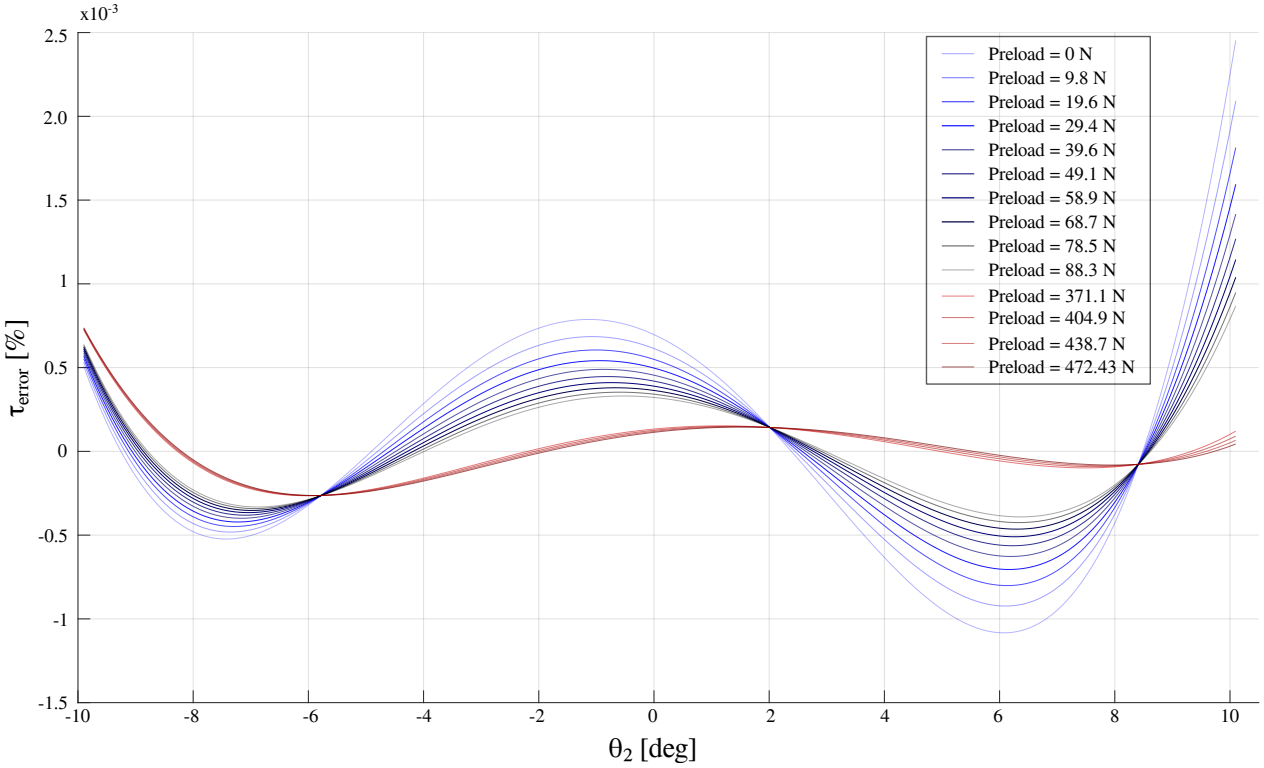

Figure 3.19: Interaction torque error of the approximate model compared to the analytic results.

the preload are directly proportional, the ratio between them is lower than $3.24e-2$. These ratios allowed to compare the output (e.g., interaction torque or stiffness) to the input (e.g., preload) given a poor performance.

The hip ab/adduction motion is commonly included in LLE's design as an unactuated joint such as HAL-3 [43], eLegs [86], and ReWalk [45]. Similarly, Vanderbilt University's LLE has adjustable compliance for the hip ab/adduction motion through a composite material and aluminum inserts, increasing its weight [87]. However, these unactuated joints have several limitations that can be overcome using the lightweight proposed passive joint.

Other LLEs also included active and quasi-passive actuators to provided energy to the hip joint, even though these devices focus on the sagittal plane. Lee et al. studied a hip-exoskeleton that provides similar interaction torque compared to the proposed passive joint adjusted at a 371.1 N. However, the hip-exoskeleton is heavier and generates a maximum

torque of 12 N [88].

Similarly, Di Natali et al. studied the XoSoft which uses quasi-passive actuators through elastic bands and an electro-magnetic clutch [89], [90]. This device generates passive energy along the motion, providing to the user's hip a maximum torque of 3 Nm. In contrast to the proposed joint that provides a higher interaction torque adjusting the preload between 0 to 88.3 N, as presented in Fig. 3.17. Additionally, the XoSoft needs an electro-magnetic clutch.

The proposed passive hip joint in this work presented a advantages compared to other devices, regarding the lightweight and the interaction torque. Nevertheless, this joint has limitations. One of these limitations is the preload's magnitude needed to achieve higher interaction torque. To reduce the preload's magnitude, the four-bar mechanism could be optimized to increase the interaction torque, modifying the links' length or layout.

Another limitation is related to the stiffness generated to the user's joint. Even though the proposed passive joint provides a range of stiffness, the amount required to support the user should be higher. However, the design could be improved by including an arrangement of bio-inspired tendons in a parallel layout to significantly increase the joint's stiffness.

3.5 Conclusions

This chapter compresses the current development of the AGoRA-LLE by extending the improvement of the AGoRA-LLE's physical interfaces and the understanding of the passive frontal hip joint through a mathematical model and simulation. The embedded version of the physical interfaces is presented to address the vibration within the previous design's mechanical structure. Besides, ergonomic considerations are also presented to enhance the comfort of the user.

The proposed passive joint is characterized through mathematical modeling and simulation providing an interaction torque and stiffness. These outcomes allow configuring the pas-

sive joint regarding a preload for a specific interaction torque and stiffness. Moreover, the passive joint's design provides a suitable solution for secondary planes of motion instead of heavyweight actuators.

Besides, the passive frontal hip joint interaction is quantified considering multiple scenarios throughout the variable stiffness configuration. Moreover, the interaction torque is divided according to the stiffness of the bio-inspired tendons which the lower stiffness provides an interaction torque between 1.8 Nm to 4.1 Nm. In contrast, setting the higher range's stiffness produces an interaction torque between 7.5 Nm to 15.4 Nm. Besides, the stiffness provided by the proposed hip joint is defined between 0.56 Nm/deg to 4.24 Nm/deg. These joint's outcomes were not enough to provide support to the user. However, this first study allowed to improve and optimize the joint's performance. Finally, enhancing the AGoRA-LLE's physical interfaces and comprehending the joint's interaction accomplish the second and third objectives proposed in this thesis.

Chapter 4

Assessment of the AGoRA lower-limb exoskeleton's physical interfaces

Performance indicators have been used to assess the LLE's performance in different groups such as goal task, kinematics or kinetics variables and HRI [14]. These groups could evaluate the overall performance or focus on a particular feature of the device. Focusing on the LLE's physical interfaces, the performance indicators poorly describe the HRI and a specific task as addressed in the previous chapters.

Therefore, a three-dimensional relative motion methodology is proposed to fully assess the HRI and understand the kinematic compatibility between the user and the exoskeleton. Moreover, the proposed three-dimensional relative motion methodology is used to assess the physical interfaces of the AGoRA-LLE. In this sense, this chapter details the three-dimensional relative motion methodology employed to an LLE. Afterward, the methodology is used to assess the physical interfaces of the AGoRA-LLE.

4.1 3D relative motion methodology

The proposed methodology extends the understanding of the relative motion analysis to three dimensions, in contrast to other approaches that only have analyzed one dimension [69], [72]. Besides, the interaction along the secondary planes allows identifying undesirable motions among the task. To measure the relative motion of the exoskeleton and the user's limb is essential to comprehend the theoretical base in which the difference of orientation between two bodies is established. To perform this analysis is used an optoelectronic system, as a reference method for movement analysis [91]. In this sense, a lower-limb scenario is presented to explain the optoelectronic system's markers setup and how the methodology is applied utilizing the AGoRA-LLE.

4.1.1 Theoretical base

Within a three-dimensional context, the body's motion can be defined through a local frame that establishes their orientation compared to a global frame located at the origin (F_O) [92]. This concept can extend to two bodies given that two local frames for body A (i.e., $F_{a/o}$) and body B (i.e., $F_{b/o}$) are compared to the global frame. According to the global frame, a local frame's orientation is defined through a rotation matrix ($R_{local/global}$). To define the three-dimensional orientation each body needs at least three points to create the local frame's three vectors. For instance, the reference geometry can be created by points or director vectors such as shown in Fig. 4.1. In this sense, the rotation matrices of the bodies are fully defined using the reference geometry.

Each rotation matrix has its director vectors that define the orientations regarding the geometry reference. These rotation matrices are essential to define the orientation as an indicator of how similar is the motion of the bodies by comparing the difference of orientation between the local frames of both bodies. Similarly to articular kinematics, two body segments are compared through their local frames given consecutive angles that define their difference of

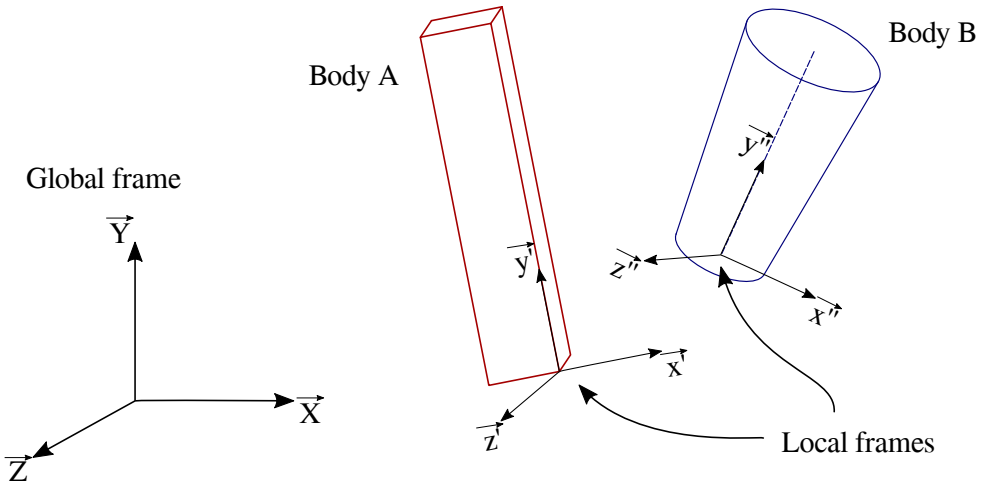

Figure 4.1: Example of the global and local frame

orientation [93]. Likewise, the orientation of body A is compared to the body B as shown in Eq. 4.1. Moreover, the elements of the matrix $R_{A/B}$ are used to calculate the three main angles (i.e., α, β, γ) which define the difference of orientation between the bodies' local frames [93]. The angles' representation is consecutive given that the first difference of orientation is defined by α, as represented in Fig. 4.2A. Regarding the rotated frame, the following rotation is β, as shown in Fig. 4.2B. Similarly, the last rotation is defined as γ, as is seen in Fig. 4.2C.

$$R_{A/B} = R_{A/O}R_{B/O}^{-1} = \begin{bmatrix} \delta_{11} & \delta_{12} & \delta_{13} \\ \delta_{21} & \delta_{22} & \delta_{23} \\ \delta_{31} & \delta_{32} & \delta_{33} \end{bmatrix} \quad (4.1)$$

$$\begin{aligned} \alpha &= tan^{-1}\left(\frac{-\delta_{12}}{\delta_{22}}\right) \\ \beta &= sin^{-1}\left(\delta_{32}\right) \\ \gamma &= tan^{-1}\left(\frac{-\delta_{31}}{\delta_{33}}\right) \end{aligned} \quad (4.2)$$

4.1.2 Lower-limb scenario

In light of the 3D relative motion methodology's main concepts, the analysis aims to compare the exoskeleton's orientation and the user's thigh. This approach allows to understand and quantify the kinematic compatibility, and how the device's physical interfaces respond during the task. A lower-limb scenario is important to address the markers setup needed to estimate the local frames and how the markers are used. Each local frame's definition is presented

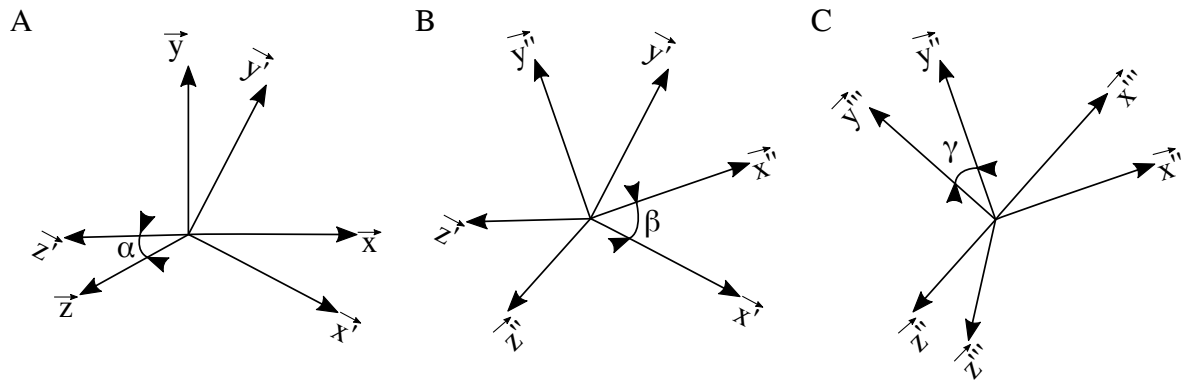

Figure 4.2: Representation for the difference of orientation. The overall difference of orientation is a consecutive rotation starting from A. α rotation, B. β rotation, and C. γ rotation.

through the rotation matrix and the difference of orientation between them.

Markers setup

The reference points aforementioned are defined by reflective markers placed in the user's thigh and exoskeleton in the motion capture system. According to the modified Helen Hayes setup for lower-limb, the thigh local frame is established using the user's hip and knee markers [30]. The hip and knee markers are highlighted in Fig. 4.3A. Moreover, the exoskeleton is also mounted with five markers distributed per leg as three markers in the lower thigh physical interface and one marker per joint (i.e., hip and knee exoskeleton joint), as presented in Fig. 4.3B. These markers are the baseline for the exoskeleton local frame.

User's thigh local frame

The user's thigh local frame is created by four markers (i.e., right postero-superior iliac spine as EPSD, right antero-superior iliac spine named as EASD, right lateral tibial condyle as CLD and right medial tibial condyle as CMD) which are defined as vectors, referenced on the F_O. To establish the thigh's first reference, this body segment is considered a truncated cone. The first diameter is the distance between EPSD to EASD and the second diameter is between CLD and CMD. The vectors $\overrightarrow{t_{up}}$ and $\overrightarrow{t_{low}}$ determine the center of the first and second diameters of the truncated cone and each vector is represented as Eq. 4.3 and Eq.

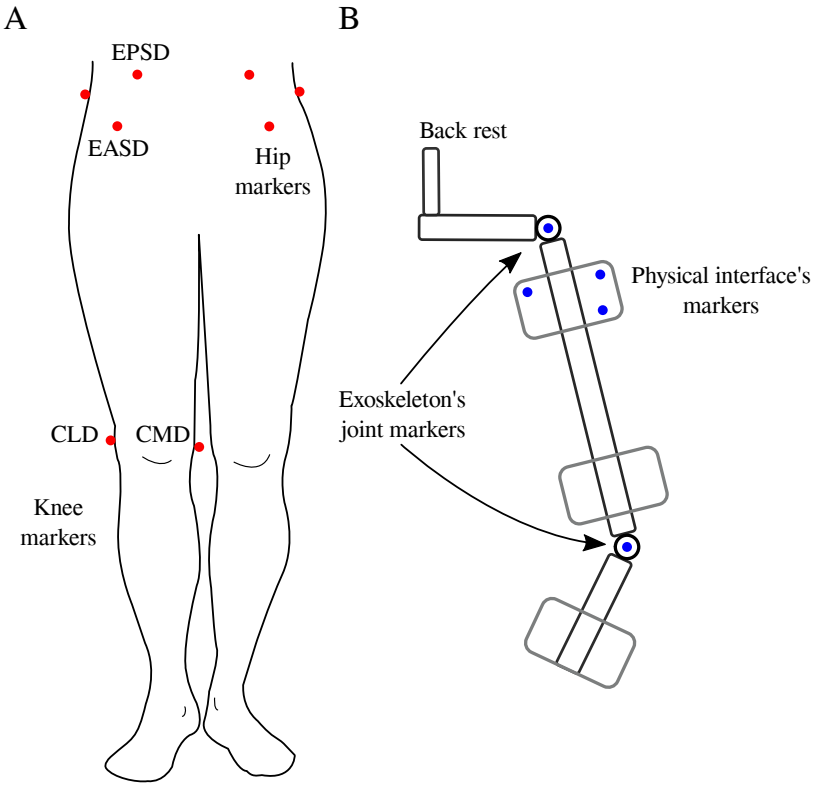

Figure 4.3: Scheme of markers setup. A. User's markers used to estimate its local frame. B. Exoskeleton's markers used to calculated its local frame.

4.4. The central axis provides the first reference ($\overrightarrow{vect_y}$) of the orientation of the thigh. The definition of these vectors are shown in Fig. 4.4 and represented in Eq. 4.5.

$$\overrightarrow{t_{up}} = \frac{1}{2} \cdot \left(\overrightarrow{OEPSD} + \overrightarrow{OEASD} \right) \tag{4.3}$$

$$\overrightarrow{t_{low}} = \frac{1}{2} \cdot \left(\overrightarrow{OCMD} + \overrightarrow{OCLD} \right) \tag{4.4}$$

$$\overrightarrow{vect_y} = \overrightarrow{t_{up}} - \overrightarrow{t_{low}} \tag{4.5}$$

The second reference ($\overrightarrow{vect_z}$) use the vectors $\overrightarrow{t_{low}}$ and $\overrightarrow{OCLD}$ as is seen in Eq. 4.6 allows finding to find the third reference ($\overrightarrow{vect_x}$) by the cross product of $\overrightarrow{vect_y}$ and $\overrightarrow{vect_z}$ as shown in Eq. 4.7. The unit vectors of the references gather together the rows of the rotation matrix ($R_{th/O}$) of the thigh compared to the global frame as shown in Eq. 4.8.

$$\overrightarrow{vect_z} = \overrightarrow{OCLD} - \overrightarrow{t_{low}} \tag{4.6}$$

$$\overrightarrow{vect_x} = \overrightarrow{vect_y} \wedge \overrightarrow{vect_z} \tag{4.7}$$

$$\left[\mathbf{R}_{th/O}\right] = \begin{bmatrix} \overrightarrow{th_x} \\ \overrightarrow{th_y} \\ \overrightarrow{th_z} \end{bmatrix} = \begin{cases} \overrightarrow{th_x} & = \frac{\overrightarrow{vect_x}}{\|\overrightarrow{vect_x}\|} \\ \overrightarrow{th_y} & = \frac{\overrightarrow{vect_y}}{\|\overrightarrow{vect_y}\|} \\ \overrightarrow{th_z} & = \frac{\overrightarrow{vect_z}}{\|\overrightarrow{vect_z}\|} \end{cases} \tag{4.8}$$

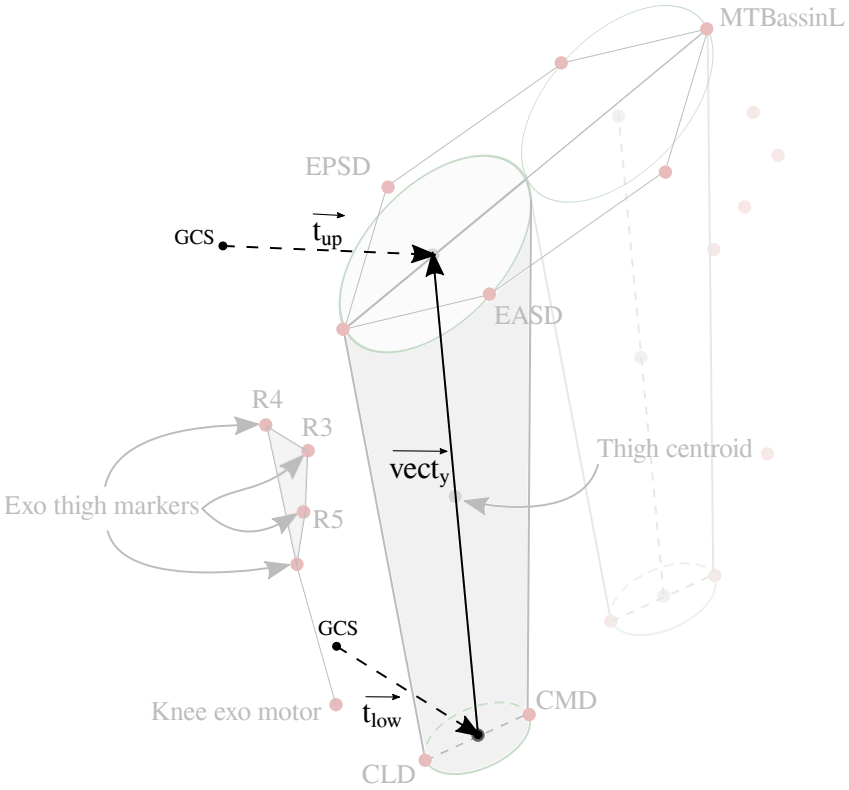

Figure 4.4: Scheme of thigh's vectors. A. Reference vectors used to establish the user's local frame. B. Reference vectors used to establish the exoskeleton's local frame

Exoskeleton local frame

The main markers to build the exoskeleton local frame are placed in the physical interface (i.e., R3, R4 and R5) and over the hip and knee actuators (i.e., exo_{HR} and exo_{KR}) as shown

in Fig. 4.5. In this case, the first reference ($\overrightarrow{vec_{exoy}}$) is defined by the markers of hip and knee actuators expressed in Eq. 4.9. Furthermore, the second reference ($\overrightarrow{vec_{exoz}}$) come from two vectors (i.e., $\overrightarrow{v_1}$ defined in Eq. 4.10 and $\overrightarrow{v_2}$ showed in Eq. 4.11) using the physical interface's markers as shown in Eq. 4.12. The third reference ($\overrightarrow{vec_{exox}}$) is calculated by a cross product of the first and second reference. Finally, the exoskeleton's rotation matrix ($R_{exo/O}$) is established as is summarized in Eq. 4.13.

$$\overrightarrow{vec_{exoy}} = \overrightarrow{Oexo_{HR}} - \overrightarrow{Oexo_{KR}} \tag{4.9}$$

$$\overrightarrow{v_1} = \overrightarrow{OR_3} - \overrightarrow{OR_4} \tag{4.10}$$

$$\overrightarrow{v_2} = \overrightarrow{OR_3} - \overrightarrow{OR_5} \tag{4.11}$$

$$\overrightarrow{vec_{exoz}} = \overrightarrow{v_1} \wedge \overrightarrow{v_2} \tag{4.12}$$

$$\left[\mathbf{R}_{exo/O}\right] = \begin{bmatrix} \overrightarrow{exo_x} \\ \overrightarrow{exo_y} \\ \overrightarrow{exo_z} \end{bmatrix} = \begin{cases} \overrightarrow{exo_x} & = \frac{\overrightarrow{vec_{exox}}}{\left\|\overrightarrow{vec_{exox}}\right\|} \\ \overrightarrow{exo_y} & = \frac{\overrightarrow{vec_{exoy}}}{\left\|\overrightarrow{vec_{exoy}}\right\|} \\ \overrightarrow{exo_z} & = \frac{\overrightarrow{vec_{exoz}}}{\left\|\overrightarrow{vec_{exoz}}\right\|} \end{cases} \tag{4.13}$$

Differences of orientation

The two local frames of the exoskeleton's knee joint and user's knee are summarized in Fig. 4.6. These are defined through two rotation matrices which define: (1) the orientation of the user's thigh ($[\mathbf{R}_{th/O}]$) placed in the knee joint, and (2) the exoskeleton's thigh ($[\mathbf{R}_{exo/O}]$) located in the knee hinge joint. These two matrices are compared to the global reference frame of the room. Following, they are computed as Eq. 4.1 to explain the exoskeleton's orientation compared to the user's thigh ($[\mathbf{R}_{exo/th}]$).

These orientations are used to estimate the exoskeleton's rotation compared to the user's thigh noted as $R_{exo/thigh}$ presented in Eq. 4.14. The elements of this rotation matrix are used

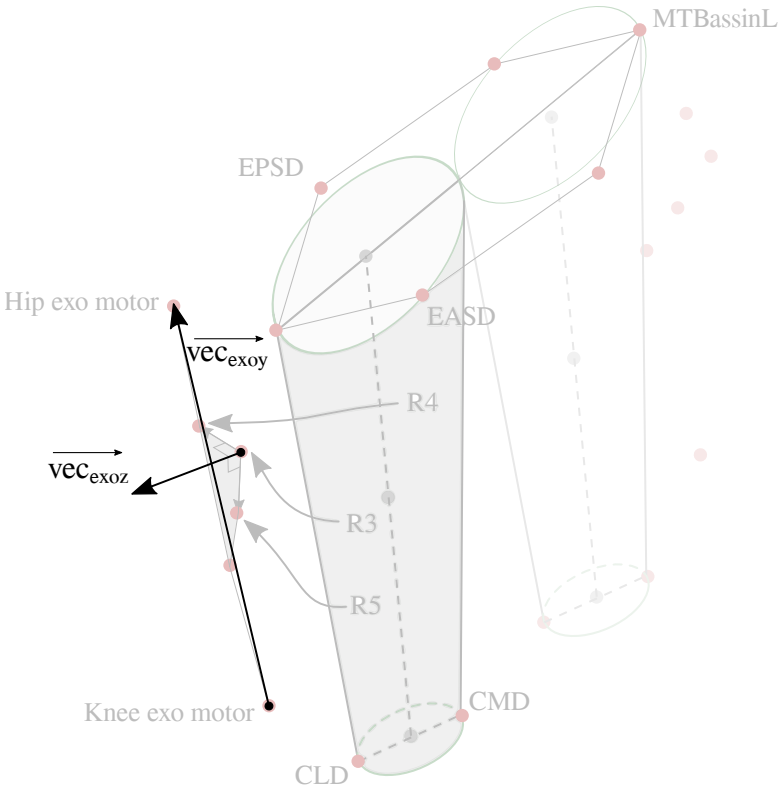

Figure 4.5: Scheme of exoskeleton's vectors. Reference vectors are used to establish the local frame of the exoskeleton.

to calculate three angles as shown in Eq. 4.2: (1) referenced to the sagittal plane (α), (2) around longitudinal rotation (β), and (3) around the frontal plane (γ). Each angle is related to an axis previously defined as β to X-axis, γ to Y-axis, and α to Z-axis. The orientation's notation is defined according to the International Society of Biomechanics recommendations establishing the following parameters: Z-axis is perpendicular to the representative sagittal plane and the Y-axis is referenced to the body segment [94].

4.2 Experimental protocol

The AGoRA-LLE is assessed through a 6-meter walking test (6-MWT) in six healthy subjects during the gait assistance mode to employ the methodology mentioned above. The three-dimensional methodology studied the HRI, regarding the exoskeleton's knee and user's knee. Each subject performed the test ten trials. The volunteers followed the inclusion and exclusion criteria to match the anthropometric measurements required by the exoskeleton

$$R_{exo/thigh} = R_{exo/O} R^{-1}_{thigh/O} \tag{4.14}$$

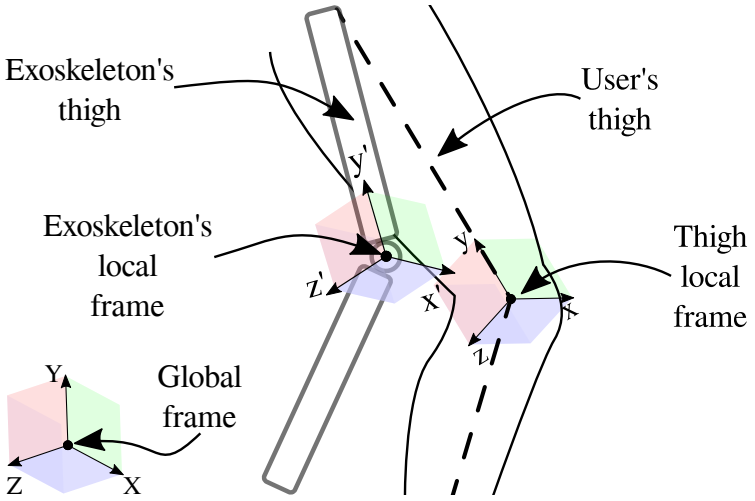

Figure 4.6: 2D-projection of the descriptive scheme of rotation matrices.

and health requirements. Besides, this experimental protocol was approved by an ethics committee at the ECIJG.

4.2.1 Subjects

The six subjects (25.5 ± 6.07 y.o., 71.5 ± 10.9 kg, 1.8 ± 0.02 m) enrolled for this pilot study were enclosed by multiple inclusion and exclusion criteria specified below.

Inclusion criteria

- Adults between 18 to 65 y.o.
- No history of neurological, neuromuscular, or physical disability that may affect their normal gait pattern.
- Height between the range of 1.70-1.85 m.
- Weight less than 100 kg.

- Anthropometric measurements of femur length between 42 to 48 cm, the distance between trochanters of 32 to 37 cm, and tibia's length within a range of 28-31 cm. According to the AGoRA-LLE's adjustable links.

Exclusion criteria

- Lower-limb abnormalities of the participant that interfere from wearing the exoskeleton.
- Cognitive impairments of the participant that restrain from reading, understanding, or signing the informed consent.
- Uncontrolled arterial hypertension or epilepsy.
- Being under the influence of alcohol, drugs, or any type of narcotic substance during the experimental procedure.

4.2.2 AGoRA-LLE layout

The unilateral version of the AGoRA-LLE presented in chapter 3 is used in the pilot study. The thigh and shank variable links are adjusted for each subject according to the user's anthropometric measurements aligning the exoskeleton joints to the user's hip and knee joints. The exoskeleton is initialized as assistance mode which is an impedance controller detailed in Fig. 4.7. The gains adjusted for all the trials allowed a resistive interaction to understand the physical interfaces' response. This modality is configured for each subject and all its trails.

4.2.3 Markers setup and equipment

Kinematic data is acquired through 11 cameras (100 Hz, accuracy 0.1 mm, Vicon Motion System, Oxford, UK) using 28 reflective markers (14 mm diameter) on the subject described in Fig. 4.8, following the modified Helen Hayes protocol for lower limb. Besides, the exoskeleton was also fitted with 20 markers distributed per leg as four markers in the lower

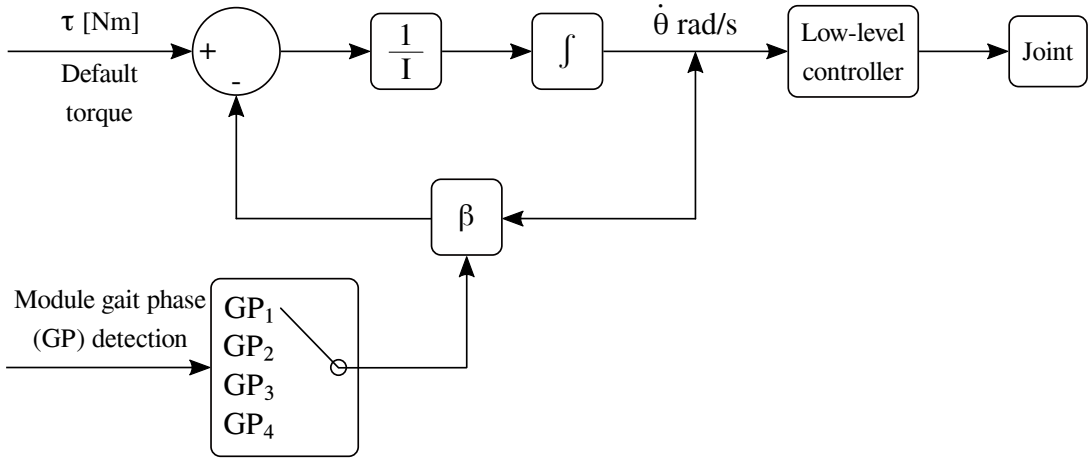

Figure 4.7: Controller scheme of the assistance mode used in the pilot study.

thigh physical interface, one marker per motor joint (i.e., hip and knee exoskeleton joint), and four markers in the shank physical interface. In this sense, the markers setup fulfilled the requirements to employ the 3D relative motion methodology as shown in Fig. 4.8. The markers were tracked using Vicon's software to identify and fill its gaps. On the other hand, the markers' placement was the same for all the trials and the exoskeleton was installed once.

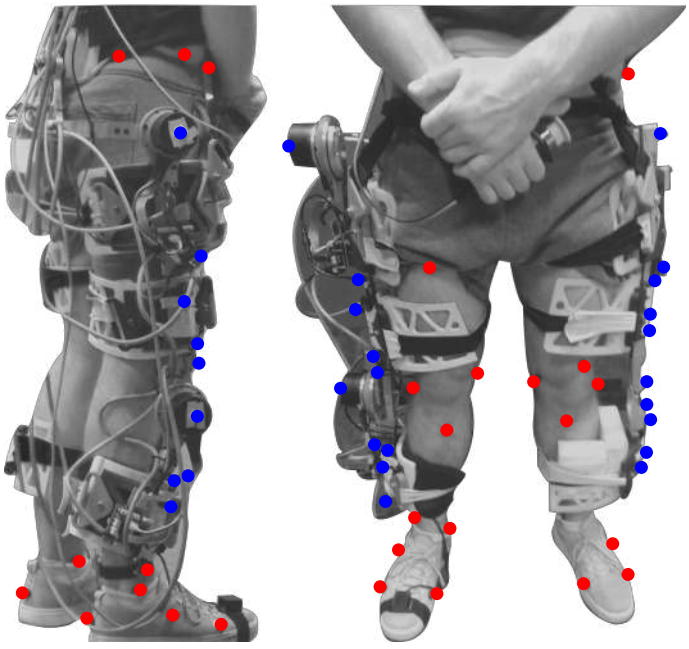

Figure 4.8: Markers setup used in the pilot study. User's markers and exoskeleton's markers are highlighted in red and blue, respectively.

4.2.4 Statistical analysis

Descriptive statistics are used to analyze the difference of orientation for each subject. The analysis is carried out in *Matlab R2018b* estimating the gait cycles by right heel's reflective marker acceleration. Besides, the first and last gait cycles were excluded due to instabilities within the signals. According to the data segmented, the mean, standard deviation, coefficient of variation, and cross-correlation values of the three angles are calculated. Besides, the cross-correlation value compared each orientation per gait cycle among themselves to establish an overall similarity outcome.

4.3 Experimental results

This pilot study implemented the novel three-dimensional methodology, detailed in previous sections, contributing to the user's interaction. The results' analysis is divided into (1) users' interaction and (2) methodology's consistency. Within the first analysis, each angle defined in the Eq. 4.2 represents the interaction of the exoskeleton compared to the user's limb given a full three-dimensional assessment. Moreover, these outcomes are analyzed through four gait phases. Finally, the methodology's consistency is examined through a cross-correlation analysis compared to each descriptive statistics angle.

4.3.1 User's interaction

The subjects' interaction is presented through the difference of orientations showed in Fig. 4.9. These results are analyzed regarding 21.3 $\pm$ 5.7 gait cycles per subject. The rotation Z (i.e., α orientation) presented a positive offset for all the subjects. Besides, the rotation Z showed that the difference of orientation varied between 20 to 45 degrees. Specifically, subjects two, three, and five presented a constant value along with the gait percentage. In contrast to subjects one, four, and six showed an increase of 10 degrees within the stance phase (i.e., 0 - 73 % gait percentage).

Similarly, the rotation X (i.e., β orientation) varied between -15 to 12 degrees. Although the orientation difference was near zero, it also presented a scatter behavior as seen in subjects one, two, three, and six. Likewise, subjects four and five revealed a sinusoidal shape and reduced scatter behavior compared to the other subjects.

Finally, the rotation Y (i.e., γ orientation) changed between -5 to 12 degrees. In this case, the difference of orientation was constant for five out of six subjects. Besides, subjects one, three, and six showed a scatter behavior. Contrary to subject two, the difference of orientation varied in 10 degrees between 18% to 60% and presented a reduced standard deviation and variation.

The outcomes are analyzed along the gait cycle through a range of rotation (e.g., subtract the highest to the lowest difference of orientation). Firstly, the overall mean is estimated in a full gait percentage (i.e., 0 to 100 % gait percentage) as is seen in Table 4.1. The overall mean is the average of the difference of orientation for all gait cycles per subject. The higher difference of orientation for Rot. Z compared to the other rotations.

In comparison to the lower difference of orientation depend on which rotation is closer to zero. For instance, subjects one, two, and six presented a Rot. X near to zero. Likewise, subjects three, four, and five showed a Rot. Y closer to zero.

Further analysis is aimed at the range of rotation calculating the mean, standard deviation, and coefficient of variation shown in Table 4.1. Within the rotation range, the coefficient of variation was greater than 20% for all the rotations and subjects. Moreover, five out of six subjects showed a coefficient of variation greater than 30% for each orientation, presenting a scatter behavior. Furthermore, the standard deviation remained lower than 4.53 except for the Rot. Z for subjects four and six.

Another approach to understanding the interaction between the user and the exoskeleton is to consider the sub-phases (i.e., heel strike at 0 or 100%, flat foot at 10%, heel off at 50%

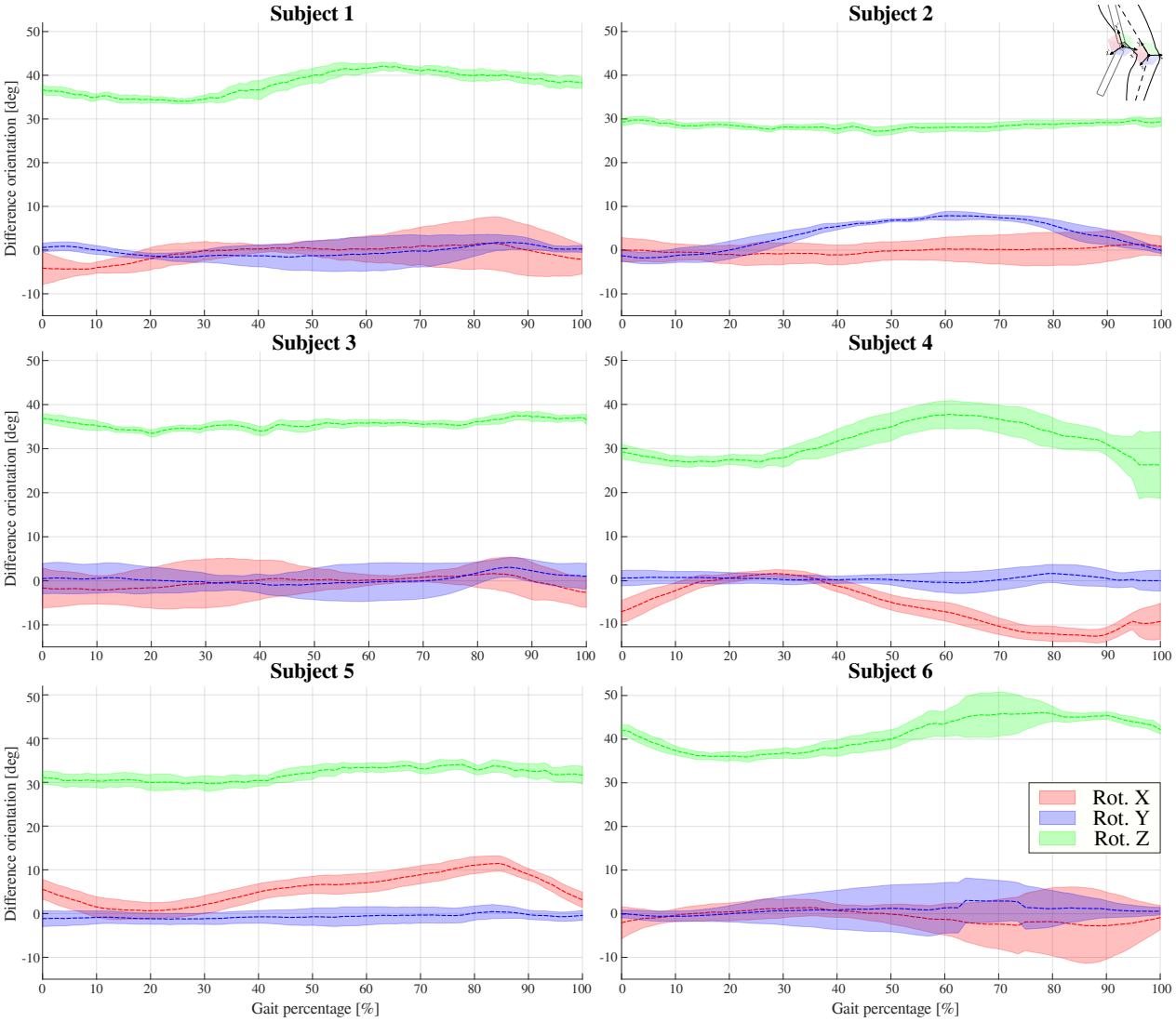

Figure 4.9: The difference of orientation results of the pilot study. Each graph represents the difference of orientation's outcomes per subject. The red curve represents the Rot. X. The blue curve represents the Rot. Y. The green curve represents the Rot. Z.

and toe-off at 73%) along the gait [3]. The ranges of rotation are also estimated within the sub-phases to analyze the transitions in the same sub-phase. These results are showed in Table 4.2. In the first phase (i.e., 0 to 10 %), the Rot. Y showed a closer range of orientation to zero compared to Rot. X and Z showing an increase or decrease in changes of 4.947 or -5.048 *deg*, respectively.

Within the second phase (i.e., 10 to 50 %), the rotation ranges increase considerably compared to the first phase. Besides, 83.3% of the ranges showed a positive increasing meaning a similar

Subject	Rotation	*Overall Mean [deg]*	Range of rotation		
			Mean [deg]	***Standard deviation***	***Coefficient of variation [%]***
1	*Z*	38.15	8.12	2.81	34.58
	X	-0.72	5.34	3.26	61.04
	Y	1.11	3.55	1.76	49.6
2	*Z*	28.45	2.57	1.57	61.08
	X	-0.12	2.52	1.90	75.17
	Y	3.63	9.64	2.03	21.14
3	*Z*	35.55	4.02	1.91	47.45
	X	-0.32	4.26	2.87	67.47
	Y	0.22	5.96	2.10	35.29
4	*Z*	31.52	11.5	8.79	76.07
	X	-5.50	14.18	4.53	31.78
	Y	0.44	2.12	1.66	78.06
5	*Z*	31.79	4.39	2.94	67.0
	X	5.60	10.92	3.42	31.5
	Y	-0.67	1.73	1.90	110.12
6	*Z*	41.1	10.17	5.83	57.34
	X	-0.81	4.16	2.86	68.84
	Y	0.87	3.64	1.85	60.

Table 4.1: Descriptive statistics of the difference of rotations. The overall mean presents the average value of each rotation for all the gait cycle. The rotation range is the difference between the maximum and minimum value for the each rotation's mean curve. Units in degrees.

response of the physical interfaces during the second phase. On the contrary within third phase (i.e., 50 to 73 %), the range of rotation kept constant for the subjects one, two and three. However, the other half of subjects presented considerable changes at least in one of the rotation. Finally, the fourth phase (i.e., 73 to 100 %) revealed the higher decrease of rotation range and the 66.6% were negative ranges.

4.3.2 Methodology's consistency

The cross correlation is analyzed within the same rotation per subject to compare the similarity along the curves. These results are presented in Table 4.3. The Rot. Z revealed the higher similarity (i.e., 0.97 to 0.99) for all the subjects. Contrary to the Rot. Y, the cross correlation value was within a range of 0.03 to 0.12 except for the subject 4. Similarly, the

Subject	Rotation	Difference of rotation [deg]			
		Gait percentage			
		0-10	*10-50*	*50-73*	*73-100*
1	*Z*	1.71	4.80	1.13	2.61
	X	0.38	3.87	0.45	2.99
	Y	0.21	2.56	0.71	3.13
2	*Z*	0.65	1.15	1.14	0.80
	X	0.60	0.25	0.32	0.77
	Y	0.08	8.02	0.39	7.25
3	*Z*	1.72	0.43	0.09	1.01
	X	0.40	2.28	0.80	3.64
	Y	0.19	4.46	1.05	4.68
4	*Z*	2.01	7.97	0.79	9.71
	X	4.95	3.04	6.40	2.27
	Y	0.14	0.54	0.65	0.80
5	*Z*	0.84	1.96	1.55	2.11
	X	4.30	5.33	2.91	6.36
	Y	0.32	0.11	0.33	0.02
6	*Z*	5.05	3.01	5.76	3.58
	X	1.90	0.03	2.55	1.81
	Y	0.53	1.81	1.47	2.01

Table 4.2: Variation of rotation between gait phases. The difference of rotation is estimated according to the mean value at the corresponding gait percentage. Units in degrees.

cross correlation of Rot. X were between 0.02 to 0.07 except for subject four and five.

Subject	Rotation		
	Z	*X*	*Y*
1	**0.9969**	0.0707	0.1108
2	**0.9975**	0.0172	**0.8057**
3	**0.9977**	0.0353	0.1251
4	**0.9773**	**0.8482**	0.0293
5	**0.9946**	**0.8003**	0.0521
6	**0.9938**	0.0305	0.0237

Table 4.3: Cross-correlation for the difference of rotations. Each group of curves is compared between them to analyze the similarity for each orientation.

4.4 Discussion

The three-dimensional analysis identified a variation of 10 degrees the difference of rotation at least in one orientation within six subjects. These variations are related to the physical

interfaces' response due to the user's interaction among gait. Moreover, the rotation affected might or not match with the main plane of motion of the AGoRA-LLE (i.e., along with the Rot. Z) given meaningful information about the HRI and kinematic compatibility. Four out of six subjects presented an affected orientation different from the main plane of motion. In this sense, the physical interfaces allowed motion in secondary planes, enabling user's energy losses during the 6-MWT. Hence, the proposed methodology introduced new information regarding the physical HRI and the physical interfaces' analysis.

Descriptive statistics provided useful information through the cross-correlation outcomes even though the coefficient of variation was higher than 30%. Within the Rot. Z outcomes, the interaction can be accumulative to some extent considering the higher similarity of the curves and the higher variation. In this context, the same curve can be vertically shifted provoking an increase in the variation. However, the accumulative effect did not apply to Rot. X and Y. Further analysis should study the Rot. X and Y to understand their lower similarity and scatter behavior. Hence, a large amount of subjects is required to fully comprehend these rotations.

Current relative motion studies related to kinematic outcomes only analyzed translations along the sagittal plane. Langlois et al. assessed a customized physical interface by estimating the distance between two markers in the sagittal plane along the gait [69]. Even though the researchers examined the variation of the distance to the energy deployed by the exoskeleton, this analysis overlooked 66.6% of the interaction reducing the understanding of the losses of energy among the task. Moreover, the physical interface's response is only understood in one plane minimizing the improvement for a future version of the physical interfaces.

Other relative motion study analyzed an LLE's interaction during sit-to-stand along the sagittal plane. Akiyama et al. presented a deeper analysis of the thigh segment given two displacements and one rotation, as well as a physical interfaces' slippage displacements [72]. Similarly to the study mentioned above, these outcomes are only estimated within the sagittal

plane disregarding the other two planes.

Within LLE, the kinematic compatibility involved different features such as adaptable, suitable and comfortable [12]. These features are intended to assess among the studies of the AGoRA-LLE. The physical interfaces were assessed through a usability test showing the main ergonomic issues improved [79]. Additionally, the three-dimensional analysis complemented the physical interfaces' assessment. These outcomes quantified the HRI that provide an overall understanding of the physical interfaces' response, allowing undesirable DOF along the user's three main planes.

Additionally, the difference of orientations' results showed a maximum rotation of 8 *deg*, 12 *deg*, and 45 *deg* according to the X-axis, Y-axis, and Z-axis, respectively. The X-axis's value is lower than other axes, although the variation presented along the gait cycle should be reduced. Similarly, the Y-axis's value presented a considerable difference of orientation's variation. Moreover, the Z-axis's value is the highest difference in orientation, which also presented a variation among the gait. Following this analysis, these values have to be improved by better physical interfaces' design.

4.5 Conclusions

This chapter presents a novel three-dimensional relative motion methodology to assess the AGoRA-LLE's physical interfaces. A pilot study was carried out by recruiting six volunteers and performed a 6-MWT. Besides, the AGoRA-LLE used an impedance controller for all the trials. The difference of orientation was calculated by the optoelectronic system using the reflective markers placed in the user and the exoskeleton. The proposed three-dimensional relative motion methodology provided a better understanding of the HRI and kinematic compatibility. Besides, the difference of orientations has adequate accuracy to estimate each rotation compared to other one-dimensional relative motion study presented in chapter 2.

The interaction estimated by the proposed methodology quantified a difference of orientation

considerable for Rot. Z at a maximum value of 45 *deg*. It is also quantified a compensatory phenomenon regarding the difference of orientation echoed in the other rotations. Moreover, the three-dimensional analysis explained physical interfaces' response quantifying undesirable DOF that might represent losses of energy and discomfort.

This phenomenon can be seen through the coefficient of variation and the cross-correlation allowed to identify an accumulative effect in Rot. Z. These outcomes also extended the understanding of the relative motion analysis by considering two more planes (i.e., Rot. X and Y), and showing a considerable interaction in the overlooked planes. Moreover, the physical interfaces' responses are also interpreted by the difference of orientation of each rotation.

Chapter 5

Conclusions and Future works

The AGoRA lower-limb exoskeleton's physical interfaces and passive hip joint were designed and assessed to understand the kinematic compatibility during gait. The development of lower-limb exoskeletons involved several design features: anatomical concepts, targeted goal, mechanical structure, actuators, control strategies, and physical interfaces. These features were addressed by the literature review described in chapter 2. Likewise, the AGoRA lower-limb exoskeleton's development was detailed with each design feature in chapter 3.

Within chapter 3, it was presented the improvement of the AGoRA-LLE's physical interfaces addressing the vibration within the mechanical structure and considering ergonomic considerations to enhance the comfort of the user. The physical interfaces' first version showed a difficulty to fix the structure to the user, and the fasteners were loosened during the gait. Contrary to the second version, this physical interfaces' design eased the exoskeleton's adjustment to the user's limb.

Additionally, it was also presented the passive hip joint's design. These design allowed an adjustable stiffness according to user's needs. Besides, the joint's mathematical model was presented based on its design's principles, considering the kinematic and kinematic modeling. These principal outcomes were aimed at the interaction torque through multiple scenarios

provided by the variable stiffness configuration.

Within this variable stiffness configuration, the bio-inspired tendon was proposed as a light-weight spring component, and characterized by a tensile test to quantify its Young's modulus of 153.9 Mpa and 529 Mpa. These results allowed to estimate the external forces applied to the variable stiffness configuration finding the passive hip joint's kinetic outcomes.

These kinetic outcomes were divided into lower stiffness provided an interaction torque between 1.8 Nm to 4.1 Nm, and higher stiffness allowed an interaction torque between 7.5 Nm to 15.4 Nm. It was quantified the joint's stiffness was defined between 0.56 Nm/rad to 4.24 Nm/rad. However, these outcomes have to be improved to assist the hip ab/adduction motion. These joint's outcomes were not enough to provide support to the user. However, this first study allowed to improve and optimize the joint's performance.

Following chapter 4, the proposed three-dimensional relative motion methodology was presented as a result of the knowledge gap found in the literature. The theoretical base was established through biomechanical analysis and framed into a lower-limb scenario. Additionally, the AGoRA lower-limb exoskeleton's pilot study focused on assessing physical interfaces and carried out using the proposed methodology.

The proposed three-dimensional relative motion methodology provided a better understanding of the HRI and kinematic compatibility. This methodology allowed to quantify the HRI within a lower-limb scenario, and its theoretical bases eased the analysis to other scenarios and joints. Besides, the proposed methodology can be also used to assess control strategies, comparing each three-dimensional user's interaction.

The pilot study's results showed a maximum difference of orientation of 45 deg among the Rot. Z. Besides, the methodology quantified a compensatory phenomenon echoed in the difference of orientation of the other rotations. This phenomenon can be seen through the coefficient of variation and the cross-correlation allowed to identify an accumulative effect

in Rot. Z. These outcomes also extended the understanding of the relative motion analysis by considering two more planes. Besides, the kinematic compatibility is analyzed from a three-dimensional relative motion's insight.

Future works will involve a broad understanding of the HRI between AGoRA lower-limb exoskeleton and the users. Firstly, the passive frontal hip joint's model will be extended on more scenarios considering the links length's variation into the model. Besides, the joint's stiffness will be improved by reducing the preload magnitude. Likewise, the proposed passive joint will be extended by considering the passive frontal hip joint's left side and simulating the gait's cyclic motion. Afterward, the passive frontal hip joint will be assessed in different scenarios through experimental tests to analyze its influence on gait.

Further three-dimensional relative motion studies will be focused on the AGoRA-LLE physical interfaces enhanced version to reduce the difference of orientation. Following this thesis's quantitative results and previous qualitative results allowed to develop a upgrade physical interfaces' version, as shown in Fig. 5.1. The physical interfaces' design include two additional components divided into a hip's belt, and a foam component per physical interface. The hip's belt is intended to reduce the difference of orientation showed by the three-dimensional analysis, and the foam components are aimed to increase the comfort and avoid the pressure points revealed in the qualitative study, presented in [79].

New studies will compare the physical interfaces' performance between versions. Besides, the AGoRA-LLE's controllers will be assessed to improve and compare their performance. Furthermore, this methodology will be extended to estimate more interaction features such as other body segments, physical interface's slipping, and migration over time.

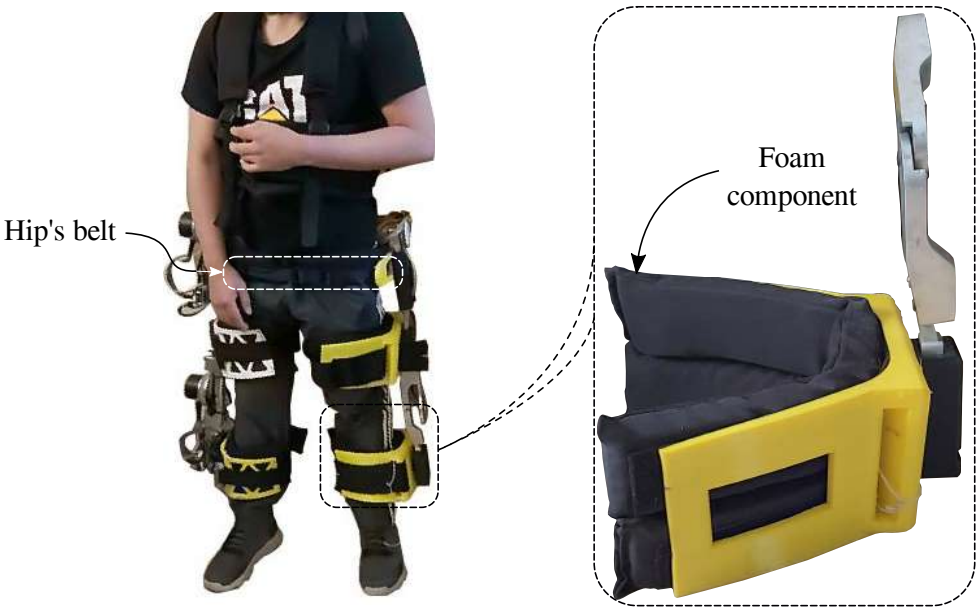

Figure 5.1: AGoRA physical interfaces' third version. The latest physical interfaces' version including the hip belt and additional foams.

Appendix A

Four-bar mechanism solutions

A.1 Kinematic modeling

A four-bar mechanism can be represented as a vector loop according to the Fig. A.1:

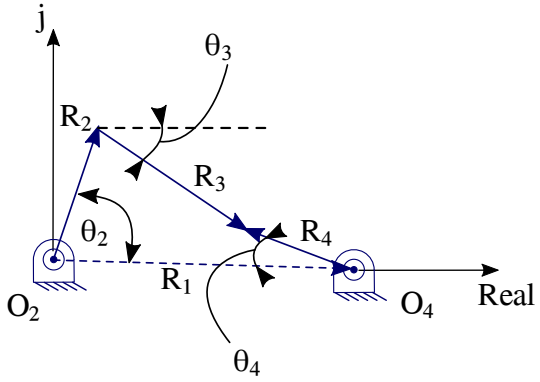

Figure A.1: Kinematic scheme of the simplified mechanism.

Each vector represent a four-bar mechanism's link which is defined in Eq. A.1:

$$\mathbf{R}_2 + \mathbf{R}_3 - \mathbf{R}_4 - \mathbf{R}_1 = 0 \tag{A.1}$$

Redefining each vector in their polar representation as presented in Eq. A.2:

$$a\exp(j\theta_2) + b\exp(j\theta_3) - c\exp(j\theta_4) - d\exp(j\theta_1) = 0 \tag{A.2}$$

Then, each term is extended following the Euler's identity, as it is showed in Eq. A.3

$$a(cos\theta_2 + jsin\theta_2) + b(cos\theta_3 + jsin\theta_3) - c(cos\theta_4 + jsin\theta_4) - d(cos\theta_1 + jsin\theta_1) = 0 \tag{A.3}$$

The previous equation is solved as it is presented by Norton et al. defining the constants shown in Eq. A.4 to Eq. A.17:

$$K_1 = \frac{d}{a} \tag{A.4}$$

$$K_4 = \frac{d}{b} \tag{A.5}$$

$$K_5 = \frac{c^2 - d^2 - a^2 - b^2}{2ab} \tag{A.6}$$

$$D = cos\theta_2 - K_1 - K_4 cos\theta_2 + K_5 \tag{A.7}$$

$$E = -2sin\theta_2 \tag{A.8}$$

$$F = K_1 - (K_4 - 1)cos\theta_2 + K_5 \tag{A.9}$$

$$\theta_3 = -2arctan\left(\frac{-E - \sqrt{E^2 - 4DF}}{2D}\right) \tag{A.10}$$

$$K_1 = \frac{d}{a} \tag{A.11}$$

$$K_2 = \frac{d}{c} \tag{A.12}$$

$$K_3 = \frac{a^2 - b^2 + c^2 + d^2}{2ac} \tag{A.13}$$

$$A = cos\theta_2 - K_1 - K_2 cos\theta_2 + K_3 \tag{A.14}$$

$$B = -2sin\theta_2 \tag{A.15}$$

$$C = K_1 - (K_2 + 1)cos\theta_2 + K_3 \tag{A.16}$$

$$\theta_4 = 2arctan\left(\frac{-B - \sqrt{B^2 - 4AC}}{2A}\right) \tag{A.17}$$

These constants are used along the *Matlab* implementation at the kinematic's function.

A.2 External forces

The external forces depends on the position of the fixation points (i.e., P_3 and P_4) as is shown in Fig. A.2:

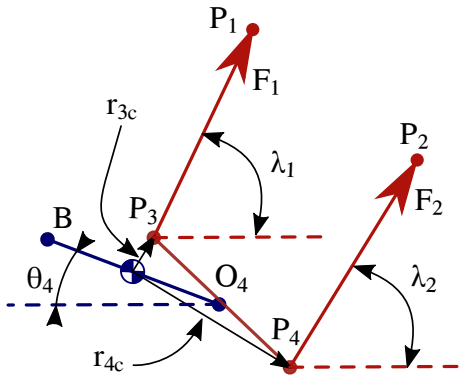

Figure A.2: Kinetic scheme of the external forces applied to the link 4.

These positions are estimated by the kinematic equations of θ_4 given the current position of the fixation points according to Eq. A.17. Moreover, the current strain can be estimated considering the initial length (i_{ini}), the current lenght ($l_\bullet$), and the initial strain (e_{ini}), as presented in Eq. A.18:

$$\epsilon_{\bullet} = \frac{|l_{ini} - l_{\bullet}|}{l_{ini}} + e_{ini} \tag{A.18}$$

Regarding the tendons' strain, the Young's modulus is defined as shown in Eq. A.19 and Eq. A.20:

$$E_A \rightarrow 0 \leq \epsilon \leq 0.1 \tag{A.19}$$

$$E_B \rightarrow 0.1 < \epsilon \leq 0.15 \tag{A.20}$$

Using these values, the force applied to the link 4 is estimated according to the Eq. A.21 to Eq. A.24:

$$F_{1x} = E_{\bullet} \cdot \epsilon_1 \cdot a \cdot cos\lambda_1 \tag{A.21}$$

$$F_{1y} = E_{\bullet} \cdot \epsilon_1 \cdot a \cdot sin\lambda_1 \tag{A.22}$$

$$F_{2x} = E_{\bullet} \cdot \epsilon_2 \cdot a \cdot cos\lambda_2 \tag{A.23}$$

$$F_{2y} = E_{\bullet} \cdot \epsilon_2 \cdot a \cdot sin\lambda_2 \tag{A.24}$$

A.3 Kinetic modeling

According to the free-body diagram (FBD) of each link presentend in Fig. A.3:

These values of the forces and torques equations are summarized for each link according to

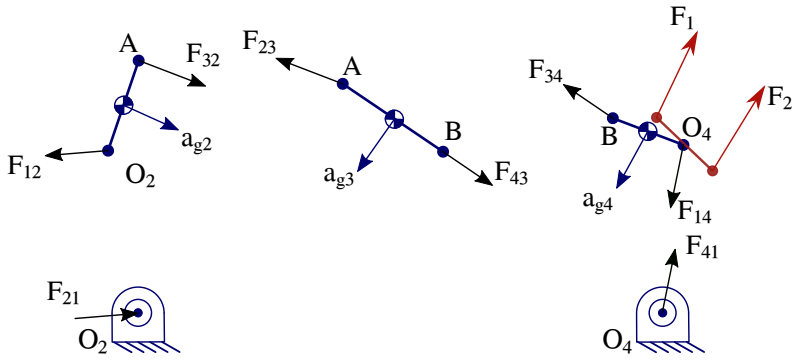

Figure A.3: Kinetic scheme of the simplified mechanism.

the sum of all forces (**F**) (Eq.A.25) and the sum of all torque (τ) (Eq. A.26):

$$\sum \overrightarrow{F} = m \cdot \overrightarrow{a} \tag{A.25}$$

$$\sum \tau = I\alpha \tag{A.26}$$

Each group of link's equations establishes rows of the matrix A and B. The equations of the link 2 correspond to the rows one to three. Similarly, the link 3 is defined by the rows four to six. Finally, the rows seven to nine relates the equations of the link 4. Overall, the matrix A is defined according to Eq. A.27

$$A = \begin{bmatrix} 1 & 0 & 1 & 0 & 0 & 0 & 0 & 0 & 0 \\ 0 & 1 & 0 & 1 & 0 & 0 & 0 & 0 & 0 \\ -R_{12y} & R_{12x} & -R_{32y} & R_{32x} & 0 & 0 & 0 & 0 & 1 \\ 0 & 0 & -1 & 0 & 1 & 0 & 0 & 0 & 0 \\ 0 & 0 & 0 & -1 & 0 & 1 & 0 & 0 & 0 \\ 0 & 0 & R_{23y} & -R_{23x} & -R_{43y} & R_{43x} & 0 & 0 & 0 \\ 0 & 0 & 0 & 0 & -1 & 0 & 1 & 0 & 0 \\ 0 & 0 & 0 & 0 & 0 & -1 & 0 & 1 & 0 \\ 0 & 0 & 0 & 0 & R_{34y} & -R_{34x} & -R_{14y} & R_{14x} & 0 \end{bmatrix} \tag{A.27}$$

On the other hand, the vector **x** is organized through the unknown internal forces of the links and the interaction torque produced by the system, defined as showed in Eq. A.28:

$$\mathbf{x} = \begin{bmatrix} F_{12x} \\ F_{12y} \\ F_{32x} \\ F_{32y} \\ F_{43x} \\ F_{43y} \\ F_{14x} \\ F_{14y} \\ T_{12} \end{bmatrix} \tag{A.28}$$

Then, the vector **B** is the dynamic equilibrium according to the internal and external forces involved in the mechanism organized as presented in Eq. A.29:

$$B = \begin{bmatrix} m_2 \cdot a_{g2x} \\ m_2 \cdot a_{g2y} \\ I_2 \cdot \alpha_2 \\ m_3 \cdot a_{g3x} \\ m_3 \cdot a_{g3y} \\ I_3 \cdot \alpha_3 \\ m_4 \cdot a_{g4x} - F_{1x} - F_{2x} \\ m_4 \cdot a_{g4y} - F_{1y} - F_{2y} \\ I_4 \cdot \alpha_4 + r_{3cx} \cdot F_{1y} - r_{3cy} \cdot F_{1x} + r_{4cx} \cdot F_{2y} + r_{4cy} \cdot F_{2x} \end{bmatrix} \tag{A.29}$$

Defining these matrix the kinetic solution is solved as $\mathbf{x} = BA^{-1}$.

Glossary

6-MWT 6-meter Walking Test.

AAN Assist-As-Needed.

ADL Activities of daily living.

AGoRA In Spanish *Desarrollo de una plataforma robótica adaptable para rehabilitación y asistencia de la marcha*.

AGoRA-LLE AGoRA Lower-Limb Exoskeleton.

AS Anthropomophic Structure.

ASTM American Society for Testing and Materials.

BWS Body Weight Support.

CAD Computer Aid Design.

CLD Right Lateral Tibial Condyle.

CMD Right Medial Tibial Condyle.

DOF Degrees of Freedom.

EASD Right Anterior-Superior Iliac Spine.

ECIJG In Spanish *Escuela Colombiana de Ingeniería Julio Garavito*.

EMG Electromyography.

EPSD Right Posterior-Superior Iliac Spine.

FIM Functional Independence Measure.

HRI Human-Robot Interaction.

LLE Lower-Limb Exoskeleton.

Minciencias In Spanish *Miisterio de Ciencia, Tecnología e Innovación*.

MT Movement Tasks.

NS Nonanthropomophic Structure.

PAM Pneumatic Artificial Muscle.

PLA Polylactic Acid.

PLA-PC Polylactic Acid Particulate with Carbon fiber.

PT Physical Therapy.

QoL Quality of Life.

QUEST Quebec User Evaluation of Satisfaction with Assistive Technology.

ROM Range of Motion.

ROS Robotic Operating System.

RPMT Ratio of Preload for Maximum interaction Torque.

SEA Series Elastic Actuator.

TPU Thermoplastic Polyurethane.

TTC Trajectory Tracking Control.

VSA Variable Stiffness Actuator.

VSP Variable stiffness's principle.

References

[1] S. Nadeau, C. Duclos, L. Bouyer, *et al.*, "Guiding task-oriented gait training after stroke or spinal cord injury by means of a biomechanical gait analysis," *Progress in Brain Research*, vol. 192, pp. 161–180, 2011, ISSN: 18757855.

[2] J. L. Pons and D. Torricelli, *Emerging Therapies in Neurorehabilitation*. Springer, 2014.

[3] J. Perry, *Gait Analysis*. Slack Incorporated, 1992, p. 524.

[4] A. Thibaut, C. Chatelle, E. Ziegler, *et al.*, "Spasticity after stroke: Physiology, assessment and treatment," *Brain Injury*, vol. 27, no. 10, pp. 1093–1105, 2013, ISSN: 02699052.

[5] B. Hobbs and P. Artemiadis, "A Review of Robot-Assisted Lower-Limb Stroke Therapy: Unexplored Paths and Future Directions in Gait Rehabilitation," *Frontiers in Neurorobotics*, vol. 14, 2020.

[6] N. K. Latham, D. U. Jette, M. Slavin, *et al.*, "Physical therapy during stroke rehabilitation for people with different walking abilities," *Archives of Physical Medicine and Rehabilitation*, vol. 86, no. 12 SUPPL. 2005.

[7] G. Chen, C. K. Chan, Z. Guo, *et al.*, "A Review of Lower Extremity Assistive Robotic Exoskeletons in Rehabilitation Therapy," *Critical Reviews in Biomedical Engineering*, vol. 41, no. 4-5, pp. 343–363, 2013.

[8] M. Pekna, M. Pekny, and M. Nilsson, "Modulation of neural plasticity as a basis for stroke rehabilitation," *Stroke*, vol. 43, no. 10, pp. 2819–2828, 2012.

[9] C. M. Stinear, C. E. Lang, S. Zeiler, *et al.*, "Advances and challenges in stroke rehabilitation," *The Lancet Neurology*, vol. 19, no. 4, pp. 348–360, 2020, ISSN: 14744465.

[10] A. Pennycott, D. Wyss, H. Vallery, *et al.*, "Towards more effective robotic gait training for stroke rehabilitation: a review," *Journal of NeuroEngineering and Rehabilitation*, vol. 9, no. 1, p. 65, 2012.

[11] J. R. Gage, M. H. Schwartz, S. E. Koop, *et al.*, "Patient assessment - introduction and overview," *The identification and treatment of gait problems in cerebral palsy*, vol. 58, no. 180, pp. 181–285, 2009.

[12] J. L. Pons, *Wearable robots: Biomechatronic Exoskeletons*. John Wiley & Sons, Feb. 2008.

[13] M. D. C. Sanchez-Villamañan, J. Gonzalez-Vargas, D. Torricelli, *et al.*, "Compliant lower limb exoskeletons: a comprehensive review on mechanical design principles," *Journal of NeuroEngineering and Rehabilitation*, vol. 16, no. 1, p. 55, Dec. 2019, ISSN: 1743-0003.

[14] D. Pinto-Fernandez, D. Torricelli, M. d. C. Sanchez-Villamanan, *et al.*, "Performance Evaluation of Lower Limb Exoskeletons: A Systematic Review," *IEEE Transactions on Neural Systems and Rehabilitation Engineering*, 2020, ISSN: 1534-4320.

[15] D. Simonetti, N. L. Tagliamonte, L. Zollo, *et al.*, *Biomechatronic design criteria of systems for robot-mediated rehabilitation therapy*. Elsevier Ltd., 2018, pp. 29–46, ISBN: 9780128119952.

[16] D. Shi, W. Zhang, W. Zhang, *et al.*, "A Review on Lower Limb Rehabilitation Exoskeleton Robots," *Chinese Journal of Mechanical Engineering (English Edition)*, vol. 32, no. 1, 2019, ISSN: 21928258.

[17] S. Sierra, L. Arciniegas, F. Ballen-Moreno, *et al.*, "Adaptable robotic platform for gait rehabilitation and assistance: Design concepts and applications," in *Exoskeleton Robots for Rehabilitation and Healthcare Devices*, Springer, 2020, pp. 67–93.

[18] N. Geifman, R. Cohen, and E. Rubin, "Redefining meaningful age groups in the context of disease," *Age*, vol. 35, no. 6, pp. 2357–2366, 2013.

[19] M. De Onis and J. P. Habicht, "Anthropometric reference data for international use: Recommendations from a World Health Organization Expert Committee," *American Journal of Clinical Nutrition*, vol. 64, no. 4, pp. 650–658, 1996.

[20] R. Á. Chaurand, L. R. P. León, and E. L. G. Muñoz, *Dimensiones antropométricas de población latinoamericana*. Universidad de Guadalajara, CUAAD, 2007.

[21] A. Schiele and F. C. T. van der Helm, "Kinematic Design to Improve Ergonomics in Human Machine Interaction," *IEEE Transactions on Neural Systems and Rehabilitation Engineering*, vol. 14, no. 4, pp. 456–469, Dec. 2006.

[22] J. C. Perry, J. Rosen, and S. Burns, "Upper-limb powered exoskeleton design," *IEEE-ASME Transactions on Mechatronics*, vol. 12, no. 4, pp. 408–417, 2007, ISSN: 10834435.

[23] T. Yamazaki, T. Watanabe, Y. Nakajima, *et al.*, "Improvement of depth position in 2-D/3-D registration of knee implants using single-plane fluoroscopy," *IEEE Transactions on Medical Imaging*, vol. 23, no. 5, pp. 602–612, 2004.

[24] T. Yamazaki, T. Watanabe, Y. Nakajima, *et al.*, "Visualization of femorotibial contact in total knee arthroplasty using X-ray fluoroscopy," *European Journal of Radiology*, vol. 53, no. 1, pp. 84–89, 2005.

[25] S. Martello, V. Pinskerova, and A. Visani, "Anatomial Investigations on the Knee by means of Computer-Dissection," *Journal of Mechanics in Medicine and Biology*, vol. 06, no. 01, pp. 55–73, Mar. 2006.

[26] P. Corke, "Robotics," *Vision and Control*, 2011.

[27] L. Saccares, I. Sarakoglou, and N. G. Tsagarakis, "It-knee: An exoskeleton with ideal torque transmission interface for ergonomic power augmentation," *IEEE International Conference on Intelligent Robots and Systems*, vol. 2016-Nov, pp. 780–786, 2016.

[28] M. Gold and M. Varacallo, *Anatomy, Bony Pelvis and Lower Limb, Hip Joint*. StatPearls Publishing, Treasure Island (FL), 2019.

[29] R. Glenister and S. Sharma, "Anatomy, bony pelvis and lower limb, hip," *StatPearls [Internet]*, 2020.

[30] M. P. Kadaba, H. K. Ramakrishnan, and M. E. Wootten, "Measurement of lower extremity kinematics during level walking," *Journal of Orthopaedic Research*, vol. 8, no. 3, pp. 383–392, May 1990.

[31] A. Ribeiro, J. Rasmussen, P. Flores, *et al.*, "Modeling of the condyle elements within a biomechanical knee model," *Multibody System Dynamics*, vol. 28, no. 1-2, pp. 181–197, 2012.

[32] A. Martino Cinnera, S. Bonnì, M. C. Pellicciari, *et al.*, "Health-related quality of life (HRQoL) after stroke: Positive relationship between lower extremity and balance recovery," *Topics in Stroke Rehabilitation*, vol. 00, no. 00, pp. 1–7, 2020.

[33] N. Koceska and S. Koceski, "Review: Robot Devices for Gait Rehabilitation," *International Journal of Computer Applications*, vol. 62, no. 13, pp. 1–8, 2013.

[34] P. W. Duncan, K. J. Sullivan, A. L. Behrman, *et al.*, "Body-weight - Supported treadmill rehabilitation after stroke," *New England Journal of Medicine*, vol. 364, no. 21, pp. 2026–2036, 2011.

[35] S. J. Park and S. Oh, "Effect of diagonal pattern training on trunk function, balance, and gait in stroke patients," *Applied Sciences (Switzerland)*, vol. 10, no. 13, 2020, ISSN: 20763417.

[36] S. K. Banala, S. H. Kim, S. K. Agrawal, *et al.*, "Robot assisted gait training with active leg exoskeleton (alex)," *IEEE transactions on neural systems and rehabilitation engineering*, vol. 17, no. 1, pp. 2–8, 2008.

[37] J. Meuleman, E. Van Asseldonk, G. Van Oort, *et al.*, "LOPES II - Design and Evaluation of an Admittance Controlled Gait Training Robot with Shadow-Leg Approach," *IEEE Transactions on Neural Systems and Rehabilitation Engineering*, vol. 24, no. 3, pp. 352–363, 2016.

[38] S. Jezernik, G. Colombo, T. Keller, *et al.*, "Robotic Orthosis Lokomat: A Rehabilitation and Research Tool," *Neuromodulation: Technology at the Neural Interface*, vol. 6, no. 2, pp. 108–115, Apr. 2003.

[39] Hocoma, *Lokomat*, 2020. [Online]. Available: `https://www.hocoma.com/solutions/lokomat-2/`, "(accessed: October 30, 2020)".

[40] S. Taki, T. Imura, Y. Iwamoto, *et al.*, "Effects of Exoskeletal Lower Limb Robot Training on the Activities of Daily Living in Stroke Patients: Retrospective Pre-Post Comparison Using Propensity Score Matched Analysis," *Journal of Stroke and Cerebrovascular Diseases*, vol. 29, no. 10, p. 105 176, Oct. 2020.

[41] R. Mustafaoglu, B. Erhan, I. Yeldan, *et al.*, "Does robot-assisted gait training improve mobility, activities of daily living and quality of life in stroke? A single-blinded, randomized controlled trial," *Acta Neurologica Belgica*, vol. 120, no. 2, pp. 335–344, 2020. [Online]. Available: `https://doi.org/10.1007/s13760-020-01276-8`.

[42] R. J. Farris, H. A. Quintero, and M. Goldfarb, "Preliminary Evaluation of a Powered Lower Limb Orthosis to Aid Walking in Paraplegic Individuals," *IEEE Transactions on Neural Systems and Rehabilitation Engineering*, vol. 19, no. 6, pp. 652–659, Dec. 2011.

[43] H. Kawamoto and Y. Sankai, "Comfortable power assist control method for walking aid by HAL-3," *Proceedings of the IEEE International Conference on Systems, Man and Cybernetics*, vol. 4, pp. 447–452, 2002.

[44] J. Gancet, M. Ilzkovitz, G. Cheron, *et al.*, "MINDWALKER: a brain controlled lower limbs exoskeleton for rehabilitation. Potential applications to space," *11th Symposium on advanced space technologies in robotics and automation*, no. 1, pp. 12–14, 2011.

[45] G. Zeilig, H. Weingarden, M. Zwecker, *et al.*, "Safety and tolerance of the ReWalk™ exoskeleton suit for ambulation by people with complete spinal cord injury: A pilot study," *Journal of Spinal Cord Medicine*, vol. 35, no. 2, pp. 96–101, 2012.

[46] M. Bortole, A. Venkatakrishnan, F. Zhu, *et al.*, "The H2 robotic exoskeleton for gait rehabilitation after stroke : early findings from a clinical study," *Journal of NeuroEngineering and Rehabilitation*, pp. 1–14, 2015.

[47] D. Accoto, F. Sergi, N. L. Tagliamonte, *et al.*, "Robomorphism: A Nonanthropomorphic Wearable Robot," *IEEE Robotics & Automation Magazine*, vol. 21, no. 4, pp. 45–55, Dec. 2014.

[48] A. Zoss, H. Kazerooni, and A. Chu, "On the mechanical design of the Berkeley Lower Extremity Exoskeleton (BLEEX)," *2005 IEEE/RSJ International Conference on Intelligent Robots and Systems, IROS*, pp. 3132–3139, 2005.

[49] H. Kawamoto, S. Lee, S. Kanbe, *et al.*, "Power assist method for hal-3 using emg-based feedback controller," in *SMC'03 Conference Proceedings. 2003 IEEE International Conference on Systems, Man and Cybernetics. Conference Theme-System Security and Assurance (Cat. No. 03CH37483)*, IEEE, vol. 2, 2003, pp. 1648–1653.

[50] M. B. Naf, K. Junius, M. Rossini, *et al.*, "Misalignment Compensation for Full Human-Exoskeleton Kinematic Compatibility: State of the Art and Evaluation," *Applied Mechanics Reviews*, vol. 70, no. 5, pp. 1–19, 2018.

[51] D. F. Machekposhti, N. Tolou, and J. L. Herder, "A review on compliant joints and rigid-body constant velocity universal joints toward the design of compliant homokinetic couplings," *Journal of Mechanical Design, Transactions of the ASME*, vol. 137, no. 3, pp. 1–12, 2015.

[52] B. Celebi, M. Yalcin, and V. Patoglu, "AssistOn-Knee: A self-aligning knee exoskeleton," in *2013 IEEE/RSJ International Conference on Intelligent Robots and Systems*, IEEE, Nov. 2013, pp. 996–1002.

[53] B. Kalita, J. Narayan, and S. K. Dwivedy, "Development of Active Lower Limb Robotic-Based Orthosis and Exoskeleton Devices: A Systematic Review," *International Journal of Social Robotics*, no. 0123456789, 2020.

[54] W. Huo, S. Mohammed, J. C. Moreno, *et al.*, "Lower Limb Wearable Robots for Assistance and Rehabilitation: A State of the Art," *IEEE Systems Journal*, vol. 10, no. 3, pp. 1068–1081, Sep. 2016, ISSN: 1932-8184.

[55] X. Zhang, Z. Yue, and J. Wang, "Robotics in Lower-Limb Rehabilitation after Stroke," *Behavioural Neurology*, vol. 2017, pp. 1–13, 2017.

[56] S. K. Banala, S. K. Agrawal, S. H. Kim, *et al.*, "Novel gait adaptation and neuromotor training results using an active leg exoskeleton," *IEEE/ASME Transactions on Mechatronics*, vol. 15, no. 2, pp. 216–225, 2010.

[57] A. T. Asbeck, R. J. Dyer, A. F. Larusson, *et al.*, "Biologically-inspired soft exosuit," *IEEE International Conference on Rehabilitation Robotics*, 2013.

[58] R. Bionics, "Rex bionics," *Web Page (www. rexbionics. com), Accessed: Oct.*, 2020.

[59] B. Vanderborght, A. Albu-Schaeffer, A. Bicchi, *et al.*, "Variable impedance actuators: A review," *Robotics and Autonomous Systems*, vol. 61, no. 12, pp. 1601–1614, Dec. 2013.

[60] P. K. Jamwal, S. Hussain, and M. H. Ghayesh, "Robotic orthoses for gait rehabilitation: An overview of mechanical design and control strategies," *Proceedings of the Institution of Mechanical Engineers, Part H: Journal of Engineering in Medicine*, vol. 234, no. 5, pp. 444–457, 2020.

[61] J. Cao, S. Q. Xie, R. Das, *et al.*, "Control strategies for effective robot assisted gait rehabilitation: The state of art and future prospects," *Medical Engineering and Physics*, vol. 36, no. 12, pp. 1555–1566, 2014, ISSN: 18734030.

[62] J. C. Moreno, J. Figueiredo, and J. L. Pons, "Exoskeletons for lower-limb rehabilitation," in *Rehabilitation Robotics*, Elsevier, 2018, pp. 89–99.

[63] A. T. Asbeck, S. M. De Rossi, K. G. Holt, *et al.*, "A biologically inspired soft exosuit for walking assistance," *The International Journal of Robotics Research*, vol. 34, no. 6, pp. 744–762, May 2015. [Online]. Available: `http://journals.sagepub.com/doi/10.1177/0278364914562476`.

[64] M. B. Näf, A. S. Koopman, S. Baltrusch, *et al.*, "Passive back support exoskeleton improves range of motion using flexible beams," *Frontiers Robotics AI*, vol. 5, no. JUN, pp. 1–16, 2018.

[65] A. Chiri, M. Cempini, S. M. M. De Rossi, *et al.*, "On the design of ergonomic wearable robotic devices for motion assistance and rehabilitation," in *2012 Annual International Conference of the IEEE Engineering in Medicine and Biology Society*, IEEE, Aug. 2012, pp. 6124–6127.

[66] J. Beil, G. Perner, and T. Asfour, "Design and control of the lower limb exoskeleton KIT-EXO-1," *IEEE International Conference on Rehabilitation Robotics*, vol. 2015-September, pp. 119–124, 2015.

[67] K. Junius, B. Brackx, V. Grosu, *et al.*, "Mechatronic design of a sit-to-stance exoskeleton," in *5th IEEE RAS/EMBS International Conference on Biomedical Robotics and Biomechatronics*, IEEE, Aug. 2014, pp. 945–950.

[68] E. Pröbsting, A. Kannenberg, and B. Zacharias, "Safety and walking ability of kafo users with the c-brace® orthotronic mobility system, a new microprocessor stance and swing control orthosis," *Prosthetics and orthotics international*, vol. 41, no. 1, pp. 65–77, 2017.

[69] K. Langlois, M. Moltedo, T. Bacek, *et al.*, "Design and Development of Customized Physical Interfaces to Reduce Relative Motion Between the User and a Powered Ankle Foot Exoskeleton," in *2018 7th IEEE International Conference on Biomedical Robotics and Biomechatronics (Biorob)*, vol. 2018-Augus, IEEE, Aug. 2018, pp. 1083–1088. [Online]. Available: `https://ieeexplore.ieee.org/document/8487706/`.

[70] M. Sposito, S. Toxiri, D. Caldwell, *et al.*, "Towards design guidelines for physical interfaces on industrial exoskeletons: Overview on evaluation metrics," in *International Symposium on Wearable Robotics*, Springer, 2018, pp. 170–174.

[71] N. D'Elia, F. Vanetti, M. Cempini, *et al.*, "Physical human-robot interaction of an active pelvis orthosis: Toward ergonomic assessment of wearable robots," *Journal of NeuroEngineering and Rehabilitation*, vol. 14, no. 1, pp. 1–14, 2017, ISSN: 17430003.

[72] Y. Akiyama, S. Okamoto, Y. Yamada, *et al.*, "Measurement of contact behavior including slippage of cuff when using wearable physical assistant robot," *IEEE Transactions on Neural Systems and Rehabilitation Engineering*, vol. 24, no. 7, pp. 784–793, 2016, ISSN: 15344320.

[73] A. Leal-Junior, A. Theodosiou, C. Díaz, *et al.*, "Fiber Bragg gratings in CYTOP fibers embedded in a 3D-printed flexible support for assessment of human-robot interaction forces," *Materials*, vol. 11, no. 11, 2018, ISSN: 19961944.

[74] A. Rathore, M. Wilcox, D. Z. M. Ramirez, *et al.*, "Quantifying the human-robot interaction forces between a lower limb exoskeleton and healthy users," *Proceedings of the Annual International Conference of the IEEE Engineering in Medicine and Biology Society, EMBS*, vol. 2016-October, pp. 586–589, 2016, ISSN: 1557170X.

[75] J. Li, S. Zuo, C. Xu, *et al.*, "Influence of a Compatible Design on Physical Human-Robot Interaction Force: a Case Study of a Self-Adapting Lower-Limb Exoskeleton Mechanism," *Journal of Intelligent and Robotic Systems: Theory and Applications*, vol. 98, no. 2, pp. 525–538, 2020, ISSN: 15730409.

[76] M. B. Yandell, B. T. Quinlivan, D. Popov, *et al.*, "Physical interface dynamics alter how robotic exosuits augment human movement: implications for optimizing wearable assistive devices," *Journal of NeuroEngineering and Rehabilitation*, vol. 14, no. 1, p. 40, Dec. 2017.

[77] D. R. Louie and J. J. Eng, "Powered robotic exoskeletons in post-stroke rehabilitation of gait: A scoping review," *Journal of NeuroEngineering and Rehabilitation*, vol. 13, no. 1, pp. 1–10, 2016, ISSN: 17430003. [Online]. Available: `http://dx.doi.org/10.1186/s12984-016-0162-5`.

[78] J. T. Meyer, S. O. Schrade, O. Lambercy, *et al.*, "User-centered Design and Evaluation of Physical Interfaces for an Exoskeleton for Paraplegic Users," in *2019 IEEE 16th International Conference on Rehabilitation Robotics (ICORR)*, IEEE, Jun. 2019, pp. 1159–1166.

[79] M. Sanchez-Manchola, "A Robotic Lower-limb Exoskeleton for Patients with Mobility Impairments," Master's thesis, Escuela Colombiana de Ingeniería Julio Garavito, 2019, p. 146.

[80] L. J. Arciniegas Mayag, "Miembro Inferior en Actividades de la Vida Diaria," Master's thesis, Universidad del Rosario & Escuela Colombiana de Ingeniería Julio Garavito, 2020, p. 99.

[81] M. Sanchez-Manchola, D. Gomez-Vargas, D. Casas-Bocanegra, *et al.*, "Development of a Robotic Lower-Limb Exoskeleton for Gait Rehabilitation: AGoRA Exoskeleton," in *2018 IEEE ANDESCON*, IEEE, Aug. 2018, pp. 1–6.

[82] A. Stienen, E. Hekman, F. van der Helm, *et al.*, "Self-Aligning Exoskeleton Axes Through Decoupling of Joint Rotations and Translations," *IEEE Transactions on Robotics*, vol. 25, no. 3, pp. 628–633, Jun. 2009, ISSN: 1552-3098.

[83] H. Nolle, "Linkage coupler curve synthesis: A historical review - I. Developments up to 1875," *Mechanism and Machine Theory*, vol. 9, no. 2, pp. 147–168, 1974, ISSN: 0094114X.

[84] R. L. Norton, *Diseño de Maquinaria: Sintesis y análisis de máquinas y mecanismos*, Cuarta. Mexico D.F.: McGrawHill, 2009, p. 754, ISBN: 978-970-10-6884-7.

[85] ASTM C1557-14, *Standard Test Method for Tensile Strength and Young's Modulus of Fibers*, West Conshohocken, PA, 2014. [Online]. Available: `https://www.astm.org/DATABASE.CART/HISTORICAL/C1557-14.htm`.

[86] K. A. Strausser, T. A. Swift, A. B. Zoss, *et al.*, "Prototype Medical Exoskeleton for Paraplegic Mobility: First Experimental Results," in *ASME 2010 Dynamic Systems and Control Conference, Volume 1*, ASMEDC, Jan. 2010, pp. 453–458, ISBN: 978-0-7918-4417-5.

[87] H. A. Quintero, R. J. Farris, and M. Goldfarb, "Control and implementation of a powered lower limb orthosis to aid walking in paraplegic individuals," in *2011 IEEE International Conference on Rehabilitation Robotics*, IEEE, Jun. 2011, pp. 1–6, ISBN: 978-1-4244-9862-8.

[88] J. Lee, K. Seo, B. Lim, *et al.*, "Effects of assistance timing on metabolic cost, assistance power, and gait parameters for a hip-type exoskeleton," in *2017 International Conference on Rehabilitation Robotics (ICORR)*, IEEE, Jul. 2017, pp. 498–504, ISBN: 978-1-5386-2296-4.

[89] T. Poliero, C. Di Natali, M. Sposito, *et al.*, "Soft wearable device for lower limb assistance: Assessment of an optimized energy efficient actuation prototype," *2018 IEEE International Conference on Soft Robotics, RoboSoft 2018*, pp. 559–564, 2018.

[90] C. Di Natali, T. Poliero, M. Sposito, *et al.*, "Design and Evaluation of a Soft Assistive Lower Limb Exoskeleton," *Robotica*, vol. 37, no. 12, pp. 2014–2034, 2019, ISSN: 14698668.

[91] M. Topley and J. G. Richards, "A comparison of currently available optoelectronic motion capture systems," *Journal of Biomechanics*, vol. 106, p. 109 820, 2020, ISSN: 18732380.

[92] R. Hibbeler, *Engineering Mechanics: Dynamics*. Pearson Education, 2011.

[93] L. Chèze, *Kinematic Analysis of Human Movement*. John Wiley & Sons, Inc., 2014, pp. 1–130, ISBN: 9781119058144.

[94] G. Wu, S. Siegler, P. Allard, *et al.*, "Isb recommendation on definitions of joint coordinate system of various joints for the reporting of human joint motion—part i: Ankle, hip, and spine," *Journal of biomechanics*, pp. 543–548, 2002.